RhoV, a Potential Notch Target Gene in Murine Skin, Does not Play an Essential Role in Epidermis Development and Homeostasis

THÈSE N^{O} 4679 (2010)

PRÉSENTÉE LE 30 AVRIL 2010

À LA FACULTÉ SCIENCES DE LA VIE

UNITÉ DU PROF. RADTKE

PROGRAMME DOCTORAL EN BIOLOGIE MOLÉCULAIRE DU CANCER ET DE L'INFECTION

ÉCOLE POLYTECHNIQUE FÉDÉRALE DE LAUSANNE

POUR L'OBTENTION DU GRADE DE DOCTEUR ÈS SCIENCES

PAR

April BEZDEK POMEY

acceptée sur proposition du jury:

Prof. J. Lingner, président du jury
Prof. F. Radtke, directeur de thèse
Prof. Y. Barrandon, rapporteur
Dr E. Hummler, rapporteur
Prof. T. Pedrazzini, rapporteur

ÉCOLE POLYTECHNIQUE
FÉDÉRALE DE LAUSANNE

Suisse
2010

Table of Contents

Table of Contents

Résumé

Résumé

La voie de signalisation Notch joue un rôle central dans la régulation de processus fondamentaux tels que la maintenance des cellules souches, la prolifération ou encore la différentiation. Récemment, nous avons enquêté sur les gènes potentiellement régulés par Notch1 durant la différentiation de l'épiderme. Pour cela, nous avons fait une analyse de puce à ADN de 14'000 gènes de la souris lors de gain et de perte de fonction de Notch1 dans des keratinocytes primaires murins. Treize gènes furent ensuite choisis selon leurs niveaux d'expression et l'importance de leur voie de signalisation pour une validation par PCR en temps réel. Parmi ceux-ci, nous nous sommes concentrés sur une Rho GTPase nommée RhoV qui démontrait une différence de régulation consistante dans les deux conditions. Nous avons donc généré des souris transgéniques exprimant une forme dominante active ou négative de RhoV spécifiquement dans la peau.

Les analyses morphologiques et histologiques n'ont pas révélé de phénotype apparent chez les souris transgéniques. De plus, des expériences sur la cicatrisation démontrèrent une guérison des plaies normale chez les souris transgéniques et aucun dysfonctionnement de la migration et/ou de la différentiation des keratinocytes. Ainsi nos résultats suggèrent que ni le gain ni la perte de RhoV ne perturbe le développement et l'homéostasie de la peau, et n'affecte pas non plus le processus de cicatrisation.

En outre, nous avons généré un modèle de souris à invalidation conditionnelle du gène Jagged2 ainsi qu'une souris transgénique reporter spécifique pour Notch2. La souris « floxée » Jagged2 permettrait la délétion du ligand pour étudier son rôle dans un contexte de perte de fonction.

La souris reporter Notch2-spécifique est un outil permettant l'analyse *in vivo* de cellules ayant reçu un signal par activation du récepteur Notch2. La stratégie utilise des éléments du système Tet-Off et permet l'identification de cellules recevant un signal spécifiquement par Notch2 dans un tissu choisi et à n'importe quel moment.

Mots-clés	Voie de signalisation Notch, peau, Rho GTPase, souris transgéniques, système Tet-Off

Abstract

Abstract

The evolutionarily conserved Notch signaling cascade plays a pivotal role in the regulation of many fundamental processes such as stem cell maintenance, proliferation, and differentiation. Recently, we aimed to identify downstream target genes regulated by Notch1 during epidermal differentiation. For this purpose an Affymetrix mouse gene chip array of 14.000 genes was performed in both Notch1 gain and loss of function experiments using murine primary keratinocytes. Thirteen genes positively or negatively regulated, based on expression levels and relevance of the involved signaling pathways, were further validated by real-time PCR. Among these, we decided to focus on the Rho GTPase RhoV because it showed robust up- and down-regulation under both gain- and loss-of-function conditions. Therefore, we generated different transgenic mice expressing either a dominant active or a dominant negative form of RhoV specifically in the skin.

Morphological and histological analyses did not reveal any overt skin phenotype in transgenic mice. In addition, challenging the system by performing wound healing assays demonstrated that the healing process in transgenic mice occurred normally and that the migration and/or differentiation of keratinocytes was unimpaired. Taken together, our data suggest that gain or loss of RhoV function does not perturb skin development and homeostasis, and does not affect the wound healing process.

In addition to the investigation of the potential Notch target gene RhoV, we sought to generate both a floxed Jag2 gene targeted mouse line and a Notch2-specifc reporter mouse. The former was intended to enable conditional deletion of the Notch ligand Jagged2 and therefore allow its role to be studied in a loss-of-function context.

The Notch2 reporter mouse is a tool enabling the *in vivo* study of cells that receive a Notch2-mediated signal. The strategy employs elements of a Tet-Off system and allows cells receiving a Notch2 specific signal to be identified in any tissue at any given time point.

Keywords	Notch signaling, skin, Rho GTPase, transgenic mice, Tet-Off system

Introduction

Introduction

1. The Notch signaling pathway

Thomas Hunt Morgan (1866-1945), an American geneticist and embryologist, was awarded the Nobel Prize in Physiology or Medicine in 1933 for his work on genetics using *Drosophila melanogaster* as a model system. In 1917 he described a strain of fruit flies with notches at the margin of their wing blades (Morgan, 1917). The gene causing this haplo-insufficiency phenotype - that was named Notch - was cloned in the mid-1980s and found to be a single-pass transmembrane receptor consisting of a ligand-binding extracellular domain and a signal transduction cytoplasmic domain (Kidd et al., 1986; Wharton et al., 1985). The family of Notch receptors is evolutionarily conserved through worms to humans (Greenwald, 1998).

1.1 Structure of Notch receptors and ligands

In mammals there are four Notch receptors (Notch1-4) (del Amo et al., 1993; Lardelli et al., 1994; Uyttendaele et al., 1996; Weinmaster et al., 1992) and five ligands (Jagged1-2 and Delta-like1, 3 and 4) (Bettenhausen et al., 1995; Dunwoodie et al., 1997; Lindsell et al., 1995; Nye and Kopan, 1995; Shawber et al., 1996; Shutter et al., 2000). The Notch receptors are expressed as heterodimers at the cell surface and initiate signaling by interaction with their DSL (Delta/Serrate/LAG2) ligands expressed by neighboring cells. The Notch receptors and their ligands contain several protein domains important for interaction and modulation of the signaling which are depicted in Fig.1.

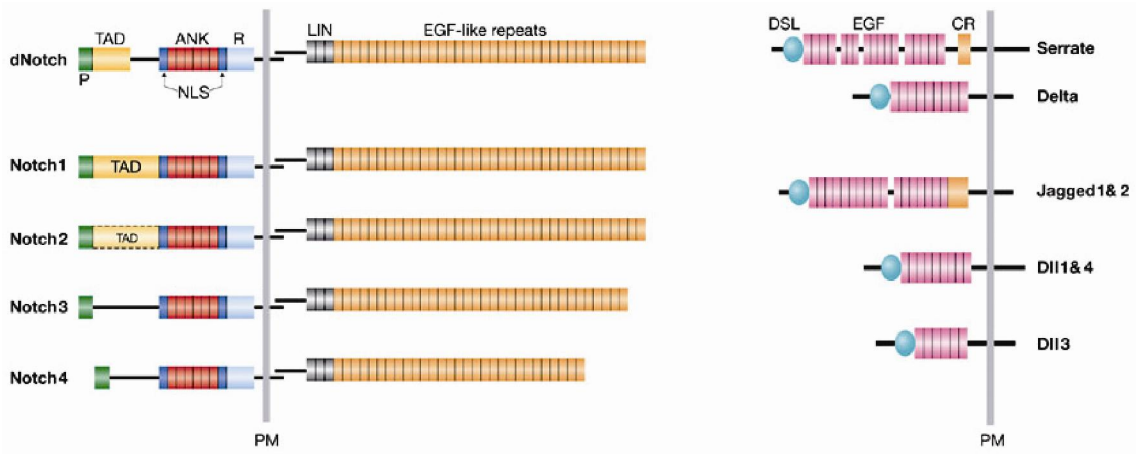

Figure 1. Structure of Notch receptors and their ligands. *Drosophila* flies contain one Notch receptor (dNotch) that is bound by two transmembrane DSL-ligands (Delta and Serrate). Mammalians possess four Notch receptors (Notch1–4) and five ligands (Jagged1 and 2, which are homologous to Serrate, and Delta-like (Dll) 1, 3 and 4, which are homologous to Delta). Notch receptors are expressed on the cell surface as heterodimeric proteins. Their extracellular portion contains 29–36 epidermal growth factor (EGF)-like repeats that are associated with ligand binding, followed by three cysteine-rich LIN repeats that prevent ligand-independent signalling, and a heterodimerization domain. The intracellular portion of the receptor harbours two protein interaction domains, the RAM domain (R) and six ankyrin repeats (ANK), two nuclear localizations signals (NLS) and a transactivation domain (TAD, which has not yet been defined for Notch3 and 4), and a PEST (P) sequence. Notch ligands are also expressed as membrane-bound proteins. They all contain an amino-terminal DSL domain (Delta, Serrate and Lag2) followed by EGF-like repeats. Ligands of the Serrate family also harbour a cysteine-rich (CR) domain downstream of the EGF-like repeats. PM, plasma membrane. (Radtke et al., 2005)

Heterodimeric Notch receptors are first synthesized as single precursor proteins and then cleaved in the Golgi by a Furin-like convertase during their transport to the cell surface (Blaumueller et al., 1997; Logeat et al., 1998). During cell-cell contact, the Notch pathway activation involves direct binding of the N-terminal ligand domain of one of the membrane-anchored ligands to the epidermal growth factor (EGF)-like repeat region of the Notch receptor. Modulation of the responsiveness of the receptor to different DSL ligands is possible by *N*- and *O*-linked glycosylation, e.g. by Fringe glycosyltransferases (Moloney et al., 2000). Notch receptors modified by Fringe glycosyltransferases cannot mediate signaling via the Jagged ligands, whereas their affinity for Delta is increased (Bruckner et al., 2000; Hicks et al., 2000; Moloney et al., 2000).

1.2 Canonical Notch signaling

Upon Notch-ligand interaction, a proteolytic cleavage site in the extracellular portion of the Notch C-terminal is exposed. The subsequent cleavage by the metalloprotease ADAM10/TACE (tumor necrosis factor α-converting enzyme) releases the extracellular Notch subunit which is endocytosed by the ligand-expressing cell (Mumm et al., 2000). The next proteolytic cleavage in the transmembrane domain is mediated by the multisubunit intra-membrane aspartyl protease γ-secretase complex and releases the Notch intracellular domain (NIC or NICD). This proteolytic complex includes presenilin and nicastrin proteins, which are also involved in the cleavage of amyloid precursor proteins (dysfunctional in Alzheimer's disease) (Li et al., 2003; Wong et al., 1997).

In the absence of NIC, Notch target genes are maintained in an actively repressed state through transcriptional complexes involving the transcription factor CSL (CBF1/Su(H)/LAG1, also known as RBP-Jκ in mice) and several co-repressors such as histone deacetylase (Oswald et al., 2005). Once NIC translocates to the nucleus it binds to CSL via its RAM (regulation of amino-acid metabolism) domain and ankyrin repeats. Subsequent displacement of the co-repressors allows formation of a ternary transcriptionally active complex of NIC, CSL and Mastermind-like (MAML), which in turn recruits other co-activators (Wu et al., 2000). Expression of Notch target genes occurs through transactivation once the transcription complex is bound to CSL-binding sites found within the promoter of genes, such as the Hairy/Enhancer of Split (Hes) transcriptional repressors (Jarriault et al., 1998). Figure 2 summarizes the various steps involved in Notch signaling.

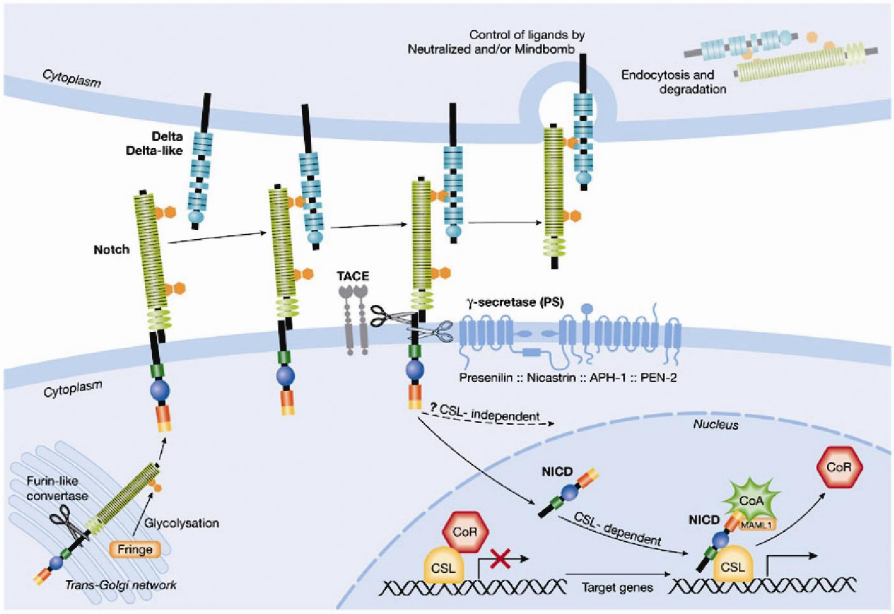

Figure 2. Notch signaling pathway. Fringe glycosyltransferases modify EGF-like repeats by adding N-acetylglucosamine within the Golgi. Notch signaling is initiated after ligand-receptor interaction, which induces two sequential proteolytic cleavages. The first cleavage within the extracellular domain is mediated by the metalloprotease TACE. The cleaved extracellular subunit of the receptor is 'trans-endocytosed' by the neighboring ligand-expressing cell. This process seems to be controlled by Neuralized and/or Mindbomb E3 ubiquitin ligases. The second cleavage occurs within the transmembrane domain and is mediated by the γ-secretase activity of the multi-protein complex of presenilins (PS), which includes Nicastrin, APH-1 and PEN-2. The liberated intracellular domain of Notch (NICD) translocates into the nucleus and binds to the transcription factor CSL (CBF1 in humans, Suppressor of Hairless in *Drosophila* and LAG in *C. elegans*). This interaction leads to transcriptional activation by displacement of co-repressors (CoR) and simultaneous recruitment of co-activators (CoA), including mastermind-like proteins (MAML1). (Radtke et al., 2005)

Finally, the proteolysis generating NIC is irreversible, and hence the turnover of the signaling molecule must be tightly controlled by ubiquitination and proteosomal degradation. One protein involved in controlling the amount of NIC in the cell is the E3 ubiquitin ligase Fbw7/Sel-10. Fbw7 acts by targeting NIC for degradation after phosphorylation on its C-terminal PEST domain by cyclin-dependent kinase 8 (Gupta-Rossi et al., 2001; Oberg et al., 2001; Wu et al., 2001).

1.3 Non-canonical Notch signaling

Another E3 ubiquitin ligase identified as Deltex in *Drosophila* suggests an alternative Notch signaling route found to be independent of CSL (or RBP-Jκ)-transcription complex

formation (Hori et al., 2005). Deltex-mediated positive regulation of Notch signaling does not require ligand interaction. Hence, this mechanism reflects a cell-intrinsic signal that evidently is not initiated by neighboring cell contact. This pathway might be utilized by some cells to maintain a basal level of Notch activation that dampens signaling noise or potentiates signaling induced by a ligand. However, gene targeting of two mammalian homologues Deltex-1 and -2 in murine T cell progenitors did not impair thymocyte development, even though Notch signaling was more potent in the double-deficient cells (Lehar and Bevan, 2006).

In vitro experiments conducted in cell lines identified another non-canonical signaling through cytosolic NIC. Notch inhibited neglect apoptosis, i.e. due to withdrawal of nutritional cues, by activation of the kinase Akt through mammalian target of rapamycin complex 2 (mTORC2) (Perumalsamy et al., 2009). Thus, this study revealed the integration of non-canonical Notch signaling with a new pathway, which ultimately promotes cell survival.

1.4 Functions of Notch signaling

Notch signaling plays many important roles during embryonic and post-natal development, such as in proliferation, cell-fate decisions and apoptosis (Fig.3) (reviewed in Artavanis-Tsakonas et al., 1999).

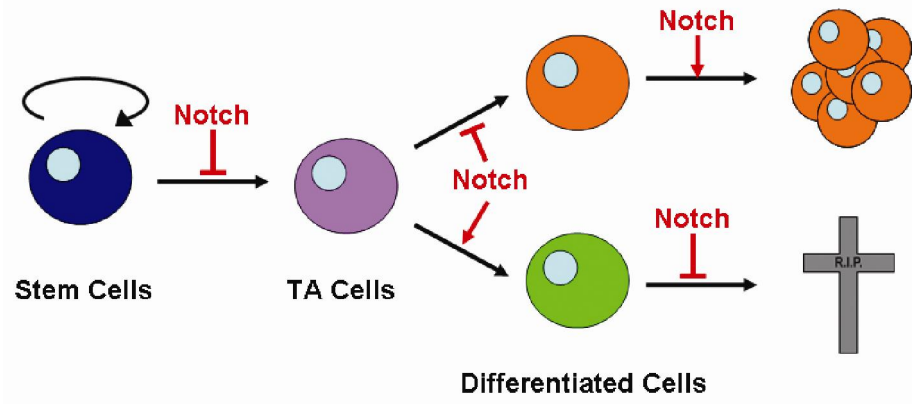

Figure 3. Multiple functions of Notch signaling. Depending on the cell context, Notch maintains stem and/or transit-amplifying (TA) cells in an undifferentiated state (e.g. intestine), specifies one cell lineage at the expense of another (e.g. T vs. B cell lineage) and promotes terminal differentiation of TA cells (e.g. skin). Notch also induces proliferation (e.g. skin) while playing an anti-apoptotic role (e.g. double-negative T cells).

The influence of Notch signaling on the proliferation of cells was shown in *Drosophila* by expression of NIC in precursor cells of the imaginal disc. Activated Notch induced mitotic activity, synergistically with the wing patterning genes Vestigial and Wingless (Go et al., 1998). In mammalian epithelial cells, activated Notch1 infected into primary murine keratinocytes *in vitro* induced an increase in the cyclin-dependant kinase inhibitor protein $p21^{WAF1/Cip1}$ and subsequent withdrawal from the cell cycle. In this context Notch1 was also shown to promote early differentiation markers of the epidermis, such as keratin1 and involucrin (Rangarajan et al., 2001).

Binary cell fate choices occur regularly during development and in self-renewing tissues. As a pathway activated by cell-cell contacts, Notch signaling plays an important role during these lineage decisions. During the developing eye of the *Drosophila*, for example, establishment of planar polarity of photoreceptors R3 and R4 is mediated by Notch and Delta signaling. Briefly, upon Wingless signaling by Frizzled and Disheveled, precursor cells of R3 cell fate up-regulate Delta expression on their surface, thereby inducing Notch signaling in the neighboring R4 precursors (Fanto and Mlodzik, 1999). In the mammalian hematopoietic system, Notch specifies T cell lineage at an early stage as induced Notch1-deficient mice illustrated a block in T cell development and an accumulation of de novo ectopic B cells in the thymus (Radtke et al., 1999; Wilson et al., 2001). Conversely, mice reconstituted with bone marrow transduced with an NIC-expressing retrovirus developed extra-thymic T cells and a B cell differentiation blockade (Pui et al., 1999).

In addition to proliferation, differentiation and cell fate decisions, Notch signaling was also shown to be involved in cell death. One example is the protective effect of Notch1 in T cell lines from T cell receptor (TCR)-dependant apoptosis. The orphan nuclear hormone receptor Nur77 is required for apoptosis of maturing thymocytes and was shown to physically interact with Notch1 in T hybridoma cells *in vitro*. This interaction inhibits Nur77-dependant cell death, and consequently, Notch1 was suggested to be an anti-apoptotic factor involved in double-negative thymocytes (Jehn et al., 1999).

1.5 Context-dependency of Notch signaling

Another feature adding to the complexity of Notch signaling is the context-dependent differences in its function. As previously mentioned, Notch promotes differentiation of epidermal keratinocytes by inducing cell cycle arrest of the transient-amplifying cells and

expression of early differentiation markers (Rangarajan et al., 2001). However, the Notch pathway can also inhibit differentiation and maintain stem and/or progenitor cells in the mammalian gastrointestinal tract. A genetic study over-expressing NIC in the intestinal epithelium resulted in an expansion of proliferating progenitors and greatly impaired cell differentiation (Fre et al., 2005). Reciprocally, gut-inducible inactivation of RBP-Jκ in mice resulted in complete loss of the progenitor compartment and conversion of transit-amplifying cells into mucus secreting goblet cells. Outcome of a pharmacological treatment of wild-type mice with a γ-secretase inhibitor, which blocked Notch signaling in the intestine, was indistinguishable from the consequences of genetic inactivation (van Es et al., 2005).

1.6 Notch: oncogene vs. tumor-suppressor

Since Notch signaling interplays in many organs with many essential pathways, it is not surprising that Notch deregulation is involved in several diseases as well as in a number of cancers. Notch was first linked to a human cancer known as T cell acute lymphoblastic leukemia (T-ALL) by investigating a chromosomal translocation breakpoint, t(7;9), found in less than 1% of patients. The sequence revealed a juxtaposition of the C-terminal region of EGF-like repeat 34 of human Notch1 (TAN1 for translocation-associated Notch homologue1) to the TCR β-enhancer. This translocation lead to the expression of a constitutive Notch1 receptor causing aberrant Notch signaling and, consequently, T cell leukemia (Ellisen et al., 1991). Constitutive Notch signaling was further associated with T-ALL tumors as activating mutations within Notch1 were found in a majority of Notch-dependent T-ALL cell lines. The mutations were localized within the heterodimerization and/or PEST domains rendering the Notch1 receptor unusually stable (Weng et al., 2004).

The oncogenic role of Notch was also described in other systems, such as the murine intestinal epithelium. Notch signaling blockade, by pharmacological treatment of a mouse model for intestinal tumorigenesis, resulted in a 50% reduction in the number of adenomas in the small intestine. The mechanism by which this reduction occurred was through the derepression of Krüppel-like factor 4 (Klf4), a zinc finger transcription factor which inhibits cell proliferation (Ghaleb et al., 2008).

The oncogenic ability of the Notch pathway, previously shown in the hematopoietic system and in the gastro-intestinal tract, is also context dependent. Evidence of the tumor-suppressive role of Notch signaling was revealed by studies in the skin (Nicolas et al., 2003).

After induced Notch1-deletion in the epidermis, mice spontaneously developed basal cell carcinoma-like tumors within 9 months after inactivation. Furthermore, tumorigenicity was facilitated after chemical-induced carcinogenesis treatment of the Notch1-deleted mice (Nicolas, 2003; Nicolas et al., 2003). Thus, Notch signaling was suggested to have a different function in the skin.

2. The skin and its appendages

The skin is the body's largest organ, typically 1.5 to 2m^2 of surface area for an adult human being, and serves as an outer covering protection against physical, biological (e.g. infectious agents) and environmental assaults. It is a waterproof barrier formed by a stratified epithelium, hair follicles, sweat and sebaceous glands. The skin also functions as a temperature regulator, conveys sensation, and allows synthesis of vitamin D. The skin is composed of three main parts: the outermost epidermis (from the Greek "epi" meaning "upon"), the dermis, where the appendages are found, and the deepest region called the hypodermis or subcutaneous adipose layer. (Fig.4)

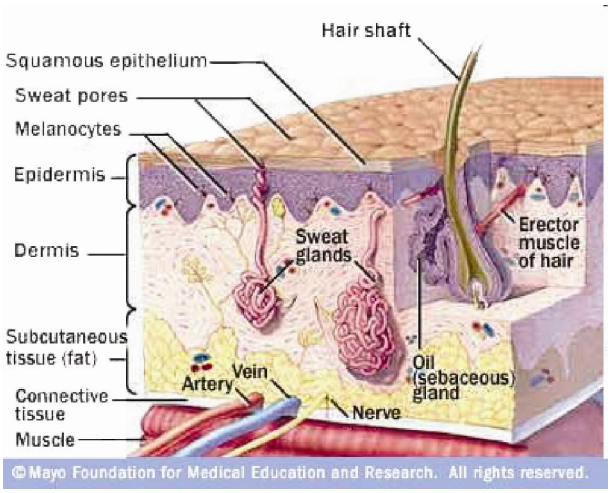

Figure 4. Structure of the skin. The epidermis, dermis, and hypodermis (or subcutaneous fat) are the three layers that form the skin. Three appendages can also be observed: the sweat and sebaceous glands, and the hair follicle. (Image from MayoClinic.com)

2.1 The epidermis

The epidermis is itself stratified in several distinct cell layers of squamous epithelium comprising mainly of keratinocytes. Other cell types that can be found are macrophages (Langerhans cells), Merkel cells associated with the sensory neurons, and the pigment-bearing melanocytes. The first layer above the basal lamina is called the basal layer from which cells migrate upwards and differentiate to form the spinous and granular layers. These cells finally

lose their nuclei and become keratinized forming the outermost cornified layer. Thus, the terminally differentiated stratum corneum has a limited lifespan and continually sheds, a process called desquamation. During embryogenesis in mice the stratification is completed by embryonic day 17.5 (E17.5). In adult mice, the homeostatic differentiation process takes approximately 14 days, whereas in humans it takes 1 month. Constant shedding of the dead cells requires a renewal of the epidermis by stem cells during homeostasis of the skin as well as in response to wounding.

Epidermal stem cells of the interfollicular epidermis (IFE) are located in the basal layer. These stem cells give rise to transit-amplifying (TA) cells which continuously execute their terminal differentiation program by moving outwards in a columnar fashion. These cells which possess proliferative potential switch off the expression of keratins 5 and 14 and concomitantly start expressing keratins 1 and 10. The latter markers of the spinous layer form a robust intermediate filament network which reinforces cell-cell junctions, thereby providing resistance to external mechanical stresses (Fuchs and Green, 1980). Cells continue to differentiate by expressing structural proteins that are deposited beneath the plasma membrane and form indestructible sacs, which gave rise to the name of the granular layer. The proteinaceous sac serves as a scaffold for lipid bilayers which confer the waterproofing of the skin surface. Several proteins are used as markers of late differentiation, such as involucrin (Rice and Green, 1979), loricrin (Mehrel et al., 1990) and filaggrin (Scott and Harding, 1986). When the cells die and form the stratum corneum, involucrin and loricrin are cross-linked by a calcium-dependent enzyme called transglutaminase for the assembly of the cornified envelope (Ishida-Yamamoto et al., 1999; Simon and Green, 1988). The stratified structures of the skin and the epidermis are summarized in Fig.5.

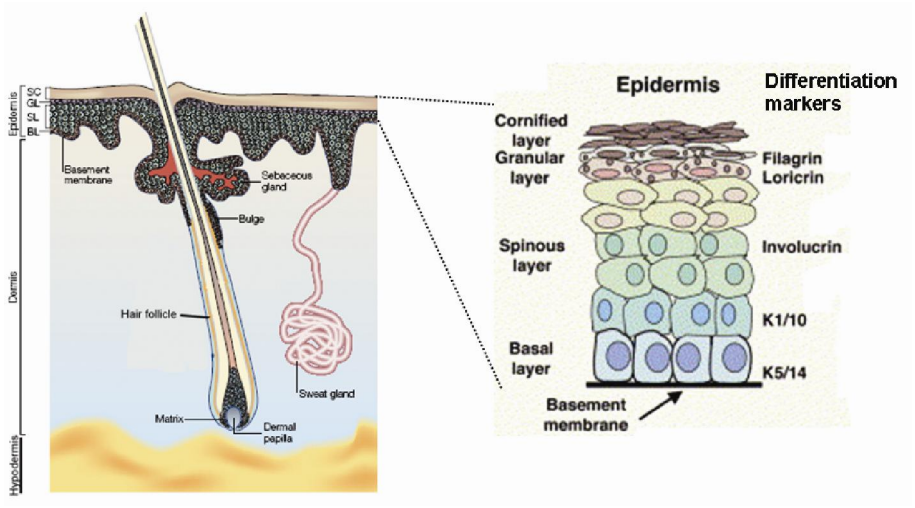

Figure 5. The skin and the structure of the epidermis. The skin is devised into three main layers: the hypoderm, the dermis and the epidermis. Three appendages are found within the dermis: the hair follicle, the sweat and the sebaceous glands. The dermis and the epidermis are separated by the basement membrane or basal lamina. (Modified from Fuchs and Raghavan, 2002) The epidermis is also stratified in several layers which consist of keratinocytes at different differentiation stages. The epidermal stem cells as well as the transit-amplifying cells are localized in the basal layer and express keratins 5 and 14. The suprabasal layers are formed by the spinous and granular layers, which express involucrin, and loricrin as well as filaggrin, respectively. Terminally differentiated cells are then enucleated and form the outermost cornified layer. (Adapted from Wilson and Radtke, 2006)

2.2 The hair follicle

In addition to its protective function, the skin also encompasses several appendages essential for survival: sweat and sebaceous glands, and hair follicles. Sweat glands secrete and excrete water and minerals which regulate the body temperature. In some mammals, such as mouse, rat and cat, these glands are restricted to the underside of the paws. The sebaceous glands, formed by sebocytes, are associated with hairs and secrete oils which protect and lubricate the hair channel as well as the skin surface. The insulation of the skin is augmented by hair follicles, or feathers and scales in vertebrates other than mammals, which can also serve as camouflage or sexual characteristics. All skin appendages arise from reciprocal interactions between the developing epidermis and the underlying mesenchyme, the dermis (Hardy, 1992).

2.3 Four murine hair types

The mouse pelage consists of four different hair types defined by size, shape and internal structure: zigzag, awl, auchene, and guard (or tylotrich). The zigzag constitutes the majority of the hairs of the pelage (approximately 70%), has two or more bends, and one single row of air spaces. The second most abundant hair type is the awl (approximately 28%) which is small (0.5cm) and straight, consisting of two or more rows of air spaces. The auchene and guard hair types are less frequently observed. The auchene has one bend and two or more rows of air spaces while the guard is straight and long (1cm) with two rows of air cells (Fig.6)

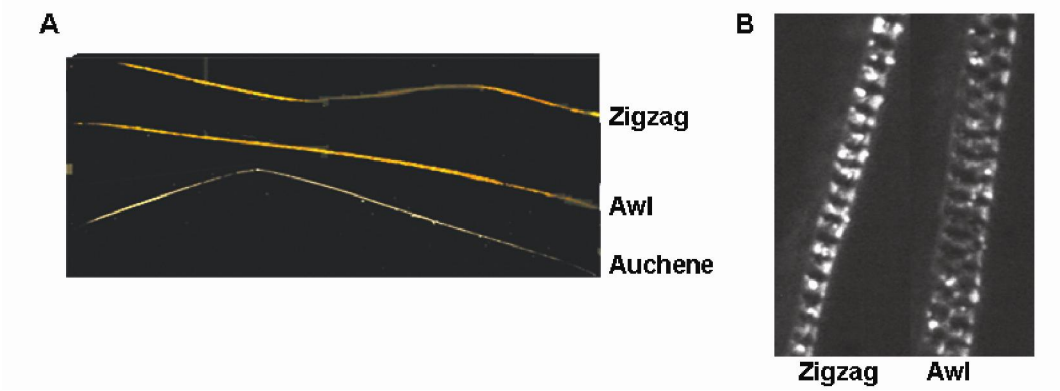

Figure 6. Three of the four hair types of the mouse pelage. (A) Stereomicroscope picture of a zigzag, an awl, and an auchene hair from a wild-type mouse back pelage. (B) Higher magnification of a zigzag and an awl hair shows 1 and 2 rows of air spaces, respectively.

2.4 Structure of the hair follicle

In the embryo, the hair follicle (HF) is produced by epithelial stem cells that grow downward at a region called the placode, contiguous with the epithelium and assuming the shape of a rod. The inner layers differentiate into concentric cylinders forming the central hair shaft (HS) and the inner root sheath (IRS). The HS consists of the hair cortex surrounded by the hair cuticle. The IRS can be sub-divided into three layers based on structure, pattern of keratinization and incorporation of trichohyalin, which stains an intermediate filament-associated protein: the cuticle, the Huxley and Henle layers. Surrounding the IRS is the outermost layer, the outer root sheath (ORS). The ORS is continuous with the epidermis and extends into the sebaceous gland (Fig.7).

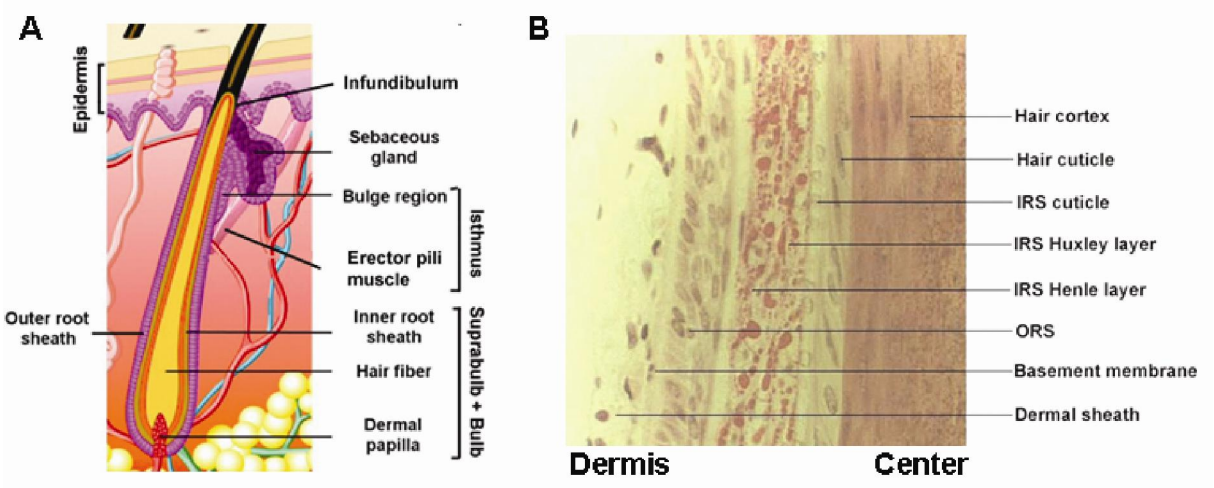

Figure 7. Structure of the hair follicle. (A) The HF is divided into three regions (from bottom to top): the bulb and suprabulb, the isthmus (from the attachment of the erector pili muscle to the entrance of the sebaceous gland duct), and the infundibulum (from the sebaceous gland duct to the follicular orifice). (B) A longitudinal cut of a HF shows the different layers from the dermis to the center of the hair cortex. (Adapted from Wikipedia)

At the base of the HF, a mesenchymal cluster called the dermal papilla (DP) becomes enveloped by the hair bulb. Once fully mature, at postnatal day 6 (P6) in mouse back skin, the proliferative matrix cells at the follicle base produce daughter cells that terminally differentiate to form the growing hair that exits the skin surface. Throughout life, the HF is renewed and cycles through growth (anagen), regression (catagen), and rest (telogen).

2.5 The hair growth cycle

During anagen, the proliferative matrix cells produce progeny cells that move upwards and differentiate into one of the six lineages, from outermost to innermost: Henley, Huxley and cuticle layers of the IRS, and cuticle, cortex and medulla layers of the HS. When the HS cells terminally differentiate, they become tightly packed with bundles of cross-linked keratins, which allow strength and flexibility. The continued proliferation and differentiation of matrix cells, which are transit-amplifying cells that undergo a limited number of cell divisions, determines the duration of anagen and the length of the hair.

As the supply of matrix cells declines, the follicle enters the destructive phase. The first catagen begins in a wave, from head to tail, at P14 at the upper back to P18 near the tail. The onset does not only vary from one skin region to another, but also between mouse strains. During catagen, the hair follicle regresses entirely by apoptosis of epithelial cells in the bulb

and the outermost layer, the ORS. The HS seals off and forms a club, which remains anchored to the permanent non-cycling upper follicle.

HF lie dormant during telogen until one or two quiescent stem cells at the base of the follicle, near the DP, are activated. Rapid proliferation produces transit-amplifying cells that will form the new HF by a new anagen phase. The new hair emerges from the orifice of the old one, and the club hair is eventually shed (exogen). The complete hair cycle, starting from the follicular morphogenesis, is depicted in Fig.8.

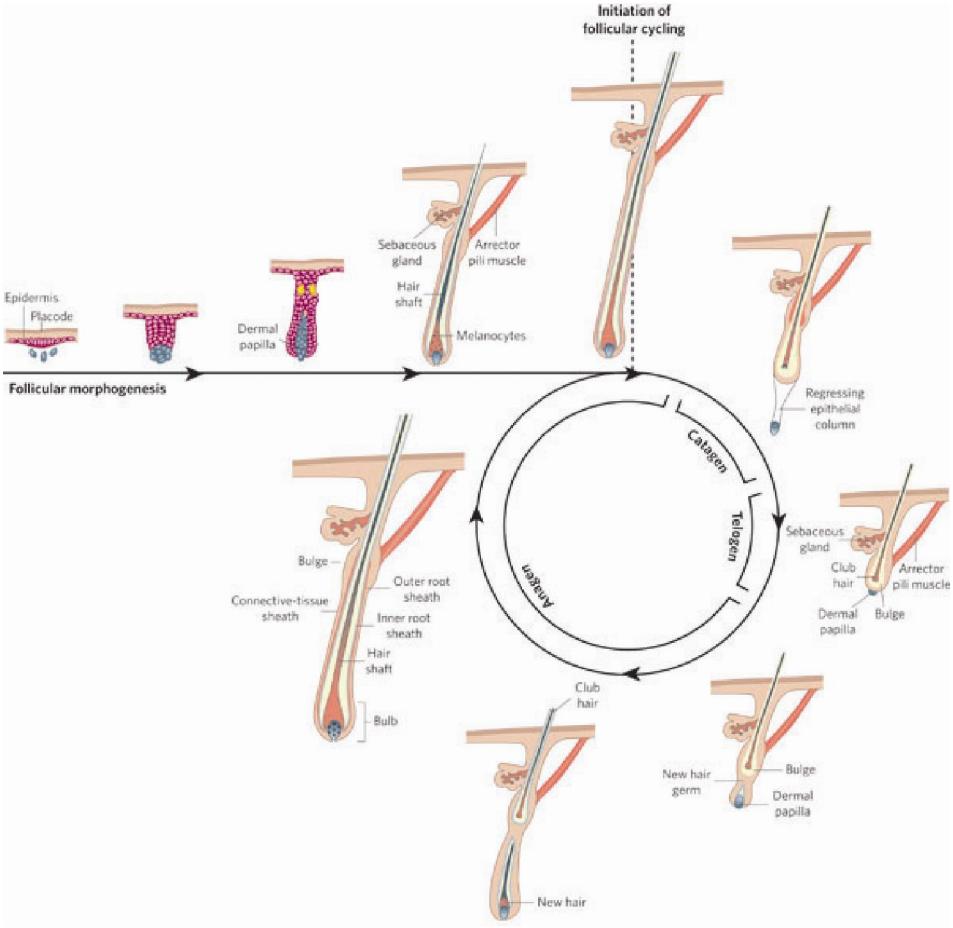

Figure 8. The hair cycle. During embryogenesis, the follicular morphogenesis is initiated by epithelial-mesenchymal interactions which occur at the ectodermal placode. After invagination into the dermal layer, the newly formed hair follicle (HF) will enter a cycle consisting of three phases: anagen, catagen, and telogen. Anagen is the growing phase of the HF, when proliferative transit-amplifying (TA) cells (matrix) migrate upwards and differentiate into the six layers of the HF. As the supply of matrix cells declines, the hair enters catagen, which is the destructive phase. The HF regresses by apoptosis of cells in the bulb and the outer root sheath. Finally, the club hair forms and lies dormant during the resting phase, or telogen. Activation of epithelial stem cells at the base of the follicle, which will produce a new pool of TA cells, resets the hair cycle. (Reviewed in Fuchs, 2007)

2.6 Factors involved in hair formation

The hair morphogenesis and subsequent hair cycle is a complex process bringing into play many different signaling pathways. Examples of factors involved in various aspects of the HF formation are the families of fibroblast growth factor (FGF), hedgehog (Hh), transforming growth factor-β (TGFβ)-related bone morphogenic protein (BMP), and Wnt signaling molecules.

FGF5, for example, is expressed in the ORS during anagen to catagen transition and was shown to be involved in inhibition of hair elongation. FGF5 null mice developed abnormally long hair identical to mice carrying the spontaneous mutation angora, which is a mutant allele of FGF5 (Hebert et al., 1994). Another member of the FGF family, the keratinocyte growth factor (KGF or FGF7), is expressed in the dermis and exerts its mitogenic activity on the epidermal cells. By ectopically expressing KGF in murine epidermis, growth and differentiation of keratinocytes were impaired, resulting in an epidermal thickening, while hair follicle morphogenesis and adipogenesis were suppressed (Guo et al., 1993).

Sonic hedgehog (Shh) is an important signaling molecule involved in epithelio-mesenchymal interactions as it is expressed in epithelial cells in the placode of the developing hair and whisker, and later in the hair bulb surrounding the dermal papilla (Iseki et al., 1996). In agreement with this expression pattern, Shh knockout mice failed to evolve any dermal papilla, and, consequently, hair follicle morphogenesis was arrested (Chiang et al., 1999).

In mature hair follicles, BMP4 is expressed in the dermal papilla, and both BMP2 and BMP4 are expressed in hair shaft precursors (Wilson et al., 1999). Ectopic expression of BMP4 in the ORS inhibited proliferation of the matrix cells and disturbed the expression pattern of cytokeratins during differentiation of the shaft cells (Blessing et al., 1993). The role of BMPs in the HF formation was consolidated by investigations using the BMP inhibitor Noggin. Transgenic mice expressing Noggin in matrix cells showed defects in differentiation of the hair shaft cortex and cuticle, as well as an inhibition of the second wave of placode formation (Botchkarev et al., 2002; Kulessa et al., 2000).

Activation of the Wnt signaling pathway involves formation of nuclear complexes between β-catenin and Tcf/Lef proteins to induce transcription of target genes (Fig.9). Both signaling molecules were found to be important in the formation of hair follicles. Lymphoid enhancer factor 1 (LEF1) is expressed in the matrix and in the developing dermal papilla cells

(Zhou et al., 1995). Confirming the role of Lef1 in hair morphogenesis, Lef1 knockout mice were completely devoid of hair (van Genderen et al., 1994). Moreover, conditional inactivation of β-catenin in the mouse embryo blocked placode formation. Deletion after formation of the HF caused a complete loss of hair, after the first cycle, and concomitant development of cysts with epidermal differentiation characteristics (Huelsken et al., 2001).

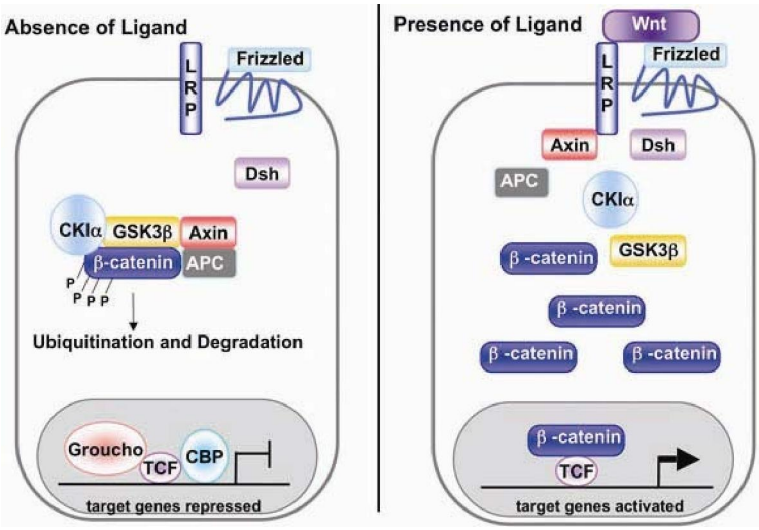

Figure 9. Canonical Wnt signaling pathway. Left scheme: In the absence of Wnt signaling molecules, β-catenin is phosphorylated by the GSK3β/axin/APC complex and subsequently degraded. Wnt target genes are repressed by Tcf/Lef proteins interacting with co-repressors. Right scheme: In the presence of Wnt molecules, LRP and Frizzled receptors are activated, thereby relieving β-catenin degradation. Consequently, the stabilized β-catenin can translocate to the nucleus and bind to the Tcf/Lef family of transcription factors. This interaction activates transcription of the formerly repressed target genes. (Wormbook.org)

2.7 Epidermal stem cells

The constant self-renewal of the epidermis and of the hair follicle is due to adult epidermal stem cells (SC). All three epidermal lineages, i.e. interfollicular epidermis, hair follicles, and glands are thought to have their own niches of epidermal stem cells (Reviewed in Ambler and Maatta, 2009).

A hair follicle region, called the bulge, was identified as a reservoir of epidermal SC by a label-retaining technique using ^{3}H-thymidine (Cotsarelis et al., 1990). The transcriptional profile of the SCs of the bulge was determined by a genetic approach to generate label-

retaining cells (LRC). A transgenic mouse strain was engineered to express a GFP-tagged protein histone H2B in epidermal cells, and the transgene can be silenced by feeding the mice tetracycline (Tet-Off system). Consequently, slow-cycling cells continue on expressing the GFP transgene while the rapidly dividing cells dilute the fluorescent protein out (Tumbar et al., 2004).

The second reservoir of epidermal SC was identified in the IFE by lineage tracing experiments. As previously described, Shh is expressed in the epidermal placode of the HF and, once the HF formed, is restricted to the cycling portion of the follicles in the skin. Consequently, the follicular stem cells in adult mice are descendants of Shh-expressing cells. By labeling these daughter cells, it was shown that the follicular SCs of the bulge do not contribute to the epidermis, implying another stem cell pool in the IFE (Levy et al., 2005). Retroviral transduction of the *lacZ* gene into mouse skin labeled IFE keratinocytes in spatially distinct epidermal proliferative units (EPU; (Allen and Potten, 1974)) independent from follicles (Ghazizadeh and Taichman, 2001).

Another population of SCs was identified in a region between the bulge and the sebaceous gland, called the upper isthmus (UI). Cells in this zone expressed the surface marker MTS24 and possessed higher clonogenic potential in vitro than MTS24-negative cells. Furthermore, transplanted UI cells were able to give rise to all three epidermal lineages, a characteristic of multipotency (Jensen et al., 2008; Nijhof et al., 2006). The various SC reservoirs described above are depicted in Fig.10.

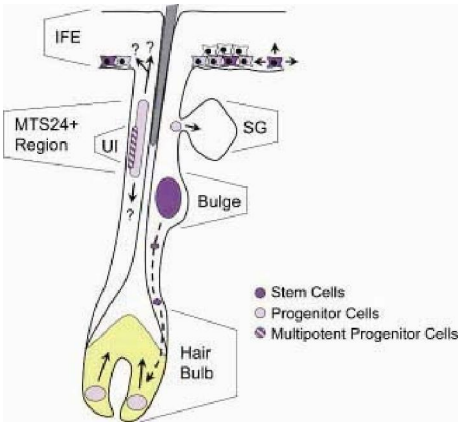

Figure 10. Locations of epidermal stem and progenitor cells in the mammalian skin. Stem cells (purple) are located in the bulge of the hair follicle and amongst the basal layer of the interfollicular epidermis. Interfollicular stem cells support the interfollicular epidermis (arrows) and bulge stem cells migrate to the hair follicle bulb (yellow) during the anagen (dashed line). Contribution of epidermal progenitor cells (lavender) has still to be defined. IFE, interfollicular epidermis; UI, upper isthmus; SG, sebaceous gland. (Ambler and Maatta, 2009)

2.8 Stem cell markers

The mechanisms by which epidermal stem cell are maintained are not fully understood. An interesting candidate is the cell-cycle regulator c-Myc (myelocytomatosis oncogene) since elevated expression in transgenic mice lead to hyperproliferation and depletion of SCs without loss of differentiation, as well as hair loss and impaired wound healing (Arnold and Watt, 2001; Waikel et al., 2001).

A member of the p53 family of transcription factors called p63 is expressed in basal stem cells and down-regulated in progenitor cells of the epithelium (Pellegrini et al., 2001). The p63 knockout mice are completely devoid of epidermis and skin appendages, suggesting an essential role for maintenance of the epidermal SC population necessary for epithelial morphogenesis and renewal (Yang et al., 1999).

Recently, leucine-rich repeats and immunoglobulin-like domain protein 1 (Lrig1) was shown to be expressed in the junctional zone between the sebaceous gland and the infundibulum of the HF. However, Lrig1 null mice did not exhibit any impairment of the sebaceous gland nor of the HF, but had an increase in IFE proliferation. These results suggested that Lrig1 is required for stem cell quiescence in adult mouse epidermis. In addition, c-Myc positively regulated Lrig1 expression, thereby consolidating the link between c-Myc activity and stem cell maintenance (Jensen et al., 2009).

Stem cells can be characterized by expression of specific markers. The hematopoietic stem and progenitor marker CD34 co-localized with LRCs in the bulge region. Isolated CD34-positive keratinocytes expressed high levels of α6-integrin, and were positive for K14 and K6 (Trempus et al., 2003). Another used marker is the bulge-specific keratin 15 (K15). By generating K15-EGFP transgenic mice, bulge SCs could be isolated and subsequently shown to have a high proliferative property *in vitro*, and to be able to generate all cutaneous lineages *in vivo* (Morris et al., 2004). More recently, the marker of intestinal stem cells called leucine-rich G protein-coupled receptor 5 (Lgr5) was shown to be expressed in actively proliferating, but yet multipotent hair follicle stem cells by generating knockin mouse models (Jaks et al., 2008).

2.9 Wound healing

Epidermal stem cells are not only essential during skin homeostasis but are also immobilized during the wound repair process. In response to injury, stem cells from both the interfollicular epidermis and the bulge rapidly respond by migrating into the damaged area. Epidermal SCs, TA cells and early differentiated cells have the ability to form fully differentiated epidermis both *in vitro* and *in vivo* (Li et al., 2004). The whole healing process comprises of three stages (Fig.11) (Reviewed in Gurtner et al., 2008).

The first response to occur is inflammation and lasts about 48h. Upon mechanical injury, the first signal is the release of pre-stored interleukin-1 (IL1) by the keratinocytes, which activates and alerts the surrounding area of the wounding. The activation cascade consists of many extracellular signals, such as tumor necrosis factor-α (TNFα) and transforming growth factor-α (TGFα) (Jiang et al., 1993; Komine et al., 2000). Theses signaling molecules induce a change in expression of keratins, such as K6, providing the keratinocytes with plasticity and flexibility for migration (Komine et al., 2001; Wong and Coulombe, 2003) The damage also induces components of the coagulation cascade and of the immune system to protect the body from losing fluids as well as from invading bacteria. Platelets form a plug in which a fibrin matrix becomes the scaffold for infiltrating neutrophils and macrophages.

In the next 2 to 10 days following injury an eschar, or scab, closes the surface of the wound and new tissue forms underneath by the inwards migration of surrounding epithelial cells. In order for keratinocytes to migrate, hemidesmosomes must be dissolved by changes in junction and adhesion proteins. Thus, activated keratinocytes produce different membrane molecules: vitronectin, fibronectin receptors and integrin α5β1 (Cavani et al., 1993). During re-epithelialization new capillaries associated with fibroblasts and macrophages replace the fibrin clot with a perfused extracellular matrix tissue called granulation tissue.

The last stage is tissue remodeling and can last for more than 1 year. Fibroblasts migrate into the wound, some of them differentiate into myofibroblasts, and both types of cells interact to produce extracellular matrix, mainly collagen, which forms the bulk of the scar and causes a slight bump at the surface of the skin. Keratinocytes are eventually deactivated and resume their normal differentiation program. However, no normal appendages, hair follicles or glands, can be found in re-epithelialized healed regions.

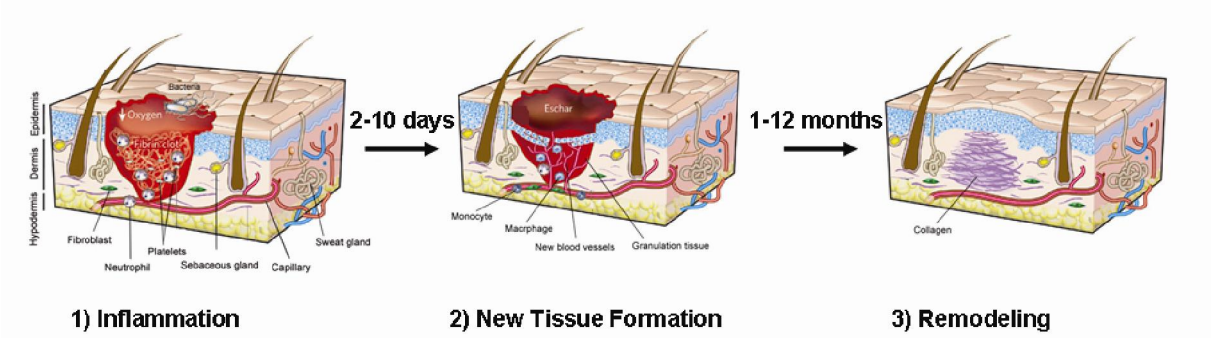

Figure 11. The three stages of skin wound healing. 1) Inflammation: a fibrin clot forms within 24-48h after the injury. Bacteria, neutrophils and platelets are abundant. 2) New tissue formation: a scab forms and epithelial cells migrate into the wound. Formation of new blood vessels occurs. 3) Remodelling: fibroblasts migrate into the wound and lay down collagen. The healed wound contracts and no normal skin appendage can be found in that area. (Adapted from Gurtner et al., 2008)

3. Notch signaling in the epidermis…

An important pathway in epidermal stem cell differentiation is the Notch signaling pathway. Expression patterns of Notch receptors and their ligands give a first insight into their role. In human epidermis, Notch1 is expressed in all epidermal layers whereas Notch2 is only seen in the basal layer. In contrast, in the murine epidermis, Notch2 is not found in the basal layer, and both Notch1 and Notch2 are expressed most strongly in the spinous layer. As for Notch ligands, they are expressed in overlapping patterns in both human and mouse epidermis (Lowell et al., 2000; Rangarajan et al., 2001).

Notch1 induces differentiation of keratinocytes by stimulating expression of early differentiation markers such as keratin1 and involucrin (Blanpain et al., 2006). Notch1 signaling directly induces expression of the cell-cycle regulator p21 (Waf/Cip1) which promotes cell cycle arrest in keratinocytes and thereby initiating terminal differentiation (Rangarajan et al., 2001). Notch1 also activates p21 indirectly, through Hes1 and the calcineurin/nuclear factors of activated T cells (NFAT) pathway. Hes1 down-regulates calcipressin, the negative regulator of the serine/threonine phosphatase calcineurin, which in turn dephosphorylates NFAT proteins (Mammucari et al., 2005).

Several other cross-talks occur between Notch and important signaling pathways, such as p63, Wnt and Shh. Notch signaling suppresses p63 expression, while sustained p63 function inhibits Notch-induced differentiation (Nguyen et al., 2006; Okuyama et al., 2007).

Wnt and Shh signaling pathways are involved in epidermal homoeostasis since Notch1 acts as a tumor suppressor notably by repressing both molecules. Notch1 deletion in murine skin activates both tumorigenic regulators resulting in basal cell carcinoma and squamous cell carcinoma (Nicolas et al., 2003). The Notch1-mediated regulation of the differentiation process in the epidermis is schematically summarized in Fig.12.

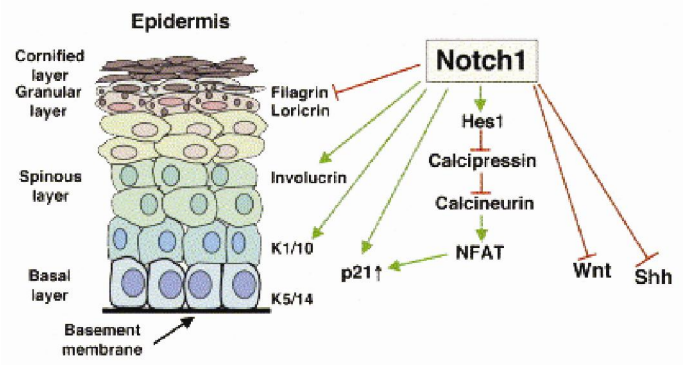

Figure 12. Notch1 signaling in the murine epidermis. Notch1-mediated differentiation of keratinocytes into the stratified layers of the epidermis involves several pathways, such as calcineurin/NFAT, Wnt and Shh. Notch1 also regulates early (K1, K10, involucrin) and late (filaggrin, loricrin) differentiation markers. (Adapted from Wilson and Radtke, 2006)

3.1 …and in the hair follicle

Thus, Notch signaling promotes epidermal differentiation in post-natal epidermis. A similar function might be assigned to Notch1 expression in the ORS of the hair follicle and the matrix cells. Its ligands Jagged1 and -2 are expressed in complementary patterns in the follicle bulb and ORS. Delta-like1 is only expressed during embryonic follicle development and is exclusive to the mesenchymal cells of the pre-papilla located beneath the follicle placode (Powell et al., 1998). An inhibitory role for Notch signaling in hair formation was described upon inactivation in mice of presenilin-1 (Psen1), a proteolytic enzyme of the γ-secretase complex. Psen1 null keratinocytes accumulate cytosolic β-catenin and have increased Lef1-mediated signaling (Xia et al., 2001). The Wnt pathway, through Lef1, was previously associated with hair differentiation.

4. Notch, skin and disease

In order to study the role of Notch in skin and the consequences of signaling deregulation, several genetic mouse models were generated. However, conventional gene targeted mice for Notch1, Notch2, RBP-Jκ, Jagged1 and Jagged2 are embryonic lethal (Hamada et al., 1999; Jiang et al., 1998; Oka et al., 1995; Swiatek et al., 1994; Xue et al., 1999). Therefore, conditional knockout strategies are necessary to study Notch signaling

during adulthood. Specific deletion in a given tissue can be achieved by the Cre/loxP technology. Firstly, the allele of interest is engineered to have two loxP sites, in the same orientation, flanking a region of the gene, exons and/or introns, which is crucial for its function. Secondly, inactivation is induced by excision of the flanked region by a Cre recombinase, which expression depends on its specific promoter.

4.1 Gene inactivation in the skin

To specifically inactivate a gene in the epidermis, K14 or K5 promoters are used to drive the Cre recombinase in basal and ORS cells. The K14Cre transgenic mice express the Cre during embryogenesis, when the K14 promoter is activated, at E12.5 (Dassule et al., 2000). To study the inactivation of a gene at later stages of development and during adulthood, an inducible Cre recombinase called Cre^{ERT} is used. The mutated ligand-binding domain of the human estrogen receptor is fused to the Cre recombinase, which allows conditional recombination dependant on the estrogen receptor antagonist 4-hydroxy-tamoxifen, and not on endogenous estradiol (Feil et al., 1996). The synthetic 4OH-tamoxifen displaces heat shock proteins by binding to the ERT, which causes translocation of the Cre into the nucleus where it exerts its recombination activity. Thus, the $K5Cre^{ERT}$ mice have an inducible expression of the Cre recombinase only upon 4OH-tamoxifen injection (Indra et al., 1999).

4.2 Mouse models of Notch inactivation in the skin

Inactivation of the Notch1 floxed allele, either embryonic (K14Cre) or induced ($K5Cre^{ERT}$), results in the excision of the leader peptide and, consequently, in Notch1 deficiency. The Notch1 conditionally deleted mice gradually lost their hair after birth and the remaining 10% were short, probably due to premature entry into catagen, and resembled no known hair type (Vauclair et al., 2005). In addition, mice with Notch1-deleted epidermis spontaneously developed basal cell carcinoma-like tumors within 9 months after inactivation. Furthermore, tumorigenicity was facilitated after chemical-induced carcinogenesis treatment (Nicolas, 2003; Nicolas et al., 2003).

Inactivation of the Notch2 floxed allele is due to a loss of reading-frame, thereby inducing expression of a truncated Notch2 protein. Notch2 conditional deletion in the epidermis did not give rise to any skin abnormality, hence the generation of Notch1Notch2 double-deficient mice. Loss of both receptors in the epidermis resulted in a severe skin

phenotype. Mice completely lost their hair, and their skin became dry, crusty and wounded (Vauclair, 2006). Double-deficient mice died rapidly after developing a myeloproliferative disorder in addition to an atopic dermatitis-like disease. Furthermore, epidermal inactivation of RBP-Jκ recapitulated the phenotype (Dumortier et al., 2010).

Inactivation of the Jagged1 floxed allele results in the excision of the two first exons encoding the leader peptide. Conditional Jagged1 deleted mice developed a similar, though more severe, phenotype than the Notch1-deficient mice. Jagged1-deficient mice completely lost their hair and developed a hyperproliferative epidermis. These mice also developed tumors, but more rapidly, within 6 months after gene inactivation (Estrach et al., 2006; Vauclair, 2006).

In addition, a double-deficient Notch1Jagged1 mouse was generated to study the cumulative effect of loss of both receptor and ligand in the epidermis. These mice completely lost their hair in several waves of growth/loss and had a thickened epidermis, similarly to both single-deficient mice. Double-deficient Notch1Jagged1 mice also developed tumors, after 6 months, which were mainly cysts derived from degenerated hair follicles (Vauclair, 2006).

Another method to study Notch signaling *in vivo* is by overexpressing Notch1 intracellular domain (NIC) in the skin. Transgenic mice with activated NIC driven by the K14 promoter developed clumped hair follicles, thus unevenly spaced, that were mainly in telogen. The data suggested that Notch activation was not sufficient to induce hair follicle growth and triggered expansion of the base of the hair follicle (Estrach et al., 2006).

4.3 Notch in human skin disorders

The mouse models described for investigating Notch signaling in the skin confirm its role as an important tumor-suppressor and its implication in skin and hair disorders. Whether Notch plays a similar role in human skin has still to be confirmed. A study investigating human diseased skin, by *in situ* hybridization of several members of the Notch family, suggested a tumor-suppressive role. Indeed, expression of Notch1-3, Jagged1 and Delta-like1 were close to non-existent in hyperproliferative keratinocytes from basal cell carcinoma, psoriasis, and during the first step of re-epithelialization in wounds. Conversely, non-lesional skin exhibited high transcription of the Notch genes in the basal cell layer (Thelu et al., 2002). Furthermore, expression of Notch receptors was observed in suprabasal layers of human unaffected skin samples whereas lesional skin from atopic-dermatitis patients showed reduced

protein expression. Notch receptor regulation was specific to the disease as two other hyperproliferative skin disorders showed strong expression of Notch receptors (Dumortier et al., 2010).

5. Rho GTPases

The retrovirus-associated DNA sequences (Ras) superfamily of GTP-hydrolyzing enzymes consists of more than 150 members and can be divided in several subfamilies. The Rho (Ras homologue) GTPase subfamily is characterized by its regulation of the actin filament system and thereby the morphogenic and migratory properties of vertebrate cells. Rho GTPases can be subdivided into 8 subfamilies, including RhoA, Rac, Cdc42 and atypical GTPases (Aspenstrom et al., 2007). The small G proteins cycle between an inactive GDP-bound and an active GTP-bound form. The latter interacts with effectors to mediate the cellular functions of the Rho GTPases.

5.1 Functions of Rho GTPases in the skin

In addition to the pathways linked to keratinocyte differentiation and/or stem cell potential described earlier, the family of small Rho GTPases was identified as a potential player (Benitah et al., 2005; Wu et al., 2006). Keratinocytes in the basal layer of the epidermis constitutively express a variety of integrin extracellular matrix (ECM) receptors, including α2β1 (collagen receptor), α3β1 and α6β4 (laminin receptors), and αvβ5 (vitronectin receptor). The β1 integrins associate with the actin cytoskeleton in focal adhesions, whereas α6β4 associates with intermediate filaments at junctions known as hemidesmosomes (Watt et al., 1993). Thus, it is not surprising that Rho GTPases are important for the dynamic cell-cell contact of epithelial cells by apical junctional complex assembly/disassembly (Fig.13) (Fukata et al., 1999; Samarin and Nusrat, 2009).

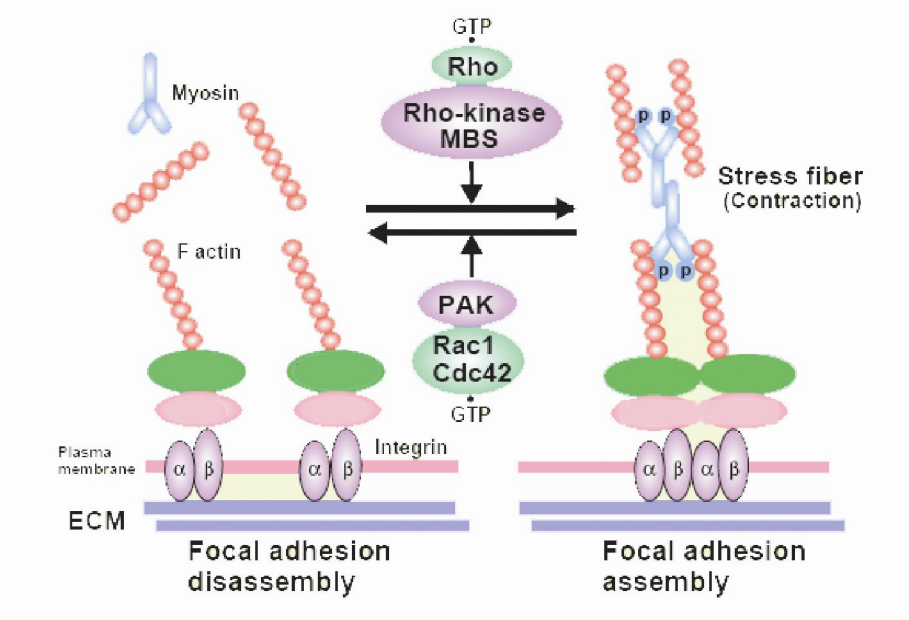

Figure 13. Rho GTPases during focal adhesion assembly/disassambly. Active Rho, i.e. the GTP-bound form, acts upon focal adhesion assembly by interacting with kinases and the myosin-binding subunit (MBS) of myosin phosphatase. The antagonistic effect of active Rac1/Cdc42 is due to the interaction with PAK effectors to disassemble the stress fibers. (Adapted from Fukata et al., 1999)

The role of Rho GTPases in the skin *in vivo* was investigated by conditional deletion of Rac1 in the epidermis. Rac1 deficiency led to epidermal stem cell depletion by disrupting adhesive interactions between stem cells and their niche (Benitah et al., 2005). Another example is Cdc42, which deletion in the skin caused epithelial progenitor cells of the hair follicle to change their fate into keratinocytes of the epidermis (Wu et al., 2006).

5.2 Rho GTPases and skin tumorigenesis

Due to their multiple roles in affecting cell morphology, Rho GTPases are potential candidates in cancer promotion (Fig.14) (Reviewed in Karlsson et al., 2009). Many Rho GTPases were deregulated in several types of human cancers. Focusing on skin disorders, RhoC was up-regulated in squamous cell carcinomas (SCC) while Rac2 was overexpressed in both non-melanoma cancers, SCC and basal cell carcinoma (BCC) (Marionnet et al., 2003).

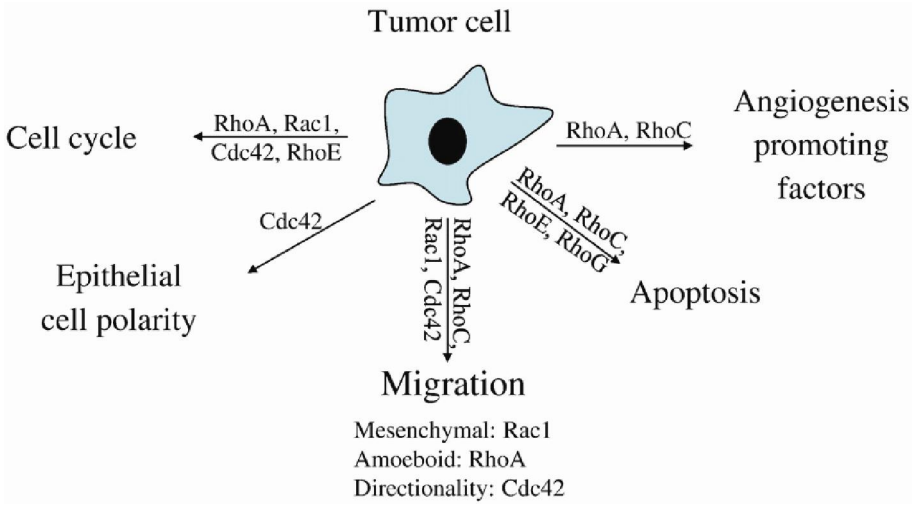

Figure 14. Potential functions of Rho GTPases during tumorigenesis. Different Rho GTPases have functions in cell cycle, epithelial cell polarity, migration, apoptosis, and angiogenesis. Any of these properties could lead to tumorigenic transformation of a cell when deregulated. (Karlsson et al., 2009)

Even though the expression of Rho GTPases was deregulated in several cancer types, transgenic animal models for the role of the small G proteins in skin tumorigenesis are scarce. Nonetheless, RhoB null mice had an increased susceptibility to skin tumor formation by induced carcinogenesis (DMBA/TPA treatment) (Liu et al., 2001). It is interesting to note that the carcinogenic chemical DMBA predominantly induces a mutation in the H-Ras gene, an early event in transformation of keratinocytes into a SCC.

5.3 Rho GTPases and Notch signaling

Investigation of the Notch-mediated tumor-suppressive mechanism in human keratinocyte cancer cell lines and SCCs revealed Notch1 to be a p53 target, and a negative regulator of Rho effectors ROCK1/2 and MRCKα kinase. The combined knockdown of these kinases counteracted the effects of Notch suppression in keratinocytes both *in vitro* and *in vivo* (Lefort et al., 2007). These results suggested an inverse relationship between Notch and Rho signaling in control of stem cell potential and tumorigenesis.

Aims

Aims

I. RhoV as a potential Notch target gene in the skin

The exact mechanism by which Notch mediates its effects in the skin, where it functions as a tumor suppressor, is currently unknown. For this purpose, potential key target genes identified by gain and loss of function assays, using murine primary keratinocytes, were validated by real-time RT-PCR. Among thirteen candidate genes, we decided to focus on RhoV, which showed robust deregulation under both conditions. Its role in differentiation of keratinocytes, during epidermal homeostasis as well as during wound healing, was investigated by the generation of skin specific transgenic mice expressing dominant active and dominant negative forms of the gene.

II. Generation of Jagged2 floxed mice

In the skin, Notch receptors interact with their ligands Jagged1 and Jagged2. The precise role of Jag2 in the epidermis can be investigated by generating floxed Jag2 mice that allow a conditional loss of function approach to determine its role in vivo. In this system, Jag2 can be deleted by crossing $Jag2^{lox/lox}$ mice with transgenic mice expressing a tissue specific Cre recombinase. This chapter describes both the generation of $Jag2^{lox/lox}$ mice and the subsequent experiments undertaken to determine the integrity of the targeted allele.

III. Generation of Notch2-mediated signaling reporter mice

Even though Notch signaling is important in the development of many organs and is linked to various diseases and cancers, there is no tool allowing *in vivo* visualization of endogenous Notch signaling in a specific tissue at any given time point. Therefore, we sought to generate a Notch2-mediated signaling reporter mouse to identify Notch2 signal-receiving cells *in vivo*. For this purpose, we generated a chimeric Notch2 fused to a transactivating domain and a secondary reporter consisting of response elements driving a red fluorescent protein. We demonstrated that both transgenes were functional *in vitro,* and thus suitable to generate transgenic mouse lines. Once generated, the mice will be crossed to obtain double transgenic animals in which cells receiving a Notch2 signal can be identified and traced *in vivo*.

I. RhoV in the skin

I. Characterization of the small Rho GTPase RhoV as a potential Notch target gene in the skin

1. Introduction

The development and the homeostasis of the skin involve a tightly-regulated coordination between epidermal cell proliferation and differentiation. Notch signaling mediates these complex processes through many downstream targets such as Hes1 and p21 (Blanpain et al., 2006; Rangarajan et al., 2001). During epidermal development Hes1 expression in suprabasal cells was shown to be directly regulated by Notch1 and loss of canonical Notch signaling, via conditional deletion of RBP-Jκ, which resulted in decreased Hes1 expression in newborn skin (Blanpain et al., 2006). Correspondingly, overexpression of Notch1 intracellular domain in transgenic NICD1 epidermis showed a dramatic increase in Hes1 throughout the epidermal layers. Loss of Hes1 by targeted deletion of its basic helix-loop-helix domain (Ishibashi et al., 1995) disrupts the spinous layers of the interfollicular epidermis, resulting in a thinner epidermis at E18.5. In addition, the proliferative potential of the basal epidermal cells is impaired in the absence of functional Hes1 (Moriyama et al., 2008).

Despite the role of Hes1 during epidermal development, conditional deletion during embryogenesis of $Hes1^{lox/lox}$, mediated by K14Cre, does not impair skin homeostasis in adult mice (Fig.1 and data not shown). Thus, in adult interfollicular epidermis, other downstream Notch target genes are involved. One mechanism by which Notch1 promotes terminal differentiation is through cell cycle withdrawal of basal keratinocytes by directly activating the expression of p21(Cdnk1a) (Nguyen et al., 2006; Rangarajan et al., 2001). The expression of cyclin-dependent kinase inhibitor $p21^{WAF1/Cip1}$ was up-regulated upon infection of keratinocytes with an adeno-virus expressing NIC. Moreover, the RBP-Jκ protein was shown to directly bind to the endogenous p21 promoter in a luciferase assay.

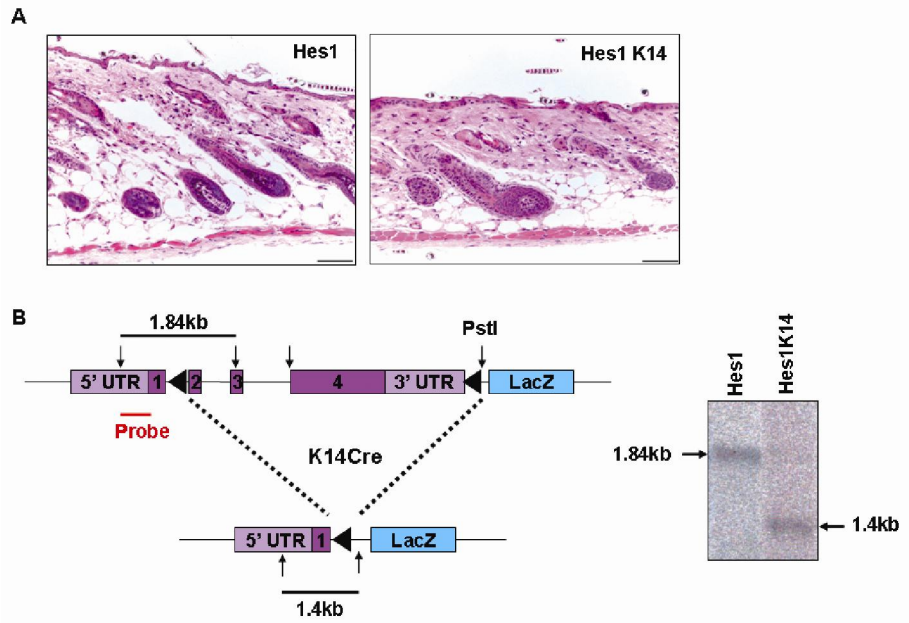

Figure 1. Conditional Hes1 deletion in the skin. (A) Skin morphology of both control (Hes1) and deleted (Hes1K14) skins show no overt phenotype by haematoxylin/eosin staining. (B) The Southern analysis of Hes1 deletion efficiency consists of a PstI digestion (arrows) of DNA from scraped epidermis and hybridization with a probe at the 5'UTR. By densitometric analysis of the phosphorimager scan we measured a deletion efficiency of 90%. Arrows show the 1.84kb wt and 1.4kb deleted bands.

In addition, Notch1 deficient epidermis showed elevated levels of free β-catenin, the effector of canonical Wnt signaling, thus suggesting a link between the Notch and Wnt signaling pathways in epidermal keratinocytes (Nicolas et al., 2003). Furthermore, the signaling-competent form of β-catenin was highly expressed in the basal cell carcinoma (BCC)-like tumors which developed in the induced deleted Notch1 mice. Notch signaling in the skin thus plays a tumor-suppressive role.

Links between Notch signaling and pathways involved in epithelial cell fate determination, cell-cycle arrest and tumorigenesis suggest many unknown target genes. In an attempt to determine these important downstream players, Affymetrix microarray analyses were performed on murine primary keratinocytes with both a gain and a loss of function assays (Vauclair, 2006). Several hundred differentially regulated genes were categorized by fold change and significance of pathways. Among thirteen candidate genes further analyzed by quantitative reverse transcription PCR (qRT-PCR), three showed robust up-regulation during forced Notch signaling, as well as down-regulation upon loss of Notch1. These three candidate genes were DEPP, Prickle2, and RhoV.

The first candidate gene to be confirmed was DEPP (decidual protein induced by progesterone), also known as fasting-induced gene (FIG) or fat-specific expressed gene (FSEG). DEPP modulates the effects of progesterone during decidualization of endometrial stromal cells, which is a crucial event for embryo implantation and placentation (Watanabe et al., 2005). Experiments done on 293 cells suggest that DEPP increases the level of phosphorylated Erk and activates the transcription factor Elk-1 (Watanabe et al., 2005). DEPP was also described as an arterial-specific gene expressed in endothelial cells of peripheral tissues, which was up-regulated in subsets of vessels in tumors and wounded skin. Nevertheless, DEPP knockout mice develop normally and show no apparent physiological defects, as well as no difference in vessel development or patterning (Shin and Anderson, 2005). The knockout mouse strain was cryopreserved and, as no skin phenotype was observed, we decided not to pursue the investigation of this gene further.

The second potential target gene robustly deregulated was Prickle2. Prickle2 was first identified *in silico* in the mouse (Katoh and Katoh, 2003). The *Drosophila* homolog Prickle plays a role in epithelial planar cell polarity (PCP). Briefly, Prickle competes with the ankyrin-repeat protein Diego for binding to the cytoplasmic protein Disheveled. Prickle thereby prevents the recruitment by Frizzled of Disheveled to the cell membrane. In the fly PCP signaling regulates the orientation of the ommatidial arrangement in the compound eye and the hair orientation in wing cells (Jenny et al., 2005). More recently, Prickle2 was shown to be highly expressed in the adult murine brain and lung. Knockdown assays by siRNA in a neuroblastoma cell line suggest a role for Prickle2 in neurite outgrowth (Okuda et al., 2007). Mouse Prickle2 cDNA consists of 8 exons for a total of 2.5kb-long coding sequence, which renders it difficult to clone. For this reason, and since the next candidate gene discussed below had a shorter cDNA sequence, we decided not to pursue investigations for Prickle2. In the meantime, a group reported cloning of the full-length murine Prickle2 cDNA together with an eGFP tag and studied the polarization of vestibular sensory epithelial cells of the inner ear. Prickle2 was localized asymmetrically at cell boundaries throughout the hair cell differentiation and polarization of the inner ear from mouse embryos (Deans et al., 2007).

The third candidate gene which showed robust deregulation under Notch gain and loss of function conditions was RhoV. This small Rho GTPase belongs to the Wrch (Wnt-regulated Cdc42 homolog) branch of the mammalian Rho GTPase family and is also known as Wrch2 or Chp. The murine RhoV gene is located on chromosome 2 and consists of 3 exons

for a 712bp-long coding sequence. It possesses additional sequences at both termini which distinguishes it from the classical Rho GTPase members (Cdc42, RhoA, and Rac1).The latter contain a carboxy-terminal CAAX (C, cysteine; A, aliphatic acid; X, terminal amino acid) motif that signals post-translational modifications crucial for their association to plasma and other cellular membranes, and, consequently, for their biological function. Although RhoV shares sequence and functional similarities with Cdc42, they diverge significantly in their mode of membrane association due to the lack of the CAAX-motif in RhoV (Chenette et al., 2005; Chenette et al., 2006). Its localization to membranes depends on the palmitoylation of its carboxy terminus *in vitro*, which is distinct from the prenylation critical for the association of the other Rho GTPases (Chenette et al., 2005; Shutes et al., 2006).

There are 23 mammalian genes encoding Rho GTPases which function as molecular switches for a multitude of tasks, including cytoskeleton remodeling and modulation of gene expression (Reviewed in Jaffe and Hall, 2005). As regulatory GTPases they cycle between an inactive GDP-bound state and an active GTP-bound state. Once activated the Rho GTPases control remodeling of the cytoskeleton, by formation and organization of actin filaments and microtubules, and, consequently, contribute to cell morphogenesis and migration. They also regulate gene expression through many signaling pathways as well as cell cycle progression. Since RhoV is potentially downstream of Notch1 and can induce a variety of cellular alterations important in the differentiation process of epithelial cells, we decided to characterize the role of RhoV in the skin. Thus, the potential role of RhoV in differentiation of keratinocytes and its relation with Notch1 was investigated by *in situ* hybridization, *in vitro* luciferase assays and by generation of skin specific transgenic mice expressing dominant active and dominant negative forms of the gene.

2. Results

2.1 Gain and loss of function assays

Three different conditions for gain and loss of function of Notch signaling were set up. Firstly, primary keratinocytes carrying floxed Notch1 alleles were cultured for 24 hours. These cells were then infected with adeno-viruses to efficiently deliver a specific gene into the primary keratinocytes, which will thus be highly expressed. In the first instance, Notch signaling was up-regulated by infection with an adeno-NIC-GFP. In the second instance, the loss of function assay, we used an adeno-Cre-GFP to induce Notch1 deletion of the floxed keratinocytes. In both cases adeno-GFP was used as infection control. RNA was isolated 12h after adeno-NIC infection, the time at which the Notch signaling activity was most potent, or 24h post adeno-Cre infection when complete Notch1 deletion was achieved. Quantitative analysis of potential Notch1 direct target genes was performed by TaqMan® real-time PCR (Fig.2).

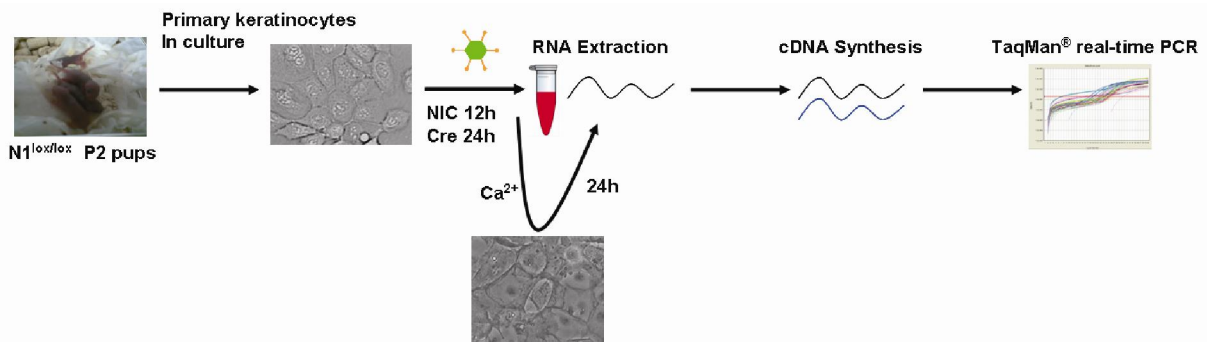

Figure 2. Experimental procedure for gain and loss of function conditions on murine primary keratinocytes involved 4 steps. First, Notch1$^{lox/lox}$ 2-day old pups were sacrificed and their skin isolated. Primary keratinocytes from the epidermis were then taken into culture. Adeno-viruses, either adeno-NIC or adeno-Cre, or control adeno-GFP, were added to the culture media and RNA was isolated after 12h and 24h, respectively. Total RNA was used as template for cDNA synthesis and subsequent TaqMan® real-time PCR analysis. A third condition consisted in the addition of Ca^{2+} to the medium to induce differentiation of the primary keratinocytes after adeno-Cre infection. Total RNA was isolated 24h later.

It is important to note that keratinocyte differentiation is dependent on a calcium gradient *in vivo* as well as *in vitro*. Epidermal calcium gradient can be mimicked in culture by increasing the concentration of calcium ions in the medium, which causes the cells to differentiate (Yuspa et al., 1989). Therefore, a third condition was tested by adding calcium to the medium of adeno-Cre infected cells to induce differentiation in absence of Notch1.

Three candidate genes, namely DEPP, Prickle2 and RhoV, were confirmed to be up-regulated during NIC signaling and decreased upon loss of Notch1 in primary keratinocytes in three independent experiments (Fig.3A and B). In addition, the RNA expression of all three candidate genes showed a slight increase during calcium-induced differentiation and a strong decrease when this differentiation process was induced after Notch1 deletion (Fig.3C and D). These observations strongly suggest a role for DEPP, Prickle2 and RhoV as downstream targets of Notch signaling in murine keratinocytes.

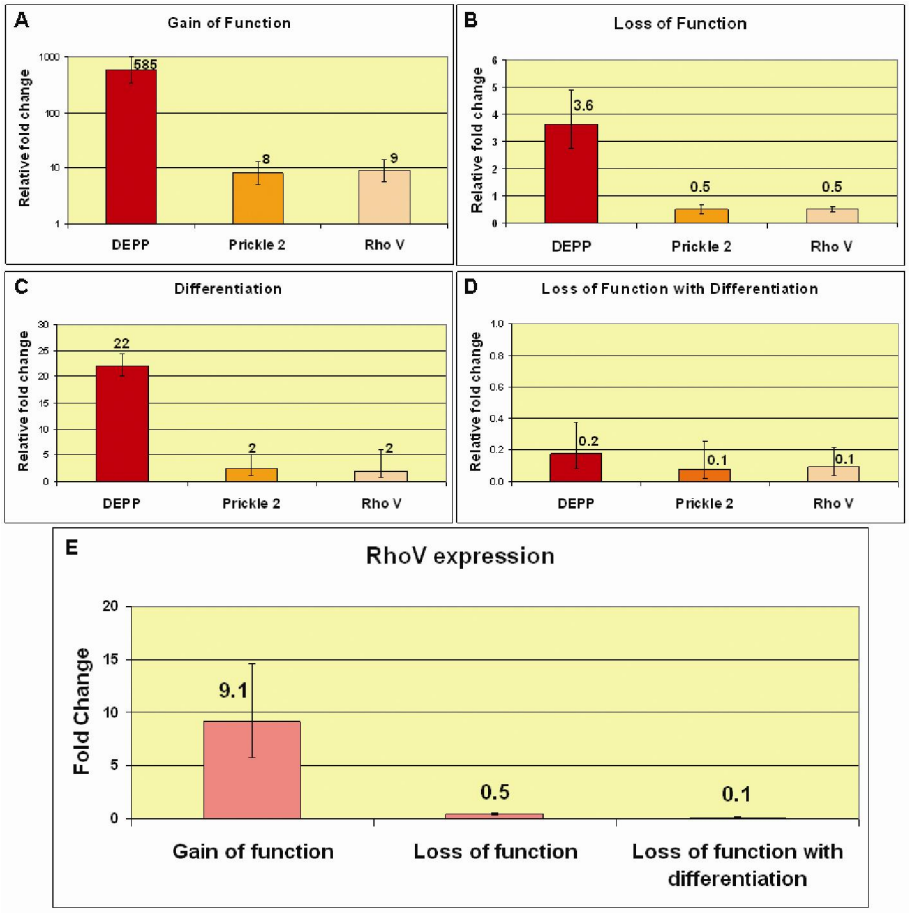

Figure 3. TaqMan® real-time analysis of the three potential candidate genes DEPP, Prickle2 and RhoV. Fold change in RNA expression upon gain of function (A), loss of function (B), differentiation (C) and differentiation after loss of function (D) represents strong up- and down-regulation depending on the condition applied. (E) RhoV RNA expression graph summarizes the differential regulation of the potential candidate gene upon all three main conditions. All bar graphs are representative of three independent experiments. Relative fold change was normalized to GAPDH expression.

We first decided to focus on DEPP and RhoV for cloning as they have short coding sequences, 618bp and 712bp, respectively. Their cDNAs were amplified from murine NIC-overexpressing keratinocytes and were subsequently cloned into the pBluescriptSK$^+$ backbone

via NotI/HindIII. The sequences were controlled by sequencing with the T7 primer, which is localized upstream of the ligated cDNA.

DEPP primer set: 5'ATCT**GCGGCCGC**CAGCACATCGTCCTGACTGTCC 3'

5'ATC**AAGCTT**CTAGGAATTGCCCAGTCCCTGC 3'

NotI **HindIII** **DEPP cDNA**

RhoV primer set: 5' AACT**GCGGCCGC**GAACCTGCTTCCCCGAGTGCC 3'

5' CAT**AAGCTT**CCCTGCCAGTACCCGATGTCTC 3'

NotI **HindIII** **RhoV cDNA**

Due to the wide array of potential functions of RhoV in keratinocyte differentiation, the small GTPase was chosen for further analysis and characterization in the skin.

2.2 RhoV as a potential direct Notch target gene

In silico analysis of the promoter region of RhoV revealed three putative RBP-Jκ transcription binding sites as well as two such sequences in its second intron (Fig.4A). Both regions were cloned into a luciferase reporter plasmid: one including the three putative binding sites upstream of the transcription start site (RhoVprom) and the other reporter containing the two sites found within intron 2 (RhoVint2). The relative luciferase units were recorded in transfection assays using Hela cells. These cells were also transfected with different amounts of a NIC-expressing plasmid. Notch signal induction efficiency was tested in parallel with a 12RBP-luciferase reporter which was strongly activated by NIC expression (data not shown). Upon NIC transfection with each RhoV reporter plasmid a slight activation of both luciferase reporters was observed, with a higher increase when using the RhoVprom (Fig.4B). Although the increase of the latter was quite low, representing less than a 2-fold change, it was nonetheless observed in three independent experiments.

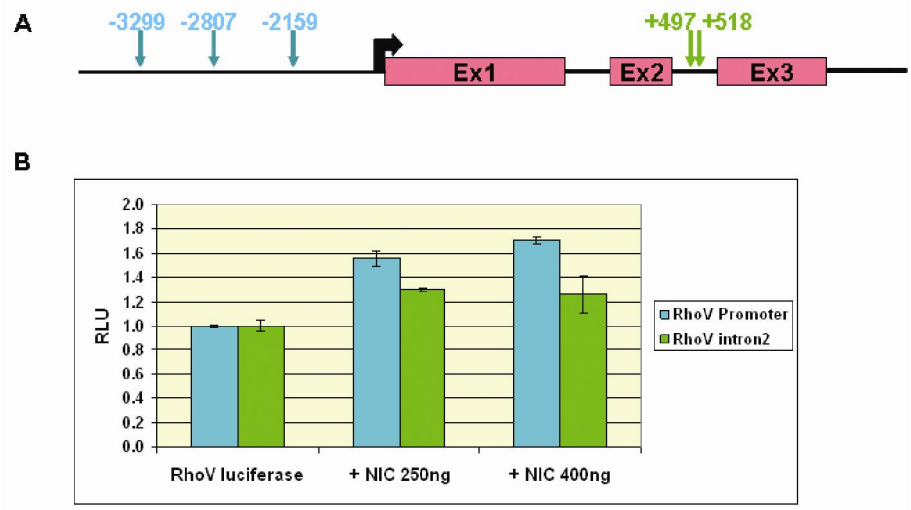

Figure 4. Luciferase assay on putative RhoV RBP-Jκ binding sites. (A) Three consensus RBP-Jκ binding sequences (blue arrows) are represented upstream of the RhoV transcription start site (black arrow). Their exact locations are indicated (blue numbers). Two putative sites are also situated within the 2nd intron (green arrows and numbers). Pink boxes: exons. (B) The bar graph represents the luciferase assay in transfected Hela cells of putative RBP-Jκ binding sites of RhoV cloned upstream of a luciferase reporter gene. When two increasing amounts of a NIC-expressing plasmid (250ng and 400ng) were co-transfected, a slight increase in luciferase expression was induced. RLU: relative luciferase units normalized to renilla luciferase.

In order to study the role of RhoV *in vivo*, we first investigated RhoV expression in wild-type (wt) epidermis. We could discriminate between genomic DNA and mRNA by using PCR primers flanking introns 1 and 2 of RhoV. The PCR amplification identified an 836bp band from genomic DNA and a 468bp product from cDNA. The difference in product sizes allowed discrimination of any contaminating genomic DNA.

RhoV RT primer set: 5'CAGCCTCATCGTCAGCTACA 3'

5' CCGAGTCGAACACCTCCTT 3'

The RT-PCR results on a sample from scraped wt epidermis indicated that transcription of RhoV does occur in wt skin (Fig.5A). In addition, to get a view of the localization of mRNA within the epidermis, we performed an *in situ* hybridization (ISH) on P1 and adult skin sections. Hybridization of the antisense probe, specific to RhoV mRNA, revealed expression in the lower layers of the epidermis as well as in the bottom region of the cortex of hair follicles (Fig.5B).

Moreover, we hypothesized that if RhoV is a downstream target of Notch signaling, the ISH signal should be stronger in mice over-expressing NIC in the epidermis and, conversely, lower in skin from mice with loss of Notch signaling. For this purpose, we used either the RosaNIC transgenic mouse line or the Notch1$^{lox/lox}$ homozygous mice. The RosaNIC allele consists of a Neo/Stop cassette, flanked by loxP sites, upstream of the intracellular domain of Notch1 and targeted to the Rosa26 locus. Cre-mediated deletion of the Stop sequence removes the transcription blockade resulting in tissue-specific NIC expression (Murtaugh et al., 2003). In order to over-express NIC in the skin, RosaNIC mice were crossed with K14Cre mice, which express the Cre recombinase in the basal layer of the epidermis. ISH on skin from NIC K14Cre P1 mice showed an increase in signal compared to the NIC control (Fig.5C). The signal in the control is barely detectable because the amount of antisense probe was decreased from 100ng to 50ng to lower the background in the NIC K14Cre sample. As for down-regulating the Notch pathway, K14Cre mice were also crossed with Notch1$^{lox/lox}$ homozygous mice. However, ISH results on Notch1-deleted skin sections were inconclusive (data not shown).

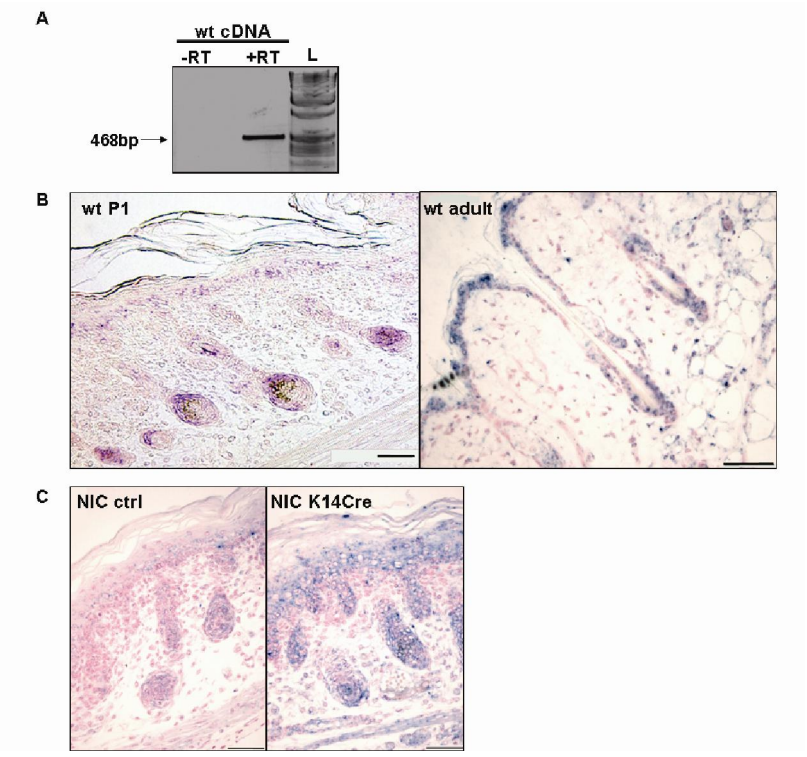

Figure 5. RhoV transcriptional expression in the skin. (A) RhoV cDNA is amplified in wt scraped epidermis when reverse transcriptase is added to the reaction (+RT vs –RT). L: 1kb DNA ladder. (B) ISH for RhoV mRNA on P1 and adult wt skin sections. (C) RhoV ISH signal increases in NIC K14Cre P1 skin. Bar: 50μm.

Taken together, the RT-PCR and ISH data demonstrate expression of RhoV, at the transcriptional level, in wild-type murine skin.

2.3 Generation of RhoV transgenic mouse lines

In the last section we have shown the expression of RhoV in the skin, although *in vitro* data did not confirm the small GTPase to be a direct downstream target gene of Notch signaling. We thus decided to investigate its function *in vivo* by generating skin-specific gain- and loss-of-function mutant mice. For this purpose two different constructs were used: a dominant active and a dominant negative form of RhoV. The constitutively active RhoV (RhoVAc) is characterized by a valine substitution at glycine 40 (G40V) which blocks GTP hydrolysis by GTPase-activating proteins (GAP) (Aronheim et al., 1998). The dominant negative version (RhoVDn) has its serine at position 45 substituted by asparagine (S45N). This mutation locks the Rho GTPase in a GDP-bound inactive form which stays bound to guanine nucleotide exchange factors (GEF) (Aronheim et al., 1998). As a result the GEF are no longer available to interact with endogenous RhoV, which are then forced to stay inactive as well (Fig.6). Both constructs were shown to be functional by RhoV-induced ubiquitin-mediated degradation of one of the Rho GTPase's direct effectors p21-activated kinase 1 (Pak1) (Weisz Hubsman et al., 2007).

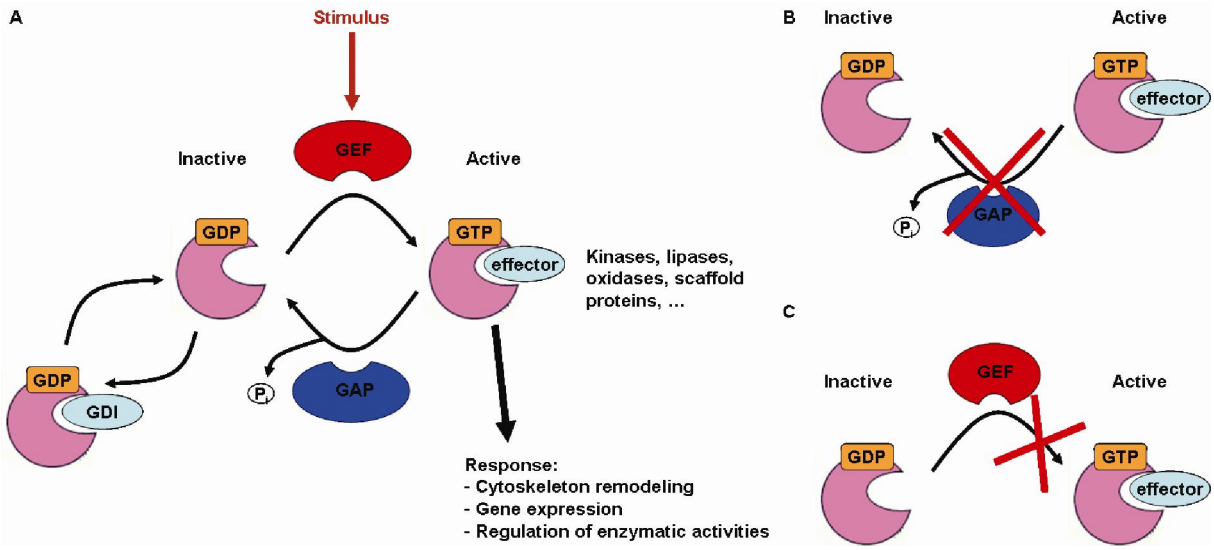

Figure 6. Schematic representation of a Rho GTPase's activity cycle. (A) Rho GTPases (pink) are found in an inactive GDP-bound form, as they bind to guanine nucleotide dissociation inhibitors (GDI), and in an active GTP-bound state. Guanine nucleotide exchange factors (GEF), upon external stimuli (red arrow), activate the Rho GTPases by exchanging the GDP for a GTP. Once in an active state the Rho GTPase can interact with effectors, thereby inducing the cell to respond, depending on the type of stimulus and the GTPase involved. GTPase-activating proteins (GAP) then catalyze the hydrolysis of the GTP, which inactivates the Rho GTPase. (B) Constitutive active form of RhoV stays bound to its GTP which can no longer by hydrolyzed by the GAP. (C) Dominant negative form of RhoV binds to the GEF permanently, thereby titrating out the GEF and blocking other RhoV molecules in a GDP-bound inactive state.

Dr. Aronheim kindly provided us with the pCEFL-Chp plasmids which consist of a myc-tagged RhoV (Chp) cDNA cloned from rat. The rat RhoV cDNA sequence shares 96% homology with murine RhoV. In order to track cells expressing the transgene, the wt as well as both mutated forms, RhoVAc and RhoVDn, were first subcloned into pcDNA3.1^{+} and subsequently coupled to an internal ribosome entry site (IRES) upstream of a GFP reporter cloned from the retroviral vector MigR1. The green fluorescence was tested by transfection of each plasmid into 293T cells and, indeed, expression of the GFP was observed using fluorescence microscopy 24h later (Fig.7). Specific mutations for the active and negative forms of RhoV, i.e. G40V and S45N respectively, were confirmed by sequencing reactions of the plasmids using the T7 primer located upstream of the transgene.

.

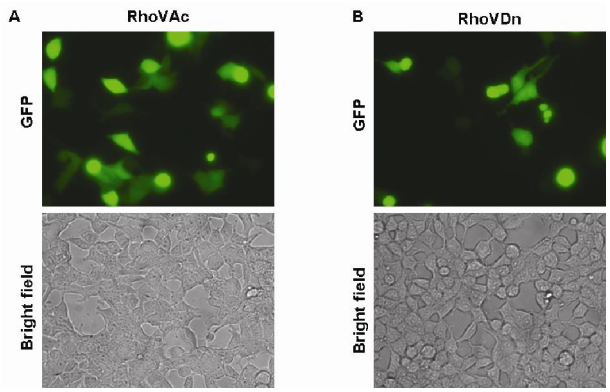

Figure 7. Expression of mutated forms of RhoV. (A and B) Cultured 293T cells were transfected with either RhoVAc (A) or RhoVDn (B) plasmids which express GFP after an internal ribosome entry site sequence.

Thereafter, according to the mRNA pattern of RhoV obtained by ISH, and knowing that Notch1 is mainly expressed in the suprabasal layers of the epidermis, we designed three different strategies to counteract Notch signaling during skin development and keratinocyte differentiation. Since our data suggest an induction of RhoV through Notch signaling, we cloned the RhoVDn transgene downstream of the involucrin promoter. This promoter will drive expression of the RhoV dominant negative form in the suprabasal layers (Fig.8A), where the Notch receptors are normally expressed, and in the inner root sheath of the hair follicle (Uyttendaele et al., 2004). Conversely, the RhoVAc transgene is expressed under the control of the human keratin14 promoter (Fig.8A), which is induced in the basal layers of the epidermis (Vassar et al., 1989).

Additionally, ISH results strongly suggest RhoV expression in the matrix region of the hair follicle. Moreover, Notch1 expression has been shown in matrix cells and precursor cells of the cortex and inner root sheath (Lin et al., 2000). Therefore, the third transgenic mouse generated comprises of the RhoVDn transgene driven by the mouse hair keratin A1 (MHKA1) promoter (Fig.8C). MHKA1 and Notch1 RNA expressions overlap (Lin et al., 2000) allowing investigation of the role of RhoV in hair development and homeostasis and its potential link to Notch signaling.

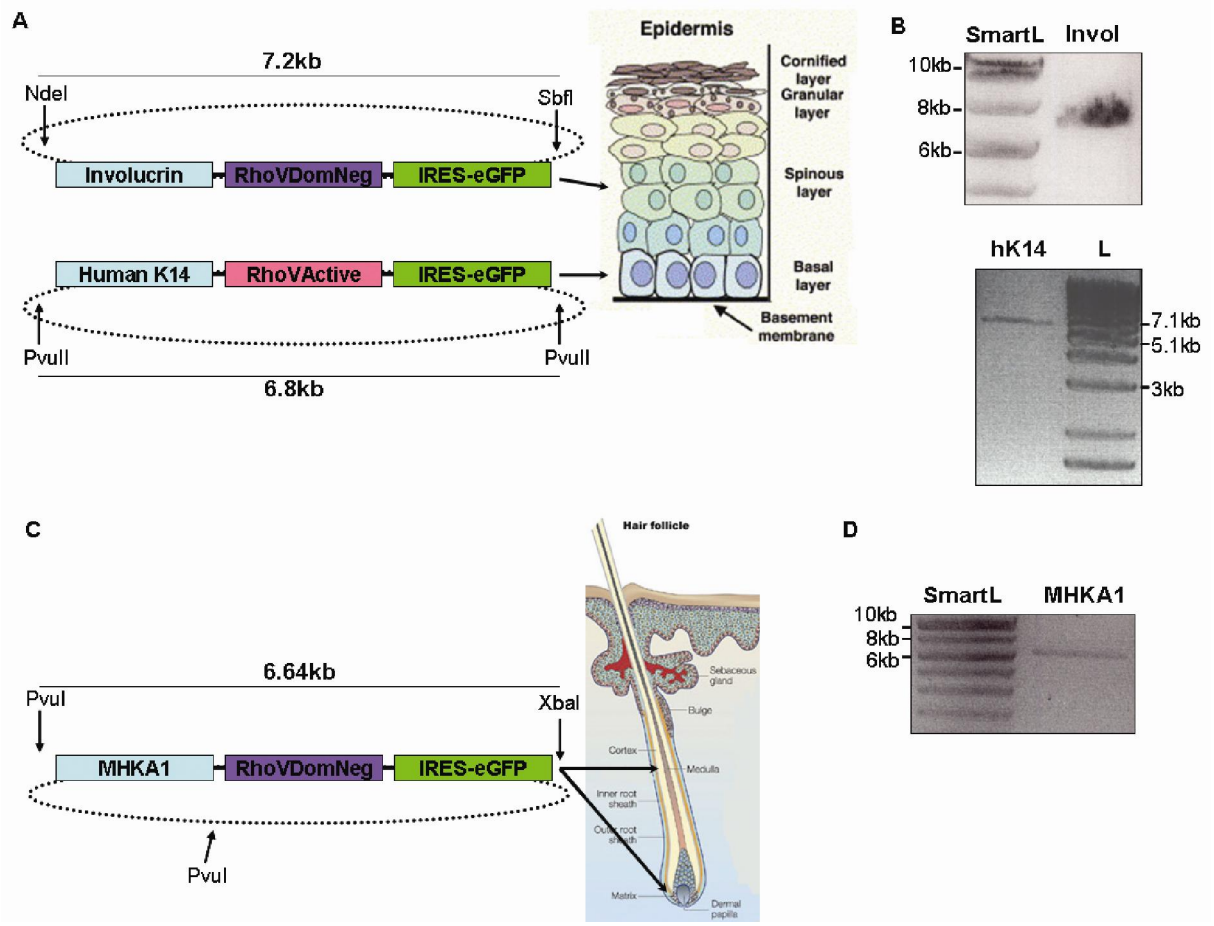

Figure 8. Schematic expression of the three different transgenes and their linearization. (A) RhoVDn driven by the involucrin promoter is expressed in the spinous layer of the epidermis and the RhoVAc driven by the human K14 promoter is expressed in basal cells. Restriction enzymes used for linearization are given by arrows and the subsequent fragment size is noted. Epidermis taken from review (Wilson and Radtke, 2006). (B) Agarose gel picture of linearized plasmids for corresponding digested transgenes. (C) RhoVDn driven by MHKA1 promoter shows expression in cortex and matrix cells of the hair follicle. Hair follicle adapted from (Fuchs and Raghavan, 2002). (D) Agarose gel picture of linearized PvuI/XbaI transgene. SmartL: DNA Smart ladder: L: 1kb DNA ladder.

After several cloning steps to generate the corresponding transgenes, each one was cut out of the backbone (Fig.8B and D) and given to the transgenic animal facility for pronuclear injections. All mice generated were screened by PCR for presence of the transgene. A total of 141 potential transgenic mice were screened as follows: 60 RhoVAc (hereafter HKRAB), 28 RhoVDn with the involucrin promoter (hereafter IRNB) and 83 for the RhoVDn driven by MHKA1 (hereafter HairKRNB).

Genotyping primer set: 5'CGCCTGGAGAAGAAACTGAA 3'

5'ACACCGGCCTTATTCCAAG 3'

Potential positive transgenic mice were confirmed by Southern blot analysis. Genomic DNA was digested with NcoI restriction enzyme and the RhoV cDNA was used as a probe to hybridize to the 3.8kb wt band and to the transgenic 1.8kb fragment. There were 5 HKRAB, 5 IRNB and 7 HairKRNB transgenic (Tg) mice confirmed by Southern blot hybridization (Fig.9). The Tg mice were then bred with C57Bl/6 mice to assess germline transmission.

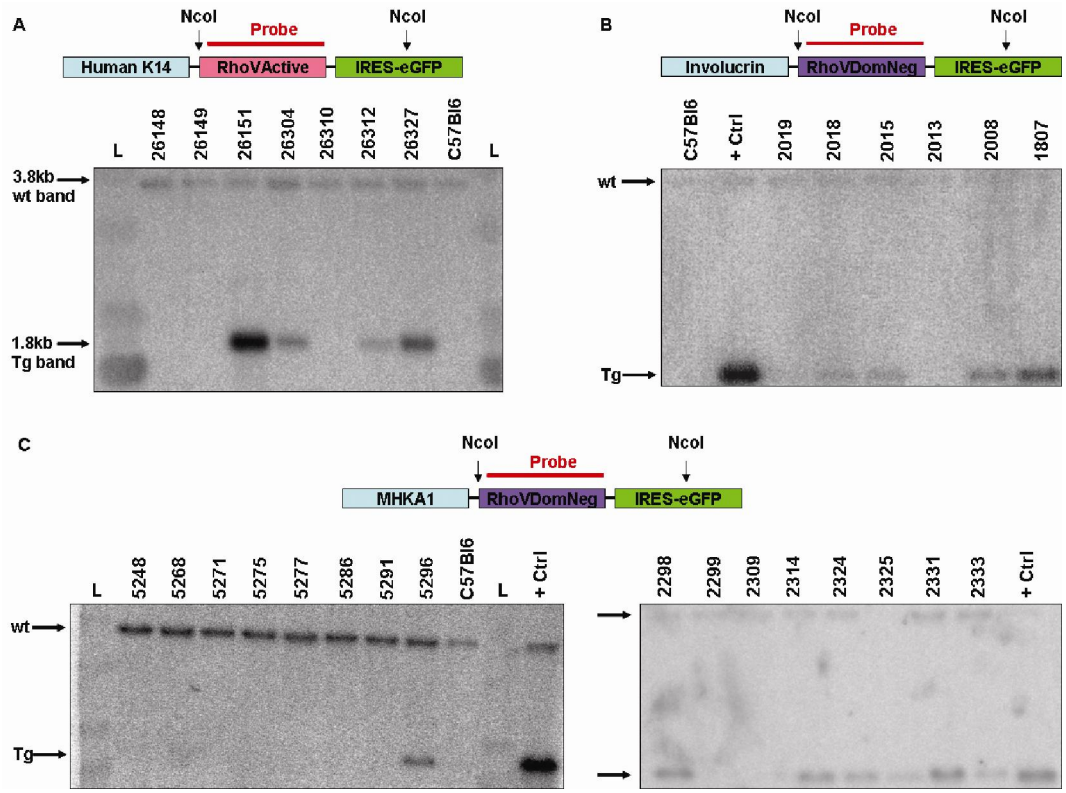

Figure 9. Screening of RhoVAc and RhoVDn transgenic founder lines by Southern blot analysis. RhoVAc transgene is driven by the human keratin14 promoter (A) while the RhoVDn is driven either by the involucrin promoter (B) or the MHKA1 promoter (C). After NcoI digestion of genomic DNA from the various potential transgenic mice, hybridization with RhoV cDNA as a probe (red bar) identified five (one not shown), five and seven founders bearing the 1.8kb transgene, respectively. The 3.8kb wt band was present in all mice.

Each founder line was then analyzed by RT-PCR for expression of the transgene in the epidermis. Western blot analysis was also performed to investigate protein expression. Finally, transgenic mice were sacrificed at several time points and their skin analyzed by immunohistochemistry for various proliferation and differentiation markers

2.4 Analysis of the active RhoV-expressing transgenic mouse line

After pronuclear injection of the RhoVAc transgene controlled by the human keratin14 promoter, 60 mice were first screened by PCR. Potential positive mice were then confirmed by Southern blot hybridization for presence of the transgene (Fig.9A). Five transgenic HKRAB founders (F0) were backcrossed into C57Bl/6 to generate offspring for each line. Four of these F0 breeders conferred germline transmission. To verify the expression of the constitutive active RhoV, several mice from each F0 line were sacrificed and their skin isolated. The epidermis was then scraped for subsequent RNA extraction. RT-PCR for RhoVAc and for GFP on samples from transgenic and littermate control mice revealed transcription of the transgene in one single founder line F0 26151 (Fig.10). The F0 26151 line also had the highest copy number of the transgene, 208 copies, as measured by densitometry of the phosphorimager scan of the Southern blot (Fig.9A).

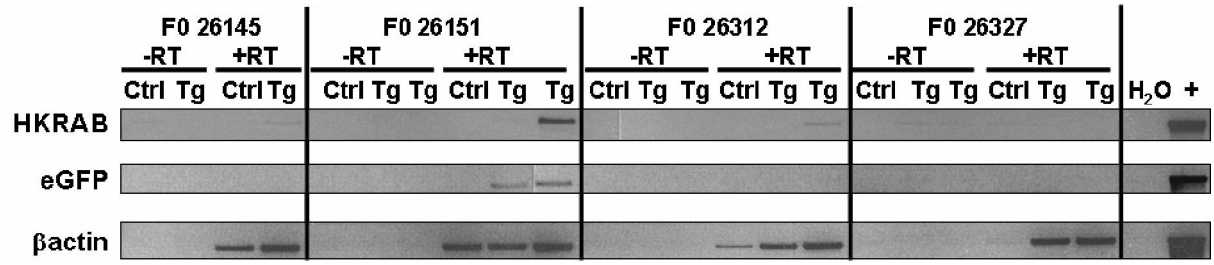

Figure 10. Expression of the RhoVAc transgene in 4 founder lines. The first panel represents the transgene-specific PCR (HKRAB), while the second panel is the GFP reporter PCR (eGFP). F0 line number 26151 expresses both transgenes, compared to the three other F0 lines (26145, 26312 and 26327). The bottom panel is the β-actin control PCR. One control and one or two transgenic mice are shown for each F0 line. Genomic DNA was used as positive control for each PCR reaction (last lane).

Since the RT-PCR for RhoVAc and eGFP both confirmed expression of the transgene in one founder line, we sought to analyze the phenotype of F0 26151 offspring. Skin was isolated from 2-day old (P2) and 18-day old (P18) HKRAB transgenic mice and their littermate controls. After 4% PFA fixation, skin sections were immunostained for several proliferation and differentiation markers. No overt skin morphology abnormality was observed by haematoxylin/eosin (H&E) staining. Proliferation was not impaired as detected by staining for the proliferation marker Ki67 on P2 sections. Immunostainings for basal cell specific K14 and spinous layer marker K1 were similar (Fig.11).

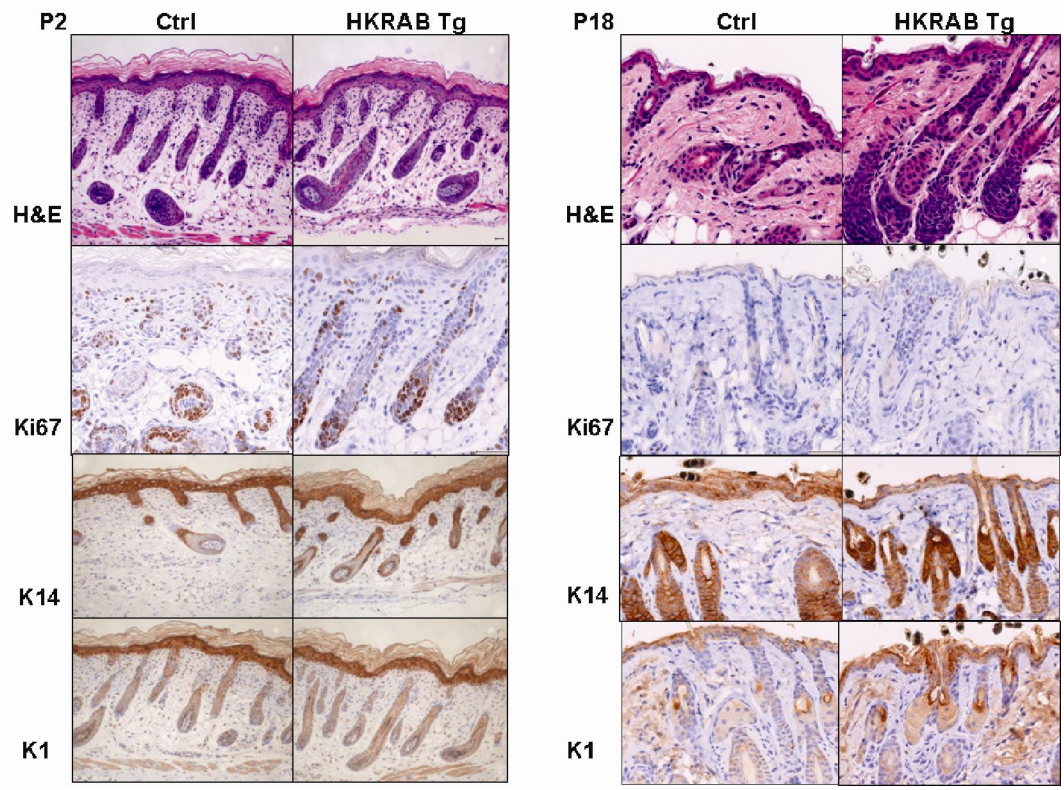

Figure 11. Histological analysis of HKRAB transgenic mice. H&E, Ki67, K14 and K1 stainings were performed on skin sections from a control (Ctrl) and a HKRAB transgenic (Tg) mouse isolated 2 days (P2) and 18 days (P18) after birth. Bar 100µm.

The immunological stainings suggest that overexpression of the RhoVAc in the basal layer of the epidermis does not effect skin homeostasis. Nonetheless, Rho GTPases are involved in cytoskeleton remodeling and regulation of cell migration. Moreover, RhoV was shown to induce lamellipodia in porcine endothelial cells (Aronheim et al., 1998). Thus, we hypothesized that RhoV might play a role during re-epithelialization processes such as during wound repair. The healing process can be divided into three stages. The first reaction is inflammation when a fibrin clot forms with neutrophils and platelets to protect from incoming bacteria. Secondly, from 2 to 10 days after injury, a scab has formed at the surface and new tissue forms with new blood vessels and inward migration of epithelial cells. The final stage can last from several months to a year when the tissue is remodeled by disorganized collagen from fibroblasts and extracellular matrix proteins. A typical feature of healed skin is the absence of normal appendages such as hair follicles and sweat glands (Gurtner et al., 2008).

The role of RhoV during tissue repair was investigated by wounding control and Tg adult mice by means of 5mm biopsy punches on their formerly-shaved back skin. Wounds

were monitored and isolated 4 days and 12 days post-wounding. Stainings for morphology and proliferation were conducted on sections from the 4% PFA-fixed wounds. Both control and Tg mice showed similar healing efficiency by 4 days with strong cell proliferation at the edges of the wound (Fig.12A). After 12 days the wounds of both HKRAB Tg and control were closed and barely visible by eye (Fig12B).

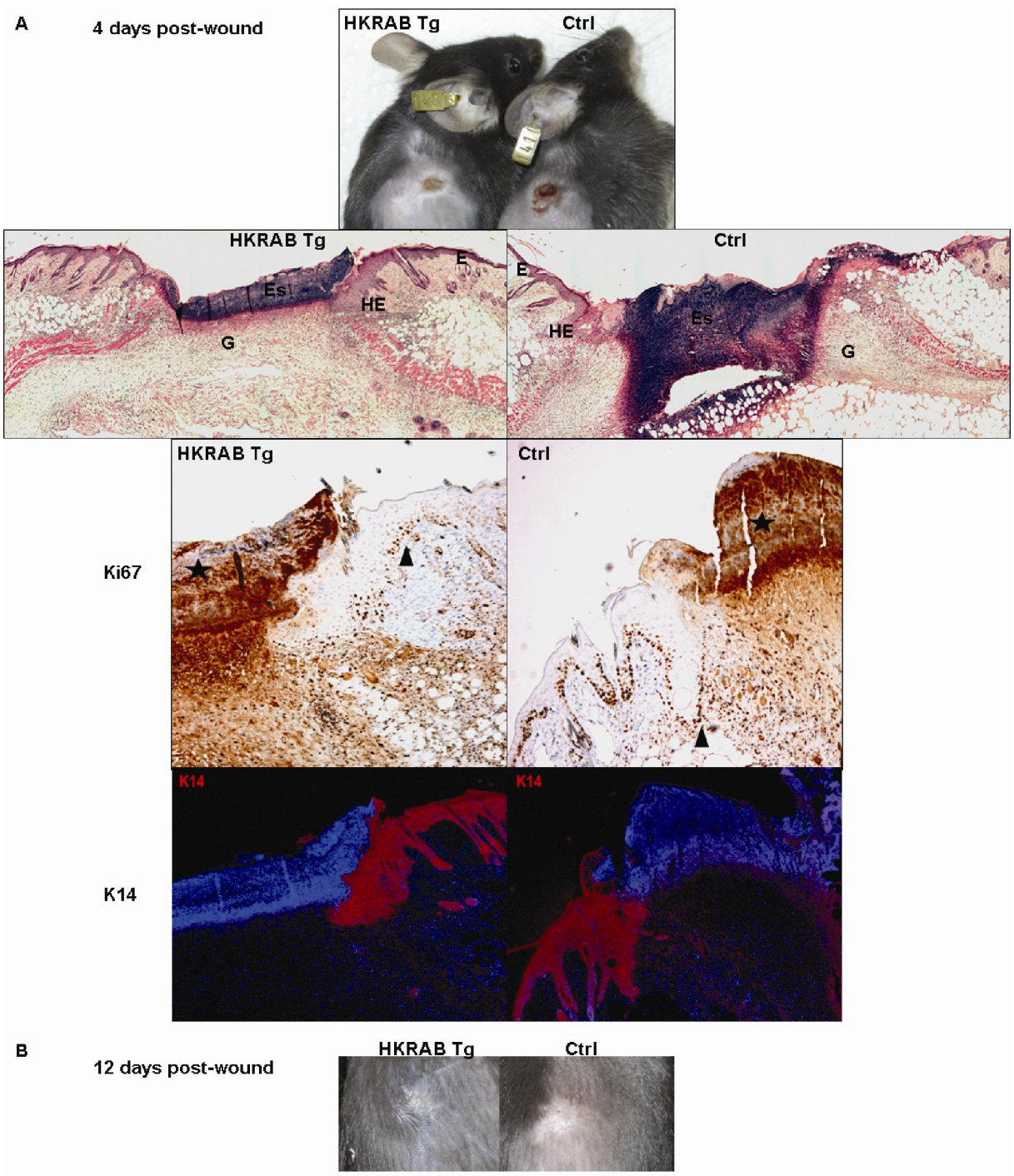

Figure 12. Wound healing in HKRAB transgenic mice. (A) Picture of an HKRAB Tg next to a littermate control represents the back wounds 4 days after injury. Similar healing processes are observed by morphology (H&E) and proliferation (Ki67 staining) where the proliferative edge of the wound is shown by an arrowhead. Immunofluorescence staining for basal layer marker K14 is marked in red. E: epidermis; Es: eschar; G: granulation tissue; HE: hyperproliferative epithelium; Star: unspecific staining of the scab. (B) Pictures from back wounds after 12 days show complete closure.

Taken together these results suggest that constitutive activation of RhoV in K14-expressing cells of the skin does not impair homeostasis or tissue re-epithelialization such as the wound healing process. However, we can not exclude that the transgene was not expressed at the protein level since Western blot analysis on scraped Tg epidermis, with an antibody against GFP, did not detect any reporter expression. We also cultured primary keratinocytes from HKRAB Tg newborns, hypothesizing that this would enrich for GFP expressing cells driven by the K14 promoter. Yet again, no green fluorescence was detected under the microscope after 24 and 48h in culture. Therefore, we conclude that the constitutively active RhoV protein is either not expressed in the Tg mice or that it is expressed at undetectable levels, which might not suffice to impede on skin homeostasis.

2.5 Analysis of the involucrin-driven dominant negative RhoV-expressing transgenic mouse line

Similarly to the generation of HKRAB Tg mice, the linearized involucrin-driven RhoVDn was injected into pronuclei by the transgenic animal facility. Thereby 28 mice were generated and 5 showed integration of the transgene (Fig.9B). Backcrossing into C57Bl/6 identified four founder lines as germline transmitters. In order to detect expression of the transgene skin was isolated from their offspring and the epidermis was scraped. The RNA was extracted and cDNA was synthesized as template for RT-PCR for the RhoVDn. One founder line F0 1807 expressed RhoVDn and the GFP reporter at the RNA level (Fig.13).

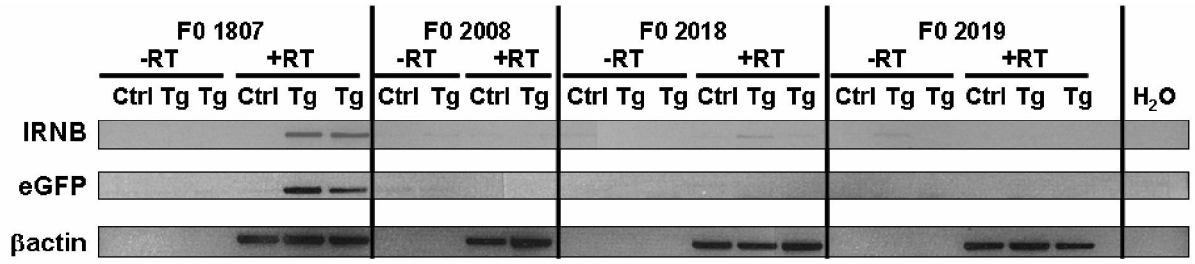

Figure 13. Expression of the RhoVDn transgene driven by involucrin in 4 founder lines. The first panel represents the transgene-specific PCR (IRNB), while the second panel is the GFP reporter PCR (eGFP). F0 line number 1807 expresses both transgenes, compared to the three other F0 lines (2008, 2018 and 2019). The bottom panel is the β-actin control PCR. One control and one or two transgenic mice are shown for each F0 line without (-RT) and with (+RT) addition of reverse transcriptase during cDNA synthesis.

As for the HKRAB Tg mouse line, the expressing F0 IRNB transgenic mouse showed the highest transgene copy number in its genome. 165 copies were measured by densitometry of the phosphorimager scan of the Southern blot (Fig.9B). Expression of the protein was investigated by Western blot analysis using an anti-GFP antibody which recognizes the 27kDa monomeric protein. Scraped epidermis from 13 and 15 days old IRNB Tg and littermate control mice were used as lysates. The RhoVDn-ires-GFP, previously cloned in the expression vector pcDNA3.1^{+}, was transfected into 293T cells and used as positive control for GFP expression. The GFP protein was detected in both Tg samples as opposed to the wt controls, thereby confirming the expression of the transgene in the IRNB Tg mice (Fig.14). Green fluorescence was confirmed in IRNB Tg primary keratinocytes taken into culture, though at a low level (data not shown).

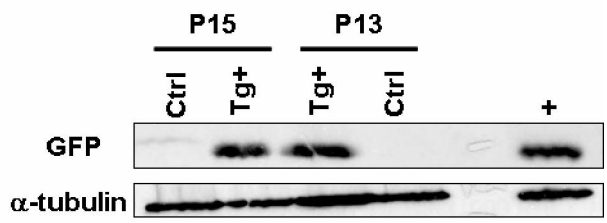

Figure 14. GFP protein expression. Top panel: Western blot using an anti-GFP antibody on scraped epidermis from P15 and P13 mice detects the protein in transgenics (Tg+). The last lane (+) is on cell lysate from 293T cells transfected with the RhoVDn-ires-GFP plasmid. Bottom panel: anti-α–tubulin Western blot for loading control.

Since IRNB Tg mice did express GFP at the protein level, we further analyzed the mice for skin morphology and proliferation status of their keratinocytes. Control and IRNB Tg mice were sacrificed at two time points, P5 and P15, and their skin was fixed in 4% PFA prior to paraffin embedding. Skin sections were then stained for H&E, Ki67 and BrdU. The latter was injected into the mice intraperitoneally two hours prior to sacrifice. Skin morphology and proliferation status of Tg mice showed no difference compared to littermate controls (Fig.15).

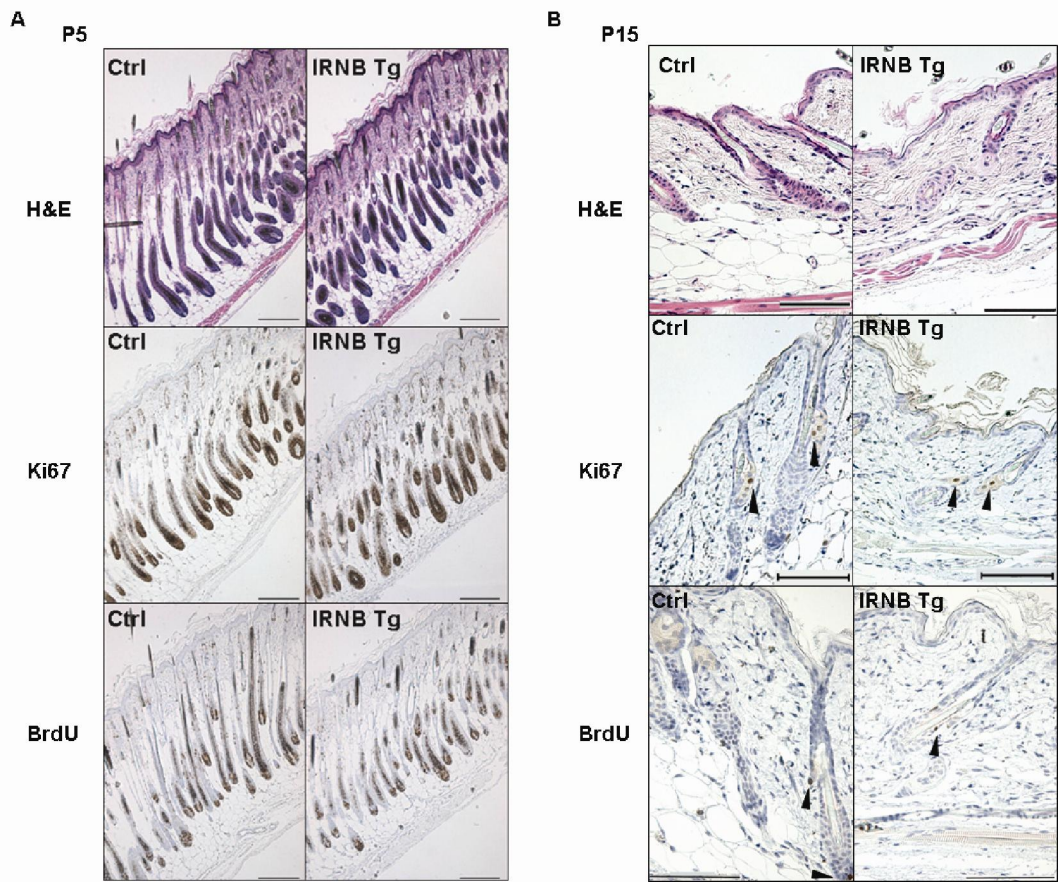

Figure 15. Morphology and proliferation state of IRNB Tg mice. (A and B) Skin sections of IRNB Tg 5 day old (P5; A) and 15 day old (P15; B) mice are undistinguishable from controls (Ctrl) by H&E, Ki67 and BrdU stainings. Arrowheads show BrdU positive cells at P15. Bar: 100μm.

Morphology and proliferation of keratinocytes were indistinguishable between IRNB Tg and control mice. Since Notch signaling is crucial during the differentiation process of the basal cells into the upper more differentiated cells of the epidermis, we performed immunostainings on the skin sections for K14, expressed in the basal layer, and K1, expressed in the spinous layer. At both time points P5 and P15, the Tg mice and their littermate controls showed similar expression patterns of both differentiation markers (Fig16).

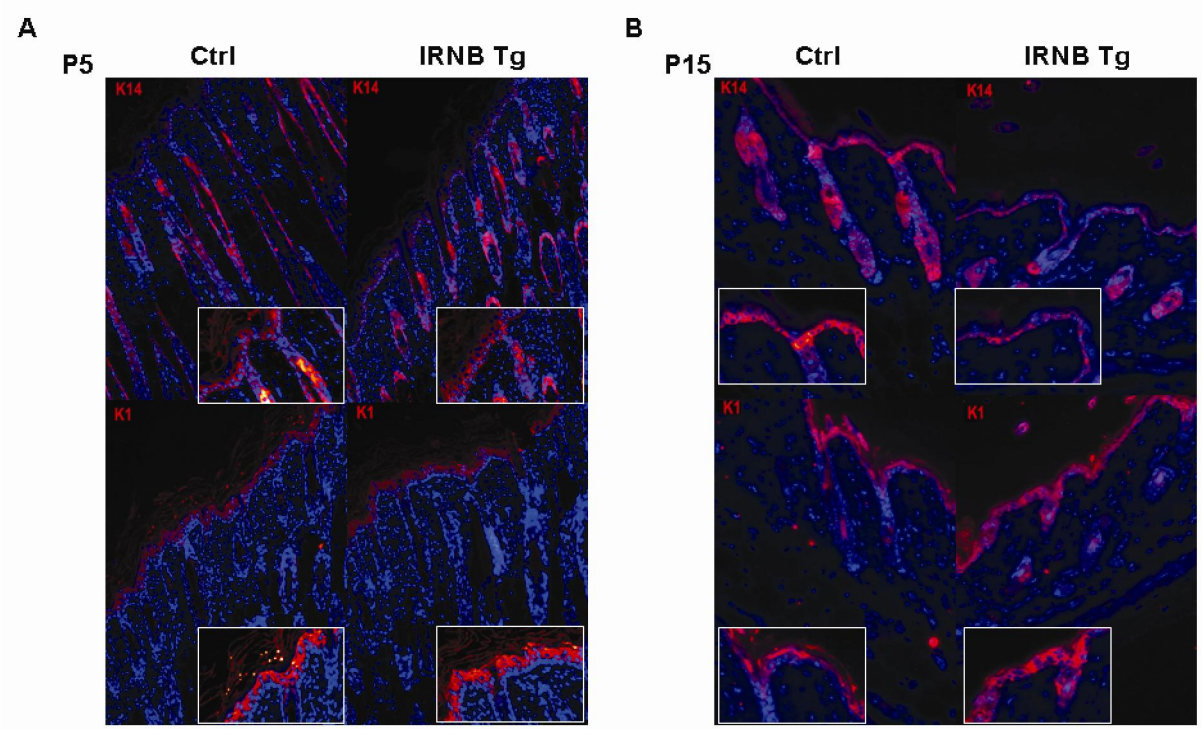

Figure 16. Immunofluorescence of the differentiation markers K14 and K1. (A and B) Skin sections of IRNB Tg 5 day old (P5; A) and 15 day old (P15; B) mice are undistinguishable from controls (Ctrl). Top panels: K14 (in red); Bottom panels: K1 (in red).

These results imply that RhoV, through its dominant negative form, does not affect skin morphology, proliferation and differentiation during homeostasis. If RhoV plays a role during skin remodeling, the dominant negative form RhoVDn would impair the healing process after injury. This hypothesis was investigated by performing 5mm biopsy punches on the formerly-shaved back skin of IRNB Tg mice. The wounds were isolated 4 days post-injury and sections were stained for morphology, proliferation by Ki67 and for the basal cell marker K14. Morphology and proliferation at the margins of the IRNB Tg wound are similar to control. Even though K14 staining was detected under the scab in the control mouse, this was not observed in other wt mice, suggesting that the wound of this particular mouse was not as deep (Fig17A). Wounds were also isolated 12 days post-wounding and were completely closed in both mice (Fig.17B). Thus, the healing process occurred equally well in both the IRNB Tg and littermate control mice.

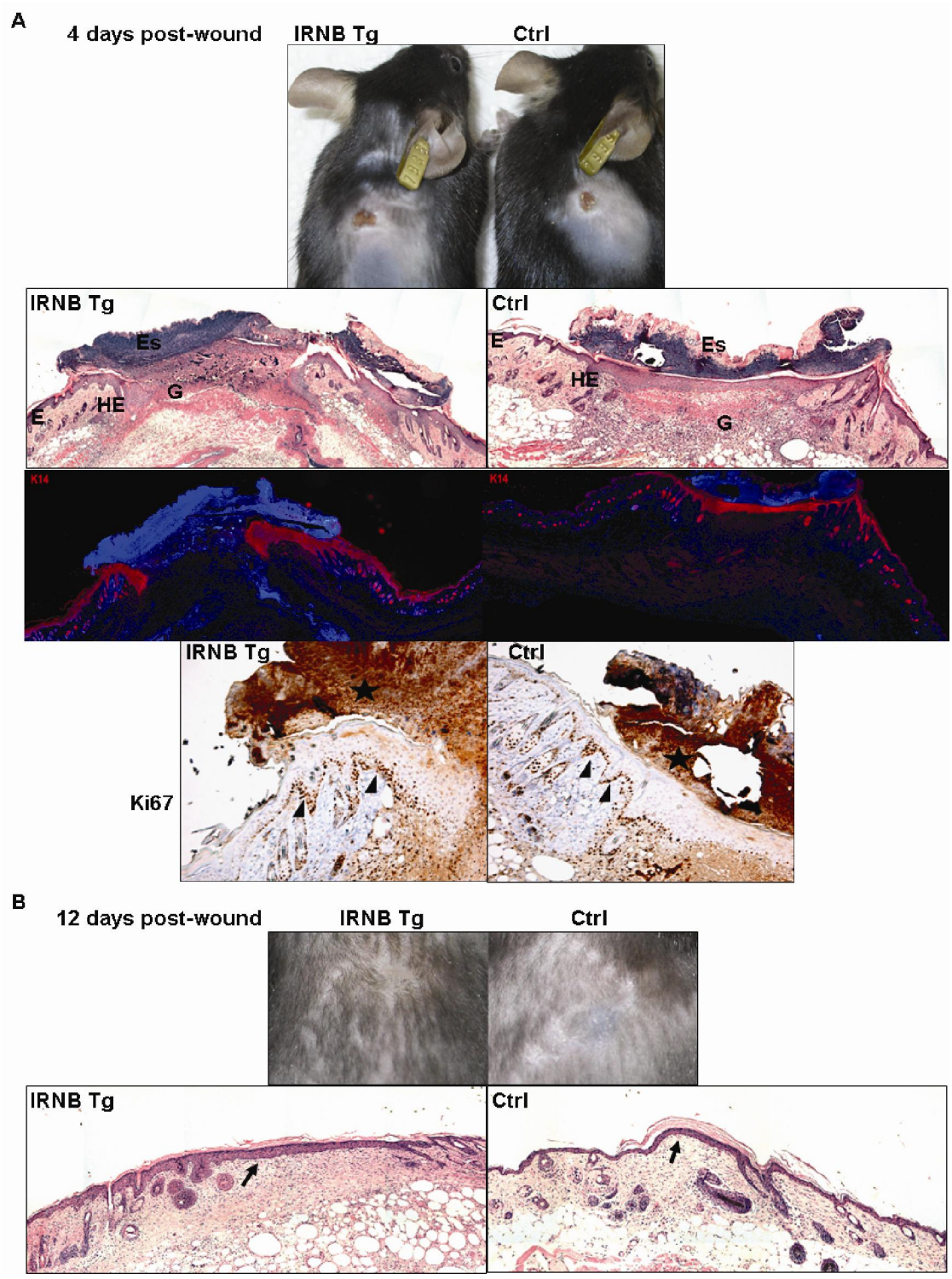

Figure 17. Wound healing in IRNB transgenic mice. (A) Picture of an IRNB Tg next to a littermate control represents the back wounds 4 days after injury. Similar healing processes are observed by morphology (H&E), K14 immunofluorescence (red) and proliferation (Ki67 staining) where the proliferative edge of the wound is shown by an arrowhead. Immunofluorescence staining for basal layer marker K14 is marked in red. E: epidermis; Es: eschar; G: granulation tissue; HE: hyperproliferative epithelium; Star: unspecific staining of the scab. (B) Picture of closed wounds 12 days after injury and H&E staining show complete healing in both IRNB Tg and control mice. Arrows point to the healed region.

Taken together, the data imply that the RhoV dominant negative form does not impair homeostasis and does not delay the re-epithelialization of the skin. In conclusion, the active and negative forms of RhoV do not impede the differentiation process of keratinocytes in the murine epidermis.

2.6 Analysis of the MHKA1-driven dominant negative RhoV-expressing transgenic mouse line

The role of RhoV in the hair follicle was studied by generating transgenic mice in two rounds. The first pronuclear injection of the MHKA1-driven RhoVDn generated 53 mice from which only 1 showed transgene integration. The transgenic animal facility thus injected a second round of pronuclei and generated 30 mice from which 6 had integrated the transgene (Fig.9C). By backcrossing into C57Bl/6 mice all HairKRNB founder lines displayed germline transmission. Transgene expression was assessed by RT-PCR on scraped skin of their offspring. The RNA was extracted and cDNA was synthesized as template for RT-PCR for the RhoVDn. Two founder lines, F0 2298 and 2331, had amplified the RhoVDn band confirming the expression of the transgene (Fig18.).

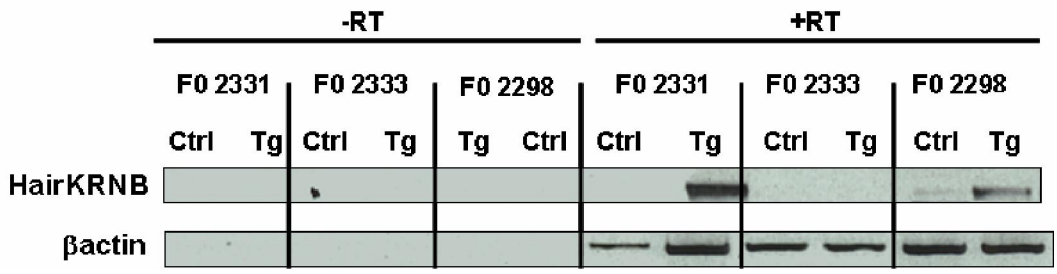

Figure 18. Expression of the RhoVDn transgene driven by MHKA1 in 6 founder lines. The first panel represents the transgene-specific PCR (HairKRNB). F0 lines 2331 and 2298 both express the transgene, compared to the non-expressing F0 2333. The bottom panel is the β-actin control PCR. One control and one transgenic mice are shown for each F0 line without (-RT) and with (+RT) addition of reverse transcriptase during cDNA synthesis.

The two expressing founder lines, 2298 and 2331, were then analyzed for skin morphology of their offspring. Hair follicles follow a life cycle of three phases: anagen, catagen and telogen. HairKRNB Tg mice were thus sacrificed at different ages corresponding to the various phases. Anagen starts during embryonic life and continues to P17 after birth. Skin was isolated from transgenic and littermate control mice for each founder at P9 or P12.

Skin sections were stained for H&E, for proliferation marker Ki67 as well as for basal cell marker K14 and no significant difference was observed in either transgenic line (Fig.19).

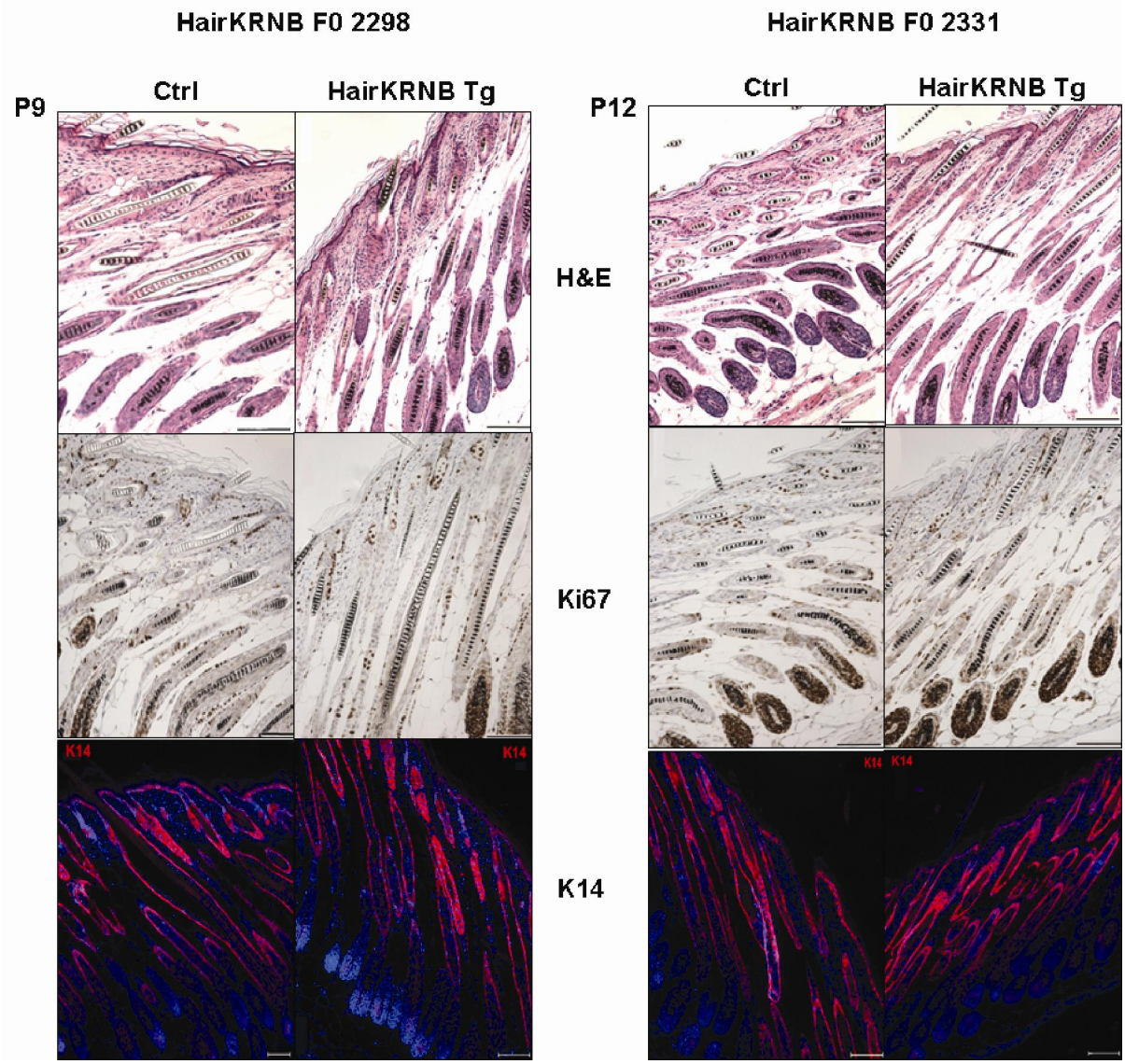

Figure 19. Morphology and proliferation state of HairKRNB Tg mice during anagen. Skin sections of HairKRNB Tg mice at P9 for founder 2298 and at P12 for F0 2331 are undistinguishable from controls (Ctrl) by H&E, Ki67 and basal cell marker K14 (red). Bar: 100μm.

The first catagen starts at P18 and the subsequent telogen lasts up to P26. Transgenic and littermate control mice were injected with BrdU two hours prior to sacrifice and their skin was isolated. Morphology, proliferation and K14 immunostainings were undistinguishable between the mice for both founder lines (Fig.20).

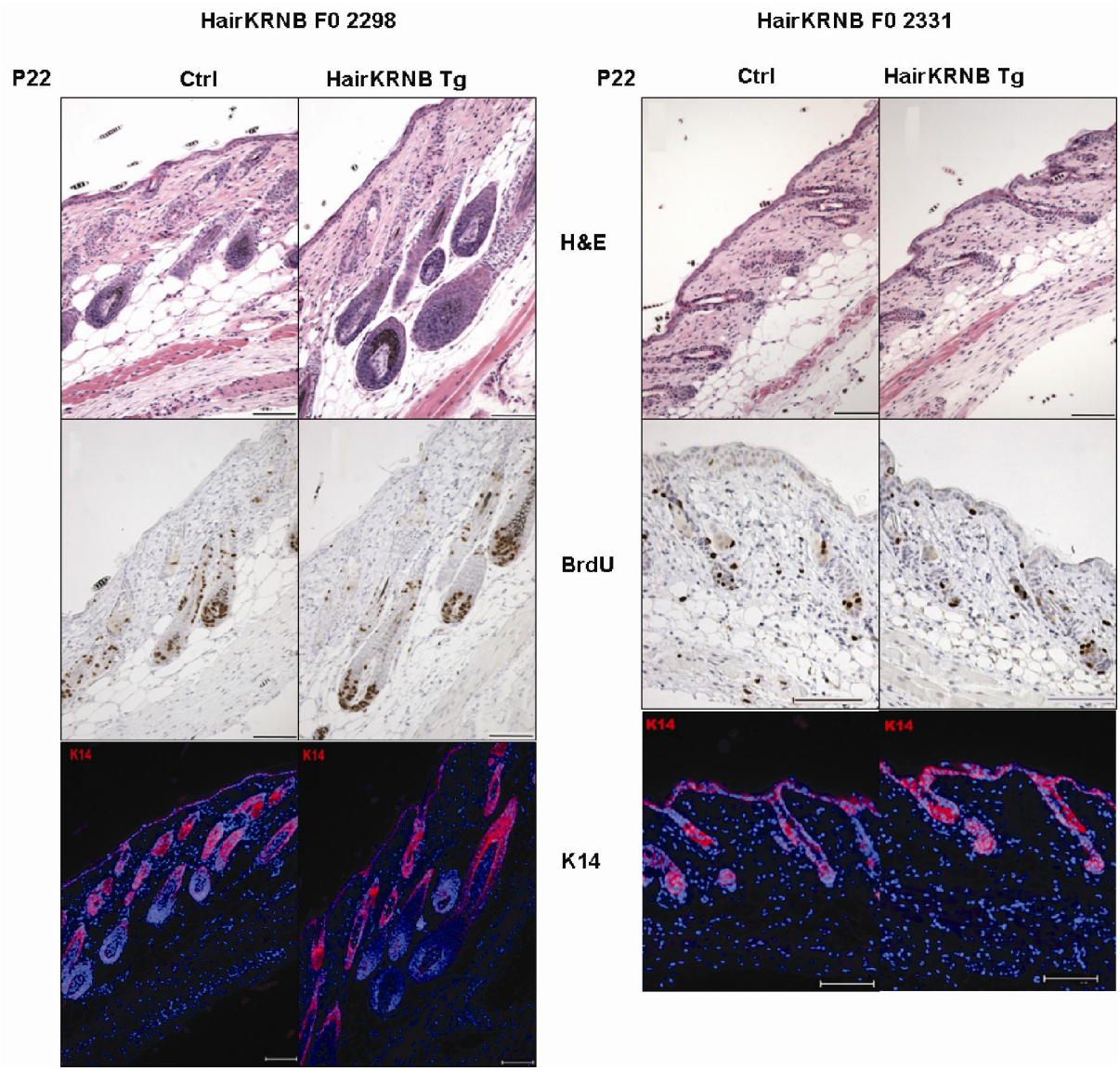

Figure 20. Morphology and proliferation state of HairKRNB Tg mice at P22. Skin sections of HairKRNB Tg mice for both founders 2298 and 2331 are undistinguishable from controls (Ctrl) by H&E, BrdU and basal cell marker K14 (red). Bar: 100μm.

Adult mice at around P35 have hair follicles which are between the second anagen and the second telogen phase. Adult P35 or P37 transgenic and littermate control mice were injected with BrdU. Two hours later their back skin was isolated and fixed in 4% PFA before paraffin embedding. Morphology, BrdU and K14 immunostainings were performed on the sections and were undistinguishable between the control and Tg mice for both founder lines (Fig.21).

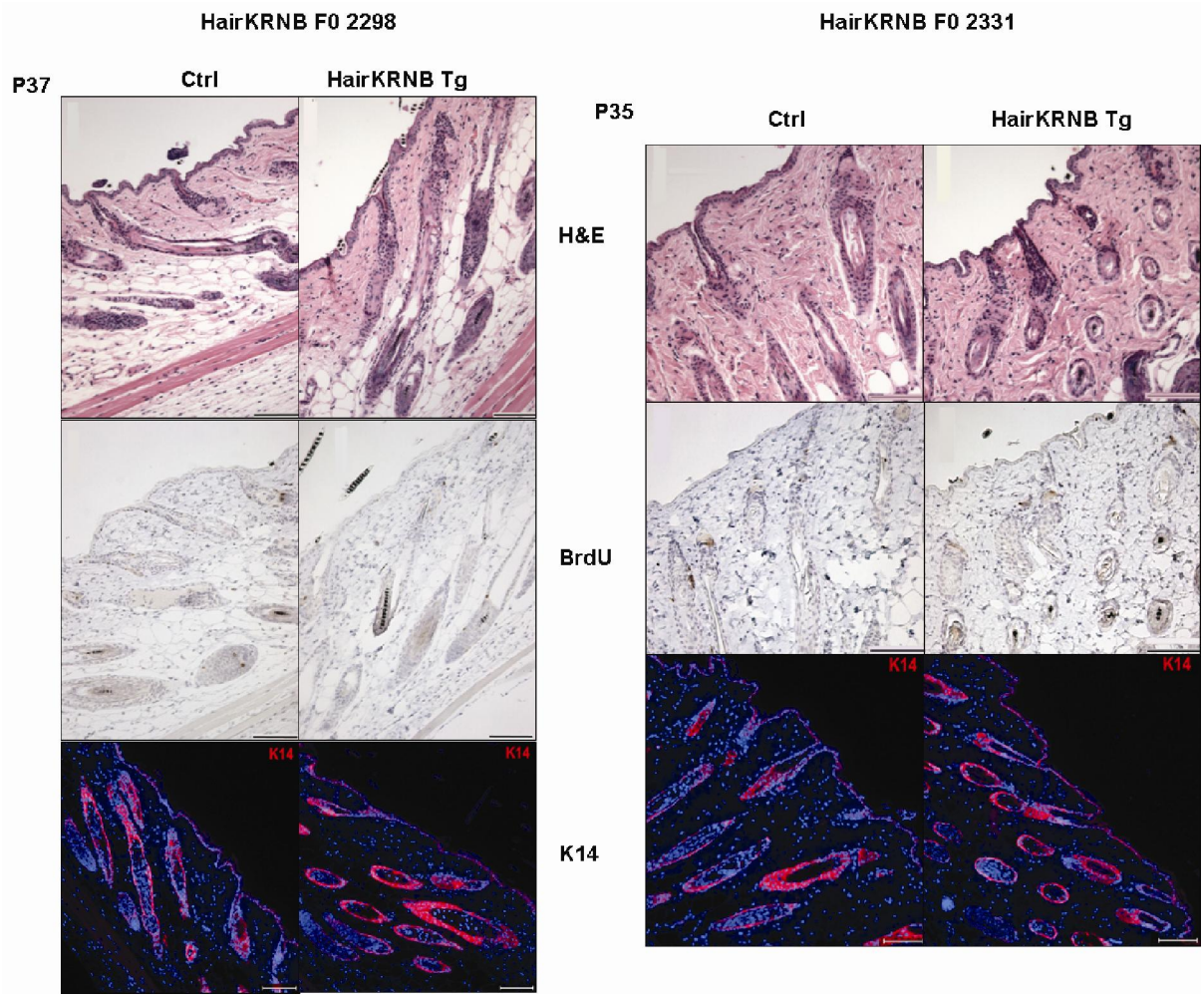

Figure 21. Morphology and proliferation state of adult HairKRNB Tg mice. Skin sections of HairKRNB Tg mice for both founders 2298 and 2331 are undistinguishable from controls (Ctrl) by H&E, BrdU and basal cell marker K14 (red). Bar: 100µm.

The data of the various hair cycle phases suggest no phenotypic difference in hair follicle growth when the dominant negative form RhoVDn was expressed by the MHKA1 promoter. Moreover, no overt phenotype was observed in either one of the generated founder lines. However, RhoV might be involved in the generation of one or more of the four murine hair types (auchene, zigzag, awl, guard). To address this question we plucked approximately 100 hairs from the back pelage of two Tg mice for each founder line. Phenotypically the hairs were similar to hairs from littermate controls (Fig.22A and B). We then counted the different hair types using a stereo microscope. The three main hair types were identified in both Tg and control mice (Fig22C). Preliminary results suggest no hair abnormality and a distribution of hair types comparable to wt (data not shown).

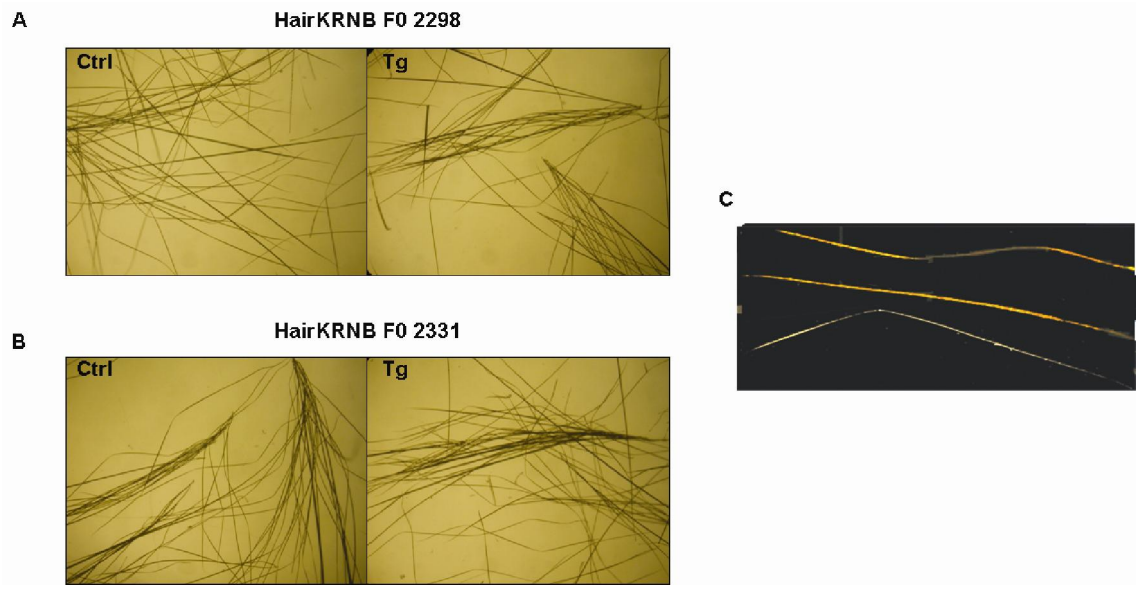

Figure 22. Different hair types of HairKRNB Tg mice. (A and B) Pictures of hairs visualized under the stereo microscope for founder 2298 (A) and founder 2331 (B) are undistinguishable from control (Ctrl). (C) Picture of three hair types found in all mice, Tg and ctrl: zigzag, awl and auchene.

In conclusion, all hair types were generated and no gross hair growth abnormality was observed by immunohistochemical analyses of HairKRNB Tg mice. Therefore, if protein expression of the dominant negative RhoV is confirmed, its expression in the cortex of the hair follicle does not hamper normal development of any hair type.

3. Discussion and perspectives

In an attempt to decipher the mechanisms of Notch signaling in the skin, we have identified and confirmed by quantitative RT-PCR three potential downstream Notch1 target genes. DEPP, Prickle2 and RhoV were up-regulated upon NIC-overexpression and down-regulated after Notch1 deletion in cultured murine primary keratinocytes.

As briefly mentioned in the introduction, the DEPP knockout mice were generated by targeting an eGFP-Cre fusion gene into the DEPP locus, thereby replacing the entire predicted coding sequence of the gene. This strategy allowed visualization of DEPP expression in subsets of endothelial cells and in settings of adult neo-vascularization, such as during tumorigenesis and skin wound healing. Even though DEPP was expressed in several organs, e.g. kidney, lung and liver, homozygous mutant mice develop normally and do not exhibit any physiological defect (Shin and Anderson, 2005). Since the DEPP knockout mice were cryopreserved and that no skin phenotype was observed, we decided not to investigate this gene further.

The second potential target gene Prickle2 was identified as an antagonist of the planar cell polarity (PCP) pathway involved, for example, in polarization of vestibular sensory cells of the inner ear (Deans et al., 2007). The PCP pathway was characterized in *Drosophila* and is conserved in vertebrates. PCP signaling is triggered by non-canonical Wnt proteins which interact with the Frizzled family of seven-transmembrane receptors to transduce signaling to the c-Jun-N-terminal kinase (JNK) pathway, possibly via Rho/Rac GTPases (Reviewed in Jenny and Mlodzik, 2006). The potential link between Notch and PCP signaling was investigated in cell fate determination of photoreceptors of the *Drosophila* eye. Experiments with dominant negative and dominant active forms of several components of the Rho/Rac GTPases and JNK cascade did not alter Notch signaling in the R3/R4 cells (Strutt et al., 2002). These investigations suggested that the PCP pathway was not sufficient to regulate Notch signaling in the fly photoreceptors. These observations, in addition to the fact that the murine Prickle2 cDNA was difficult to clone, prompted us not to pursue the characterization of this potential Notch target gene.

The focus of this study was the role of the potential Notch target gene RhoV in the skin. We first demonstrated the expression of the mRNA in wt murine epidermis by RT-PCR and by ISH. The ISH results detected RhoV mRNA in the epidermis as well as in the hair follicle

matrix region. In addition, we conducted luciferase assays *in vitro* to investigate a potential direct interaction of the NIC/transcription factor RBP-Jκ complex with putative binding sites localized upstream of the transcription start site and within the 2nd intron. The slight increase in luciferase activity observed opens the question of RhoV as a direct vs. indirect target gene. To test if direct binding to a site within the RhoV genomic sequence occurs upon Notch activation, a chromatin immunoprecipitation should be performed. In addition, RT-PCR of RhoV mRNA from cells treated with an inhibitor of protein synthesis, e.g. cyclohexamide, could also indicate if *de novo* proteins are necessary for its transcription. Furthermore, *in silico* analysis revealed another RBP-Jκ putative binding site in the 3rd exon as well as a RBP-Ebox-RBP motif localized 212bp downstream of the 3rd exon, which should be investigated.

We have shown RhoV expression in wild-type skin and hence decided to generate three different transgenic mice to study the role of RhoV *in vivo*. We expressed either constitutively active or dominant negative RhoV in various parts of the skin by using different promoters. The RohVAc form was driven by the K14 promoter and we generated the HKRAB Tg mice. The RhoVDn form was either driven by the involucrin promoter or the MHKA1 promoter, thereby generating the IRNB Tg and the HairKRNB Tg mice, respectively.

The generated transgenic lines were first backcrossed into C57Bl/6 to assess germline transmission. Skin samples from the offspring were then analyzed by RT-PCR for transgene expression. One HKRAB Tg, one IRNB Tg and two HairKRNB Tg mice expressed the corresponding mutated form of RhoV, RhoVAc or RhoVDn. Protein expression was then investigated by Western blot analysis for GFP as readout of transgene expression.

HKRAB Tg mice were first tested for protein expression. No GFP was detected in scraped epidermis samples from the HKRAB Tg mouse line. Moreover, no green fluorescence was observed in HKRAB Tg primary keratinocytes taken into culture to enrich for K14-expressing non-differentiated cells. The GFP expression was also investigated by directly observing, by fluorescence microscopy, sections of skin fixed in OCT, or by immunostaining for GFP. Both methods were inconclusive and could be explained by a level of protein expression below detection. However, we can not rule out the possibility that the RhoVAc protein is not expressed in the HKRAB Tg mice.

In contrast to HKRAB Tg mice, GFP expression was detected in scraped epidermis from IRNB Tg offspring. Green fluorescence was confirmed in primary keratinocytes in

culture, though at a low expression level. RhoV expression was also investigated directly by Western blot analysis with an anti-RhoV. This polyclonal antibody was generated against a peptide from a unique region at the carboxyl terminus of RhoV (Aronheim et al., 1998). The 36kDa protein was detected in 293T cells transfected with a RhoV-expressing plasmid, but no protein could be detected in lysates from epidermis. Consequently, the conditions for the anti-RhoV using epidermal samples need to be improved.

Finally, HairKRNB Tg mice were analyzed for protein expression. Western blot analysis on hair follicles was hindered by the highly keratinized structure of the hair, which contains a large amount of hard α-keratins. To increase the protein extraction yield a non-detergent lysis, described as the Shindai method (Nakamura et al., 2002), was tested on hairs plucked from the back pelage of transgenic mice. The first extraction following this protocol was non-conclusive and needs to be repeated.

Once the expression of the transgene confirmed by RT-PCR, and by Western blot analysis for the IRNB Tg mouse line, all three strains of transgenic mice were investigated by histological analyses of their skin at several ages. Morphology by H&E and proliferation state by Ki67 or BrdU stainings showed no developmental abnormalities. Differentiation was not impaired in any of the Tg as investigated by K14 and K1 immunostainings. Immunostainings for more differentiation markers, such as loricrin and filaggrin, could be performed in order to confirm the absence of differentiation defects.

Histological analyses suggested that disruption of RhoV does not impair homeostasis of the skin, implying that the small GTPase may play a role in challenged conditions. This hypothesis was tested by wounding both HKRAB and IRNB Tg mice and following the healing process. No overt defect in morphology and re-epithelialization of the epidermis of the wound was observed after 4 and 12 days post-wounding in any of the Tg lines. Further *in vitro* characterization of the migratory capacity of the keratinocytes should also be undertaken. Migration can be estimated by a scratch assay on primary keratinocytes. The cells in culture are treated with mitomycin C, to inhibit DNA synthesis and thus proliferation, and monitored after 24 hours for potential migratory defects.

Furthermore, the immediate reaction to injury is an inflammatory response, consisting of inward migration of platelets at the wound and subsequent formation of new blood vessels. We can thus also investigate the inflammation and angiogenesis responses induced by the

wounding in RhoVAc- and RhoVDn-expressing mice. For this purpose, CD31 expression was analyzed on wound sections. The CD31 glycoprotein is expressed on endothelial cells as well as in platelets and is involved in cell signaling and adhesion. The CD31 immunostaining on 4 days post-wounding skin sections, from both HKRAB and IRNB Tg mice, were not conclusive. The immunostaining can be repeated by changing the conditions and another specific staining for neutrophils, for example, can be performed.

In order to verify if RhoV is indeed downstream of Notch signaling, HKRAB and IRNB transgenic mice were crossed with Notch1$^{lox/lox}$ K14Cre mice. As Notch1-deleted mice lose their hair and spontaneously develop BCC tumors, the triple transgenic mice were monitored for either a rescue or an increased severity of the phenotype. Preliminary observations of HKRAB Tg Notch1$^{lox/lox}$ K14Cre mice suggest similar phenotypes since they exhibit a hair loss comparable to their Notch1-deleted littermates. However, the mice analyzed range from 6 to 8 months old, and thus have not developed any skin cancer, yet. Monitoring of the phenotype progression, as well as IRNB Tg crosses with Notch1$^{lox/lox}$ K14Cre mice, are ongoing.

Taken together, the data suggest a non-essential role of RhoV during skin homeostasis and wound healing. Active and negative forms of RhoV did not impair skin development and tissue remodeling even though RhoV was expressed in the epidermis and hair follicle. Therefore, a deeper understanding of the potential roles of the candidate target gene should be characterized by more gain- and loss-of-function assays. One method is overexpression of the gene *in vitro*, which can be induced by infection of cultured murine primary keratinocytes. The adeno-virus specifically expressing RhoV can be generated by cloning the cDNA into an adenoviral vector. Infected cells can then be analyzed for their differentiation status by investigating the expression levels of markers such as K1 or loricrin. Deciphering the pathways activated or down-regulated by this potential Notch downstream target gene can be undertaken by Western analysis of proteins involved in keratinocyte differentiation and migration, or of proteins which are potentially downstream of Rho GTPases.

In combination with overexpression, another method to analyze the function of the candidate gene is siRNA knock-down. After transfection into primary keratinocytes of the siRNA specific for RhoV, potential downstream signaling pathways can be investigated by Western blot analysis or microarray studies.

One hypothesis for the non-essential role of RhoV in the skin, suggested by this project, is a partial or complete compensatory effect of other Rho GTPases. In mammals, the Rho GTPase family is composed of 23 genes. The best-characterized members of the small Rho GTPase family are RhoA, Rac1 and Cdc42. Phylogenetic studies have revealed a remarkable conservation among the Rho GTPases throughout evolution, from yeast to humans. Gene duplication and divergence has expanded the family to several closely related subfamilies with each gene playing slightly different roles (Wherlock and Mellor, 2002). RhoV and RhoU, also known as Wrch1, are the two members of a subfamily sharing over 50% amino-acid sequence identity with Cdc42. RhoV and RhoU differ by additional unique sequence extensions at both N- and C-termini and they share a 54% amino-acid sequence identity.

RhoU was first described as a gene increased in response to Wnt1-mediated signaling, such as in Wnt1 transgene-induced mouse mammary tumors and Wnt1 retrovirus infected cells. Infection of Swiss 3T3 cells with a recombinant RhoU-expressing adenovirus induced filopodia and stimulated quiescent cells to reenter the cell cycle (Tao et al., 2001). Furthermore, RhoU was shown to regulate focal adhesion formation and cell migration *in vitro*. Indeed, RhoU siRNA knockdown in HelaS3 cells increased focal adhesion formation and inhibited cell migration in response to wound healing (Chuang et al., 2007). In order to test redundancy between RhoU and RhoV, RhoU expression should first be investigated in murine skin by RT-PCR and ISH. If both expressions do overlap, deleting both RhoV and RhoU in the epidermis might impair skin development and/or homeostasis. However, deregulation of RhoU was not detected in the Affymetrix microarray analysis conducted originally.

Several studies investigated the involvement of Rho GTPases in adhesion and migration of keratinocytes (Benitah et al., 2005; Lock and Hotchin, 2009). Most recently, RhoA was shown to signal through ROCK effectors in human keratinocytes and thereby regulate cell adhesion to fibronectin and terminal differentiation (Lock and Hotchin, 2009). In mouse epidermis, Rac1 was expressed in undifferentiated cells of the basal layer, in the bulge and the bulb of the hair follicle. Conditional deletion of Rac1 led to epidermal stem cell depletion by disrupting adhesive interactions between stem cells and their niche. Consequently, basal cells lacking Rac1 divided and underwent terminal differentiation inducing partial or complete loss of the IFE cell layers (Benitah et al., 2005). In fact, Rac1 was identified during the Affymetrix gene chip analysis in two conditions, the gain- and the loss-of-function with calcium-induced

differentiation. Nonetheless, quantitative RT-PCR in both settings did not determine Rac1 as a robustly deregulated potential downstream target gene of Notch1. Rac1 expression was slightly increased by 1.4 fold upon NIC-adenovirus infection of primary keratinocytes and a modest 0.8 fold change was detected upon adeno-Cre infection with Ca^{2+} addition (data not shown). No significant change in mRNA expression was detected upon loss of Notch1 alone. Hence, if the effects of RhoVAc and/or RhoVDn in the transgenic mice were rescued by another Rho GTPase, Rac1 may be a minor but not the sole contributor.

In addition, the Rho GTPases share common downstream effectors such as the serine/threonine protein kinase family known as p21-activated kinases (PAK). PAK proteins specifically interact with Cdc42, Rac (Manser et al., 1994; Zhao and Manser, 2005) and RhoV (Aronheim et al., 1998). The activated forms of the Rho GTPases bind to a p21 binding domain which induces autophosphorylation of PAK and subsequent kinase activity. Whereas Rac1 was shown to negatively regulate c-Myc through phosphorylation of PAK2 in mouse epidermis (Benitah et al., 2005), RhoV and Cdc42 triggered autophosphorylation-dependent degradation of PAK1, 2 and 3 *in vitro* (Weisz Hubsman et al., 2007). Common characteristics in effector-binding and in signaling potential might contribute to the redundancy among Rho GTPases. As Cdc42 was detected during the Affymetrix microarray analysis, it might also be a Notch1 target gene and have overlapping functions with RhoV. Nevertheless, Cdc42 deregulation upon Notch signaling needs to be confirmed by qRT-PCR.

In summary, RhoV is dispensable during skin homeostasis and re-epithelialization during wound healing, but its function might be more complex due to interplay with other small Rho GTPases and effectors. In order to investigate its effects in a more direct setting, one could generate RhoV straight knockout mice or conditionally delete the RhoV allele in the epidermis.

II. Jagged2 floxed mice

II. Generation of Jagged2 floxed mice

1. Introduction

Notch signaling is initiated through the direct interaction of the Notch receptors with their specific ligands. All four Notch receptors are activated by either the Delta-like (Dll) family of ligands and/or the Jagged (Jag) ligands. The Jagged2 gene encoding the transmembrane protein was cloned in mammals in 1996 (Shawber et al., 1996) and was shown to be expressed during rat embryogenesis. Co-expression of both Jag2 and Notch1 in the apical ectodermal ridge, as early as embryonic day 12.5 (E12.5), suggests a receptor-ligand interaction during limb development (Shawber et al., 1996). Interaction of Jag2 and Notch1 was also suggested to play a role at a later stage in other tissues such as the developing thymus, the epidermis and hair follicles as shown by immunohistochemical co-expression (Luo et al., 1997). A few years later, the mouse Jag2 gene was isolated from a multipotent hematopoietic cell line. The full-length Jag2 promoted survival of bone marrow progenitors *in vitro* through direct cell-to-cell contact (Tsai et al., 2000), even though the receptor to which it bound was not described.

In adult mice, the interplay between Notch receptors and their ligands has also been investigated through their differential expression patterns. For example, Notch receptors 1 to 3 exhibit differential expression patterns not only during thymus development, but also in adult thymocyte subpopulations (Felli et al., 1999). The investigators also characterized the expression of the Jagged ligands. Whereas Jag1 mRNA expression decreased in the post-natal thymus, expression of Jag2 was stable. In addition to the thymus, expression of members of the Notch signaling pathway has been well described in the skin. Both Notch1 and Notch2 are expressed in the suprabasal layers of the epidermis. While Notch1 is also expressed in the basal cells, Notch2 is absent (Rangarajan et al., 2001). Three Notch ligands were shown by *in situ* hybridization to be expressed in murine epidermis and developing hair follicles, Jag1 and 2, and Dll1, the latter being only detectable in embryonic skin exclusively in mesenchymal cells of the pre-papilla (Powell et al., 1998). More precisely, in the interfollicular epidermis (IFE), both Jag1 (Nicolas, 2003) and Jag2 (Fig.1) are primarily found in the suprabasal layers. As for the hair follicle, Jag1 is expressed in the upper outer root sheath (ORS) and bulb pre-cortex while Jag2 shows a complementary expression pattern in the follicle bulb and basal layer of the ORS (Watt et al., 2008).

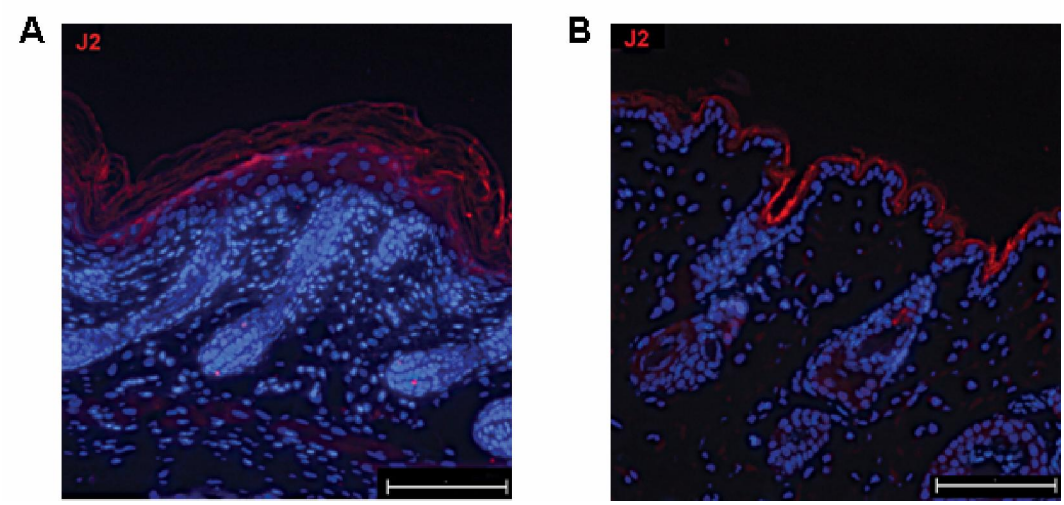

Figure 1. Jagged2 expression in murine skin. (A and B) Jag2 immunofluorescence (red) shows Jag2 expression in murine epidermis of a 2-day old newborn (A) and of a 7-week old adult (B), when expression is also seen in the hair follicle. Bar: 100μm

Gene targeting in mice further validated the importance of Notch ligands in skin development and homeostasis. Specifically, inactivation of Dll1 in embryonic epidermis caused increase proliferation and thickness of the IFE (Estrach et al., 2008) whereas loss of Jag1 in the mouse epidermis inhibited hair growth and induced conversion of hair follicles into cysts (Estrach et al., 2006). The Jag1 conditional knockout mice developed skin tumors within 6 months after gene inactivation confirming the tumor-suppressor activity of Notch signaling in this self-renewing tissue (Vauclair, 2006). Jag1 inactivation in the skin did not phenocopy conditional deletion of Notch1. Gene targeting of Notch1 lead to a gradual hair loss and only 10% of hairs remained (Rangarajan et al., 2001; Vauclair, 2006) while Jag1 deficient mice lost all hairs within a few months. The conditional inactivation of both Notch1 and Notch2 caused a much stronger phenotype since the mice developed an atopic dermatitis (AD)-like disease (Dumortier et al., 2010). The N1N2 inducible inactivation rapidly caused severe skin abnormalities, such as complete and irreversible hair loss and hyperproliferative epidermoid cysts, and the mice died within 7 weeks post deletion (Dumortier et al., 2010; Vauclair, 2006). This premature death and AD-like disease was not recapitulated by the inactivation of Jag1 alone, as previously mentioned. This discrepancy suggested a non-redundant role for Jag2 in the skin.

Although Jag2 is suggested to play a complementary role to Jag1 in the skin, this Notch ligand has not been extensively characterized during epidermal homeostasis. Investigating the

function of Jag2 in the adult skin is hampered by the fact that conventional gene targeting of Jag2 is embryonic lethal. Mice that died at or shortly after birth, due to craniofacial morphogenesis defects, were homozygous for a targeted mutation which removed the DSL domain of the Jag2 protein ($Jag2^{\Delta DSL}$). This domain is required for receptor interaction (Jiang et al., 1998). $Jag2^{\Delta DSL}$ homozygous mice exhibited fusion of the tongue with the palatal shelves and thus were unable to breathe or accumulated air in their stomach and intestines. $Jag2^{\Delta DSL/\Delta DSL}$ mutant mice also exhibited syndactyly of the fore and hind limbs.

Moreover, the Jag2 gene was mapped near the spontaneous missense mutation *sm*. $Jag2^{sm}$ homozygous mice displayed a similar phenotype, such as fusion of the digits, hyperplastic apical ectodermal ridge at the limb buds and postnatal mortality (Gruneberg, 1956; Sidow et al., 1997). Interestingly, epidermal hyperplasia, producing excessive thickness of epidermal cells, was observed in circumscribed areas of the limb epidermis. Additionally, premature keratinization, or parakeratosis, occurred from E13 onwards. The latter observations suggest a function of Jag2 in keratinocyte proliferation.

In order to investigate the role of Jag2 at later stages of development and during adulthood, we focused on generating floxed Jag2 mice. Homozygous $Jag2^{lox/lox}$ mice could then be crossed with specific Cre transgenic mouse strains to conditionally delete the Notch ligand in targeted tissues, such as in the hematopoietic system or in the skin.

2. Results

2.1 Generation of the floxed Jag2 targeting vector

Floxed Jag2 mice are generated to investigate the role of the ligand in a loss of function context during adulthood. Generation of the Jag2 floxed mouse line was originally outsourced to the company Nucléis (Lyon, France). Nucléis went bankrupt in 2006 and we received the targeting vector for the Jag2 gene, which is schematically shown in Fig.2. Briefly, the targeting vector consists of the 5'homologous arm upstream of the deletion arm and the 3'homologous arm was cloned downstream. The deletion arm, flanked by loxP sites, consists of exons 1 and 2 of the Jag2 gene which code for the leader peptide and the conserved N terminus of Notch ligands (MNNL). It also contains sequences 551bp upstream of the ATG and 1443bp within the 2nd intron, summing up to 2.6kb in total. Additionally, a neomycin resistance cassette, itself flanked by two 34bp FLP recognition target (FRT) sites, was inserted for positive selection and a diphtheria toxin A-chain (DTA) cassette for negative selection (Fig.2).

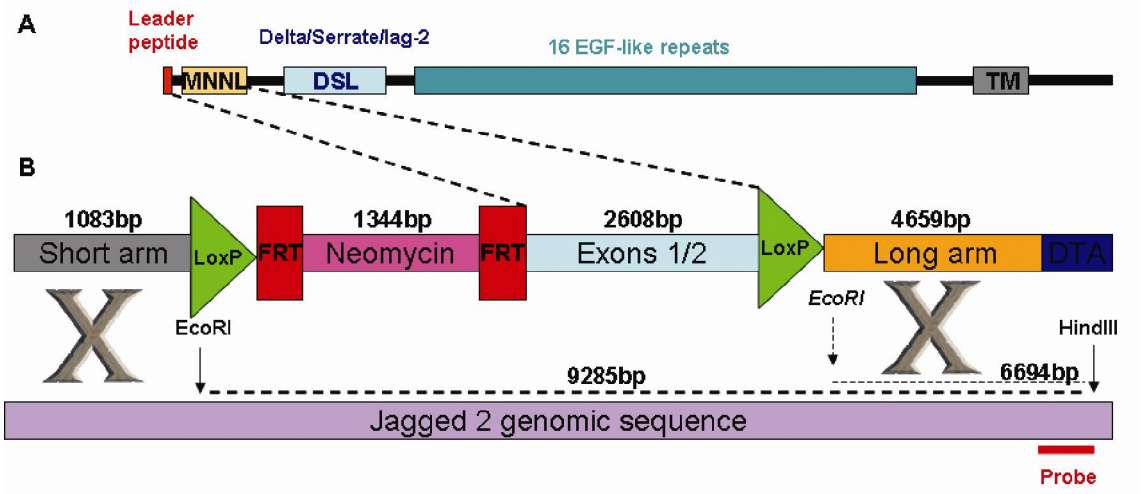

Figure 2. Inducible targeting of the Jag2 gene. (A) The Jag2 gene consists of 26 exons of which the two first ones code for a leader peptide and an N terminus common to Notch ligands (MNNL). Also encoded are the DSL region which interacts with the Notch receptors, 16 calcium-binding EGF-like repeats and the transmembrane domain (TM). (B) The targeting vector consists of the neomycin cassette (pink), flanked by FRT sites (red), and exons 1 and 2 (blue) flanked by two loxP sites (green triangles). The homologous Jag2 regions are depicted as the short arm (grey) and the long arm (orange). HindIII and EcoRI cutting sites are indicated by arrows. The red bar corresponds to the localization of the 3' probe used for Southern blot hybridization during the screening of homologous recombination events.

The targeting construct was then electroporated into mouse embryonic stem (ES) cells by the transgenic animal facility. Subsequently, 480 clones were screened by Southern blot for the floxed allele. Double digestion of the DNA with HindIII/EcoRI allowed identification of a 9.3kb wild-type band or a 6.7kb band for the correctly targeted locus (Fig.2B and 3). This analysis revealed one positive clone (Fig.3) that was confirmed to carry the most 3'loxP site by PCR, using primers within the 2nd intron of the deletion arm and upstream of the long arm (Fig.3C).

3'loxP primers: 5'CTTTTGGTTAGGGGGTCAGG 3'

5'GGGCTGCAGGAATTCGATC3'

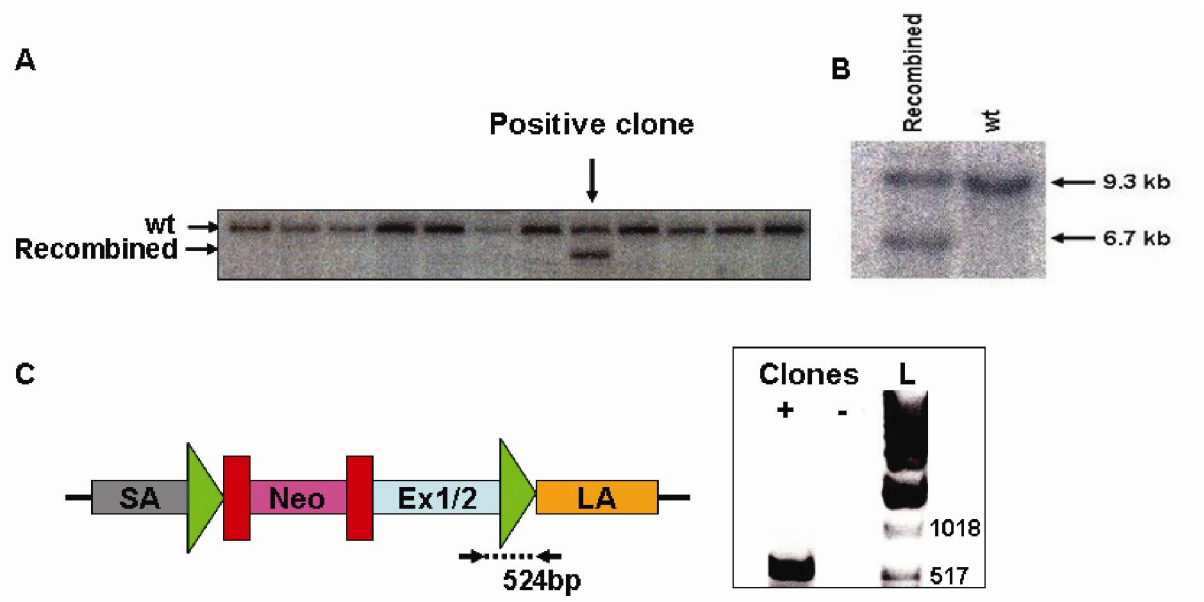

Figure 3. Southern blot analysis of Jagged2 gene targeted ES cell clones. (A) Representative phosphorimager scan from 12 of the 480 clones analyzed by the Southern blot strategy shown in Fig.2B. DNA from ES cell clones was hybridized with a probe downstream of the 3'end after double digestion with HindIII/EcoRI. One positive clone (arrow) shows the correct recombined 6.7kb band in addition to the 9.3kb wt band. (B) The recombined clone was further confirmed by an independent Southern blot analysis. (C) PCR of the most 3'loxP site amplifies a 524bp band as shown schematically on the left. PCR amplification on DNA from the positive clone (+) compared to a negative one (-) confirms the presence of the most 3'loxP site. Green triangles: loxP sites; red boxes: FRT sites; SA: short arm; Neo: neomycin cassette; Ex1/2: exons 1 and 2; LA: long arm; L: 1kb DNA ladder with two band sizes given in bp.

2.2 $Jag2^{lox/lox}$ founder lines

The correctly targeted ES cell clone described above was injected into blastocysts by the transgenic animal facility and subsequently implanted into pseudopregnant recipients. Eight chimeras were born and crossed to C57Bl/6 mice to identify germline transmitters. Since the ES cell lines were derived from SV129 substrains, two of the founder lines (F0) displayed germline transmission by virtue of the brown coat color of their offspring. The F1 generations of both founders were intercrossed and genotyped by PCR for the most 3'loxP site. Genotyping PCR resulted in only heterozygous lox/+ and wt animals determined by the 392bp lox band and 200bp wt band (Fig.4B).

Genotyping primers: 5'GCTCCAAATCGCTACCTGAG 3'

5'GTCCCCAAGACCAAGTACCA 3'

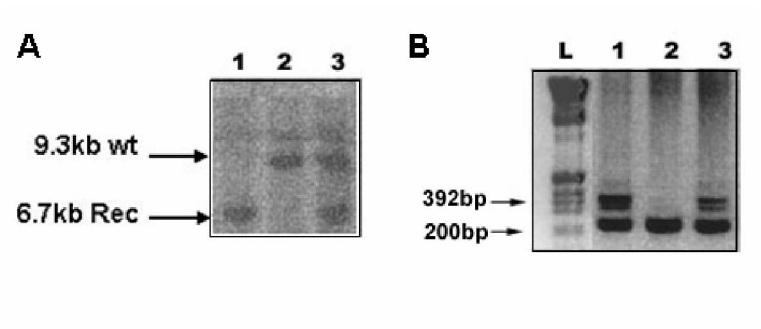

Figure 4. Southern blot analysis and PCR genotyping for floxed Jag2 gene do not correlate. Phosphorimager scan of Southern blot (A) and corresponding PCR (B) for $J2^{lox/lox}$ (lane 1), $J2^{+/+}$ (lane 2) and $J2^{lox/+}$ (lane 3). 392bp: lox band; 200bp: wt band; L: 1kb DNA ladder.

Since no homozygote $Jag2^{lox/lox}$ mice could be generated after several litters from intercrosses of both founder lines, we hypothesized that the Neo cassette, still present in the original targeting construct, might interfere with the endogenous Jag2 gene. This interference could induce hypomorphism, i.e. by reducing the level of gene activity, which could explain why no homozygote mice were born. Therefore, we decided to set up timed pregnancies and investigated three embryonic time points, namely E12.5, E13.5 and E14.5, for embryonic lethality. By examining the embryos using the stereo microscope we found no phenotypic difference among siblings and no syndactyly was observed, as previously described for $Jag2^{\Delta DSL}$ homozygous mice (Jiang et al., 1998). E12.5 and E13.5 embryos were genotyped by Southern blot and several mice were indeed $Jag2^{lox/lox}$ homozygotes. Surprisingly, the genotypes by PCR on genomic DNA from the very same mice indicated that the mice were

heterozygotes (Fig.4). The discrepancy between results obtained by Southern blot analysis and by PCR amplification suggested an incomplete homologous recombination of the targeting vector into the Jag2 gene, unless the PCR amplified an unspecific product of the same size as the wt band.

In order to rule out the possibility of an unspecific band instead of the wt band, we decided to verify the specificity of the amplified products. We thus isolated the two PCR bands, wt and most 3'loxP site, amplified from genomic DNA of a founder, a C57Bl/6 wt mouse and from the plasmid containing the original Jag2 targeting vector. Several digestion patterns were tested for diagnosis of the correct sequences (Fig.5A). Digestion of the wt and 3'loxP PCR products with three restriction enzymes, namely AflIII, HindIII and XhoI, produced distinct band patterns when analysed by electrophoresis on a high percentage agarose gel. This analysis not only revealed the expected digestion patterns for both wt and 3'loxP site PCR products, but more importantly the patterns of the wt sequence were identical (Fig.5B and C). Similar results were obtained for the digestion patterns of the 3'loxP site isolated from a $J2^{lox/+}$ mouse (data not shown). Therefore, we concluded that the products amplified by the genotyping PCR were the correct sequences and hence, that the wt allele of the Jag2 gene was indeed present in the samples genotyped by this method.

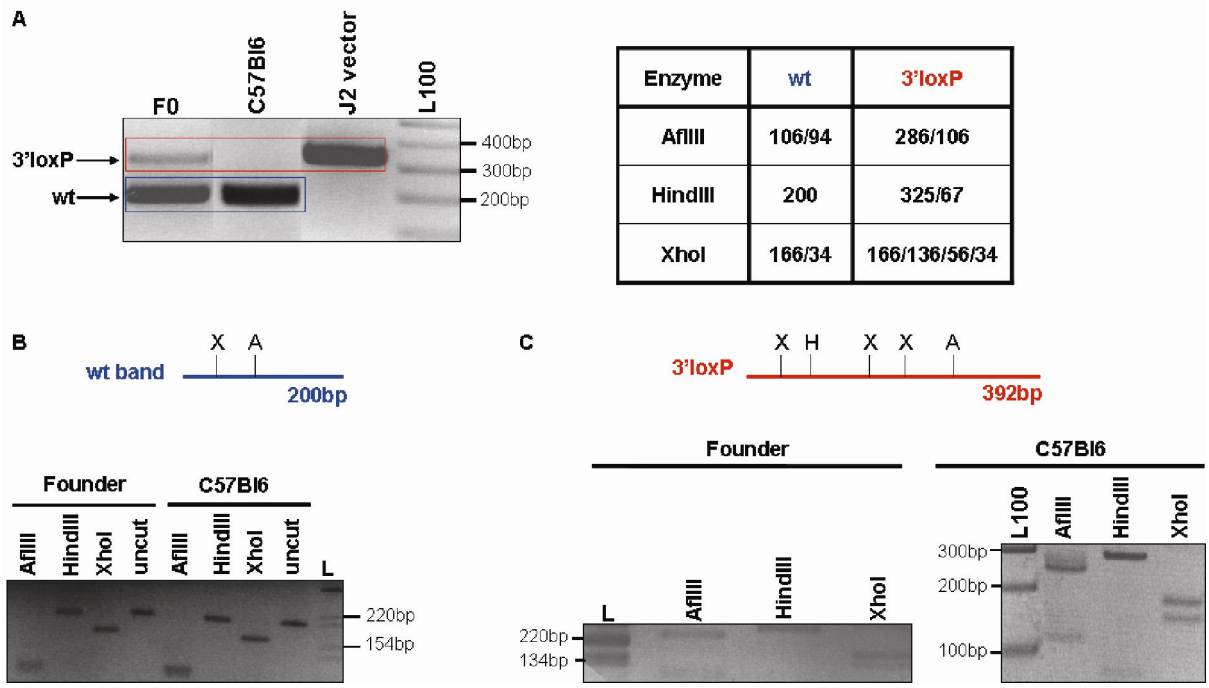

Figure 5. Specificity of wt and 3'loxP site PCR products verified by digestion patterns. (A) Genotyping PCR on founder (F0) and C57Bl6 DNA as well as on the plasmid of the original targeting vector (J2 vector) amplifies both products: the wt 200bp (boxed in blue) and the 3'loxP site 392bp (boxed in red). L100: 100bp Plus ladder. The table displays the values in bp of the diagnostic digestion pattern for each band for the three restriction enzymes used. (B and C) Isolated wt band (B; blue) and 3'loxP site band (C; red) are digested with enzymes AflIII, HindIII or XhoI. Restriction sites cutting in the PCR products are shown schematically above the corresponding agarose gel pictures. A: AflIII; H: HindIII; X: XhoI; L: 1kb DNA ladder; L100: 100bp Plus ladder.

2.3 Incomplete homologous recombination of the floxed Jag2 allele

We have shown that the failure to generate $Jag2^{lox/lox}$ homozygous mice was neither due to hypomorphism of the floxed Jag2 allele, nor to the integrity of the most 3'loxP site. We thus decided to delete the Neo sequence and to further investigate whether correct homologous recombination had occurred in the floxed Jag2 mice.

As previously described in Fig.2B, the Neo sequence is flanked by FRT sites which enable recombination through flipase activity. Excision of the intervening Neo cassette by FLP-mediated recombination was tested on the targeting vector by transformation into the 294-FLP *E.coli* strain. The bacteria were specifically engineered to express flipase and therefore efficiently recombine plasmids containing FRT recognition sites (Buchholz et al., 1996). Isolated potentially recombined vector DNA was subsequently digested with the

HindIII restriction enzyme to assess complete excision of the Neo cassette. Three HindIII restriction sites are located within the targeting vector, one in the Neo sequence and two in the backbone plasmid. Consequently, HindIII digestion of the targeting vector produces two fragments instead of three upon Neo deletion by FLP-mediated recombination (Fig.6A). Digestion patterns indeed resulted in two bands instead of three after transformation into the FLP-bearing bacteria (Fig.6B) demonstrating efficient excision of the Neo cassette from the Jag2 targeting vector.

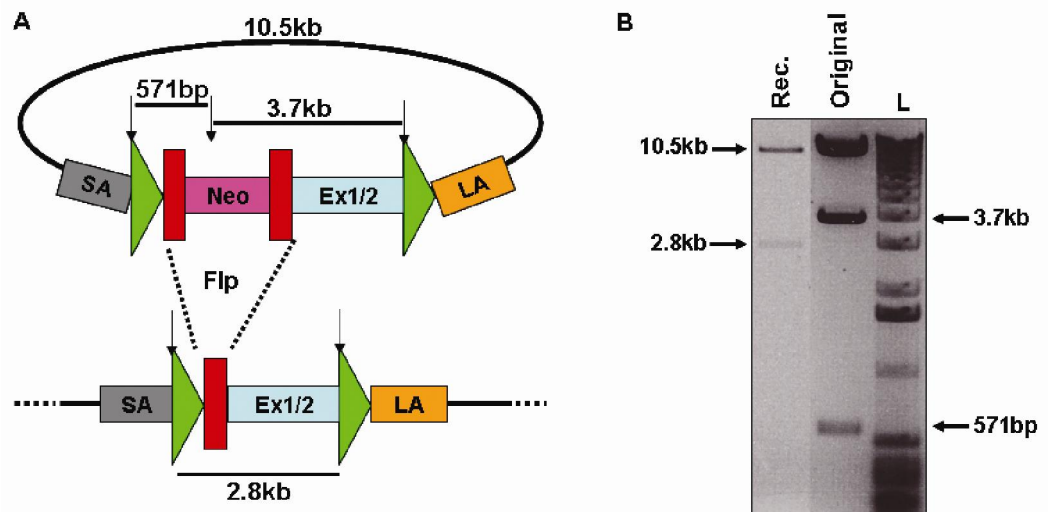

Figure 6. FLP-mediated efficient recombination of Jag2 targeting vector. (A) Efficient FLP-mediated recombination is tested by HindIII digestion (restriction sites represented by arrows) which cuts three times in the Jag2 targeting vector. After excision of the Neo sequence (dotted lines) one HindIII restriction site is lost resulting in a single 2.8kb fragment instead of the two 571bp and 3.7kb portions. (B) Agarose gel electrophoresis of the HindIII digested Jag2 targeting vector after (Rec) and before (original) transformation into 294-FLP bacteria. Diagnostic bands are highlighted by arrows with their corresponding sizes. L: 1kb DNA ladder.

Since efficient FLP-mediated recombination of the Jag2 targeting vector occurred *in vitro*, we focused on excision of the Neo cassette *in vivo*. For this purpose, the $J2^{lox/+}$ mice were crossed with a deleter mouse strain ($Flpe^{+}$ mice) harboring the enhanced thermostable FLPe recombinase gene under the human ACTB promoter. These mice express the FLPe recombinase variant in tissues such as the brain, the heart and in germ cells of adult testes and ovary (Rodriguez et al., 2000). The F1 $J2^{lox/+}$ $Flpe^{+}$ mice were then intercrossed in order to obtain hetero- and homozygous mice for the FLPe transgene for efficient expression of the recombinase. Complete deletion of the Neo cassette was analyzed by PCR with the upstream primer in the short arm region and the downstream primer within the Neo sequence (Fig.7A).

Neo deletion primers: 5'CACTCACTCCCAGGCTGTTT 3'

5'GGGGTGCCTAATGAGTGAGA 3'

As deletion of the Neo cassette resulted in the absence of the 188bp band, DNA from both founder lines was used as positive controls for its presence (Fig.7B). Not only do these PCR results confirm efficient Flp-mediated excision of the Neo sequence *in vivo* but they also prove the presence of the 5'loxP site of the targeting vector in the floxed Jag2 founders.

We have shown that floxed Jag2 $Flpe^{+}$ mice carried the FLPe transgene and that the Neo cassette was efficiently deleted. However, the wt band was still amplified during the genotyping PCR and Southern blot analyses on these same mice again revealed the presence of $Flpe^{+}$ homozygote $Jag2^{lox/lox}$ mice. This observation suggested an incomplete homologous recombination.

We thus investigated whether the presence of the wt Jag2 allele was due to a homologous integration of the targeting vector at its 5'end. In other words, we hypothesized that only the 3'end had recombined correctly. This incomplete homologous recombination would explain the PCR amplification of the wt band since the endogenous gene segment would not be replaced by the floxed Jag2 allele at its 5'end. To test this hypothesis we designed a Southern blot strategy consisting of an EcoRI digestion and subsequent hybridization with a 2.65kb fragment of the deleted region. If exons1 and 2 were correctly replaced by the targeting deletion arm, expected bands would be the wt 22kb and the 2.65kb from the targeting construct (Fig.7A). Both bands were indeed detected in $J2^{lox/+}$ and wt genomic DNA samples. However, an extra band at about 12kb was identified in both $J2^{lox/+}$ and $J2^{lox/lox}$ mice (Fig.7C) thereby confirming the presence of a third segment containing Jag2 exons 1 and 2.

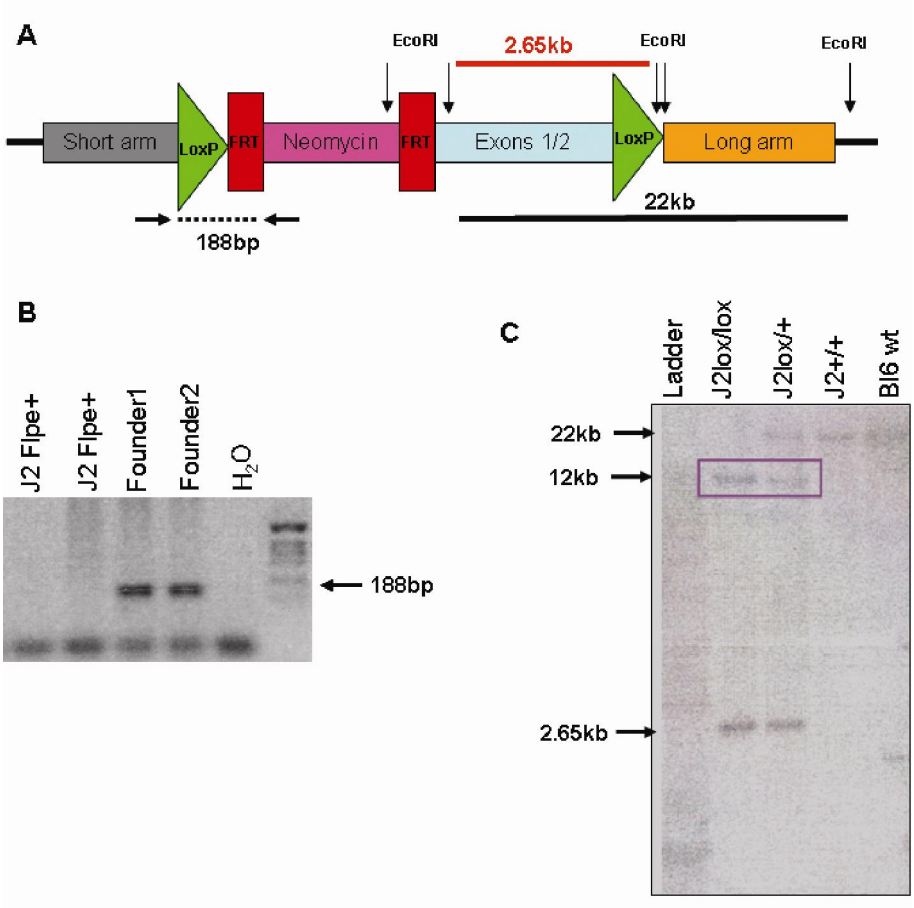

Figure 7. Efficient Neo cassette deletion and control of homologous recombination. (A) Primers designed for the PCR amplification of the 5'loxP site and Neo cassette are shown by black arrows delimiting a 188bp region. The Southern blot strategy for the integration of the deleted region (red bar represents the probe) gives a 2.65kb band for the targeting construct and a 22kb wt band after EcoRI digestion (arrows). (B) PCR amplification on genomic DNA from floxed Jag2 mice bearing the FLPe transgene shows efficient deletion of the Neo sequence. Both founders are shown as positive controls. (C) Phosphorimager scan of Southern blot on 10μg of genomic DNA from hetero-and homozygote Jag2 mice hybridized with a fragment of the deleted region as probe gives an unexpected extra band at about 12kb (violet box). Expected bands are shown by arrows with their respective sizes. Bl6wt: DNA from a C57Bl/6 wild-type mouse.

In an attempt to interpret this unexpected 12kb band and to corroborate a partial integration of the targeting vector, we designed a Southern blot strategy to investigate the 5'loxP region. We have previously shown the presence of the 5'loxP site indirectly, in the founders, by the Neo deletion PCR. However, a Southern blot analysis using a probe at the boundary of the short arm with the Jag2 genomic sequence would confirm or refute the correct homologous recombination event. Double digestion of the genomic DNA with DraIII/HindIII would then result in a 2kb band for the targeting construct and a 9.7kb wt band

(Fig.8A). Surprisingly, not only was the 2kb band not identified on the Southern blot scan but an unexpected band about 1 to 2 kb higher than the 9.7kb wt band was detected (Fig.8B).

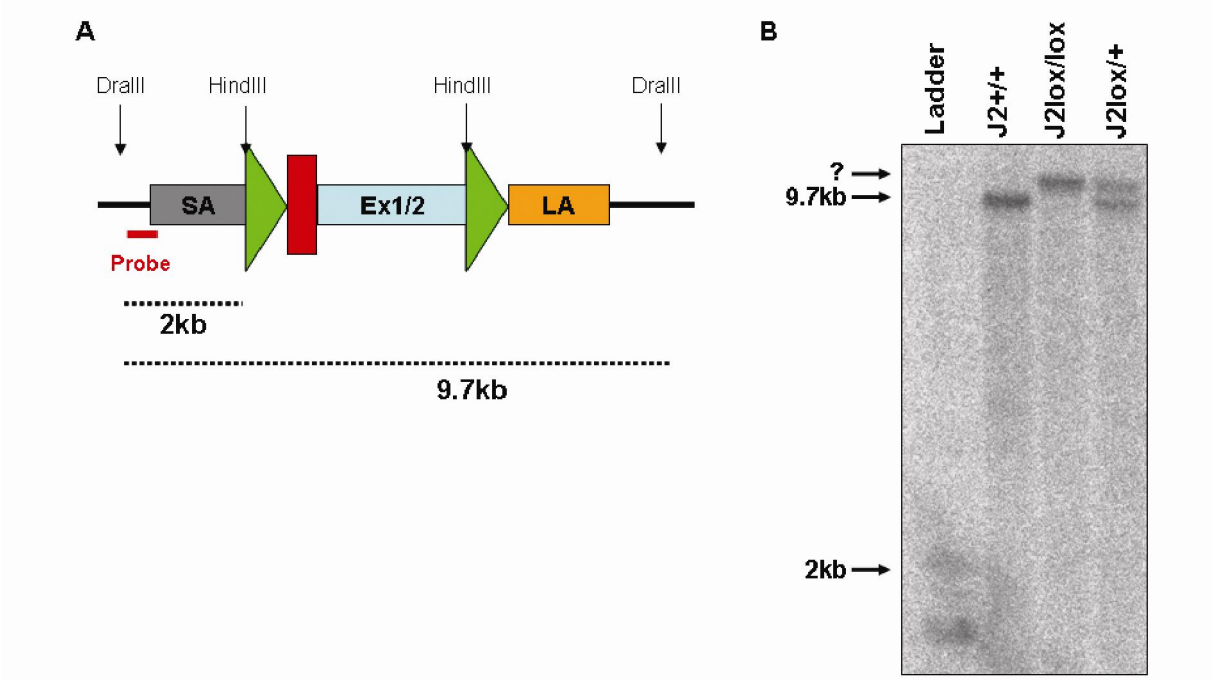

Figure 8. Southern blot analysis of the 5'loxP region of the Jag2 targeting construct. (A) Southern blot strategy for 5'loxP region uses a probe (red bar) at the boundary of the short arm with the Jag2 genomic sequence. Two restriction enzymes, DraIII and HindIII (arrows), are used in a double digestion of the DNA. Dotted lines represent the 2kb targeting construct band and the 9.7kb wt band, respectively. SA: short arm; LA: long arm; green triangles: loxP sites; red box: FRT site; Ex1/2: exons 1 and 2. (B) Phosphorimager scan of the 5'loxP region Southern blot on 10µg of DNA digested HindIII/DraIII from a wt $Jag2^{+/+}$, a homozygote $Jag2^{lox/lox}$ and a heterozygote $Jag2^{lox/+}$ mouse. The 9.7kb wt band is detected in the wt and $Jag2^{lox/+}$ lanes as expected, but no 2kb band appears in either homo- or heterozygote mice. However, an extra band at about 11kb is visible in both lanes (question mark). Ladder: 1kb DNA ladder.

In parallel, several PCR amplifications for both the 5' and the 3' loxP sites were designed (Fig.9A). The PCRs were performed on genomic DNA from E13.5 embryos of the three different genotypes, i.e. wt $J2^{+/+}$, $J2^{lox/+}$ and $Jag2^{lox/lox}$.

Primer set 1/2: 5'GCTCCAAATCGCTACCTGAG 3'

5'CCAAAGAGCGGAAATACCAA 3'

Primer set 3/4: 5'CTAGGCTCCTGCTCCATACG 3'

5'GTCCCCAAGACCAAGTACCA 3'

Primer set 5/6: 5’TGTGCAGCAGGCAGTATCTC 3’

5’GCACAGAACCAGTAGCAGCA 3’

Primer set 7/8: 5’GACAGGGAAGCTGAATTTGC 3’

Primer set 8/9: 5’ATCGATACCGTCGAAACAGC 3’

5’ACCTACCCTACCTGCGTGTG 3’

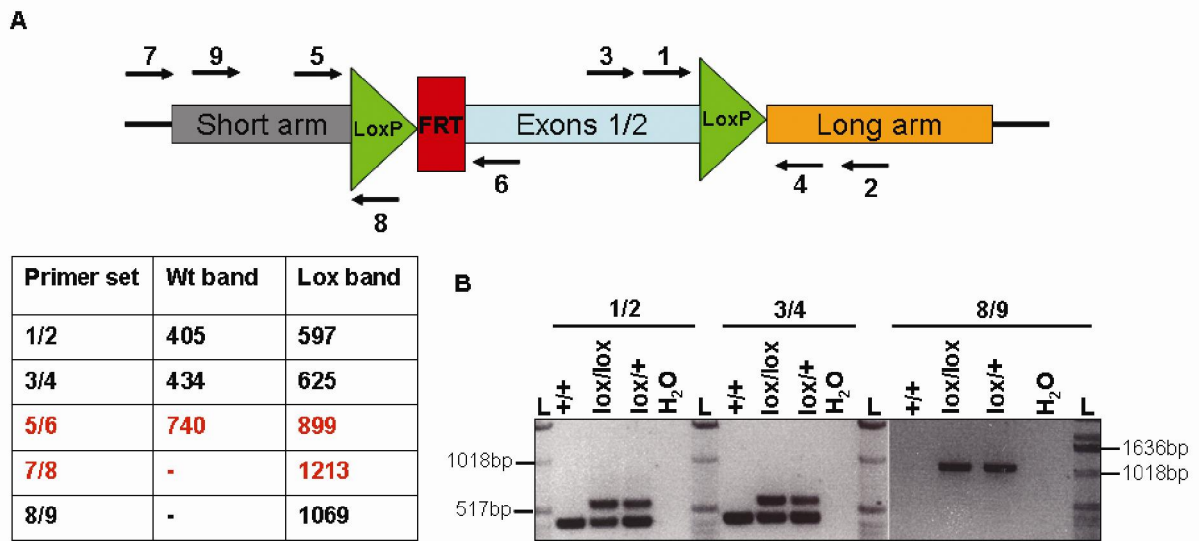

Primer set	Wt band	Lox band
1/2	405	597
3/4	434	625
5/6	740	899
7/8	-	1213
8/9	-	1069

Figure 9. PCR amplification strategies for 5’ and 3’loxP sites. (A) Schematic representation of the targeting vector shows the emplacement of the primers (arrows) designed for 5 different PCR amplifications. The primer sets are designated by numbers which can be found in the table below with their corresponding product sizes in bp (wt band and lox band). The PCR strategies that did not give any results are highlighted in red (twp rows). (B) Agarose gel pictures show products of expected sizes for the three PCR amplifications 1/2, 3/4 and 8/9, respectively. Genomic DNA from embryos of a wt +/+, a $J2^{lox/+}$ and a $J2^{lox/lox}$ genotype were used as templates. L: 1kb DNA ladder.

As depicted in Fig.8B, PCR amplifications for the two sets of primers in the 3’loxP region (1/2 and 3/4) still identified the wt band in the homozygous $Jag2^{lox/lox}$ genomic DNA. The 5’loxP site was present downstream of the short arm as amplified by the primer set 8/9 even though the two PCR reactions that did not work were within the 5’loxP region (5/6 and 7/8; Fig.9A).

Taken together, these results suggest an efficient homologous recombination event at the 3’end of the targeting construct, but not at its 5’end. An integration of the Jag2 floxed

allele in its 5'region has most likely occurred instead of a complete replacement of the endogenous Jag2 gene as the wt Jag2 allele was still present in $Jag2^{lox/lox}$ mice.

2.4 Efficiency of Jag2 inactivation

The hypothesis of integration in the 5'UTR of the 5' short arm of the targeting construct, instead of its homologous recombination, was further investigated by analyzing the inactivation efficiency of the floxed Jag2 allele. In order to recombine the loxP sites flanking the deletion arm, $Jag2^{lox/lox}$ homozygote mice were crossed with mice bearing the Cre recombinase, such as the MxCre or K14Cre mouse strains. If the hypothesis of partial homologous recombination is correct the generated $Jag^{lox/lox}$ MxCre, or K14Cre, mice would have their floxed Jag2 allele efficiently excised but nonetheless continue to transcribe a wt Jag2 allele. Consequently, the Cre-recombined $Jag^{lox/lox}$ mice would still express a functional Jag2 protein (Fig10).

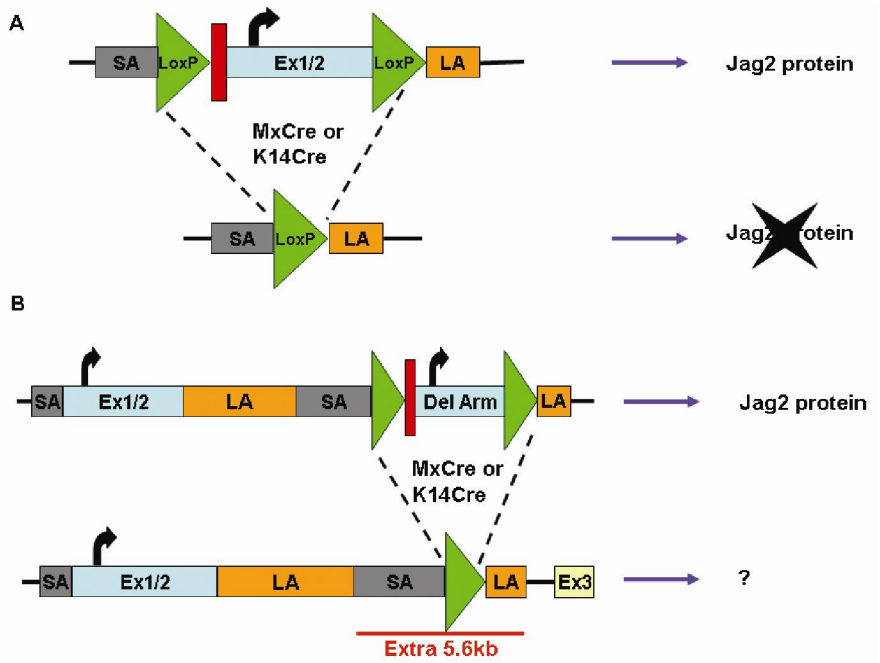

Figure 10. Hypothesis of Jag2 transcription and protein expression after Cre-mediated deletion. (A) Excision of exons 1 and 2 of correctly recombined Jag2 deletes the translation start site of the gene. Consequently, Cre-mediated deletion through MxCre or K14Cre blocks Jag2 protein expression. (B) In the case of a partial recombination event, deletion of Jag2 would cause a 5.6kb insertion (red bar) in the endogenous gene. As the wt Jag2 gene is still present, the deletion arm excision might not affect Jag2 protein expression. SA: short arm; LA: long arm; green triangles: loxP sites; red box: FRT site; Light blue boxes: exons 1 and 2 which also correspond to the deletion arm (Del Arm); black arrow represents the Jag2 translation start site (ATG).

Jag2 deletion efficiency was first studied in thymocytes, since it was previously shown that Jag2 mRNA is expressed in the thymus (Felli et al., 1999). Efficient deletion in the lymphoid organ can be achieved by the inducible MxCre mouse strain. The MxCre transgene expresses Cre recombinase under the Mx1 (myxovirus influenza resistance 1) promoter. The Mx1 promoter is inducible upon interferon (IFN)-α or –β treatment. Another method to induce this promoter is by administration of a synthetic double-stranded RNA (called pI-pC, polyinosinic-polycytidylic acid) which stimulates endogenous IFN production. Upon MxCre induction floxed alleles are efficiently deleted in many organs, such as the liver, the spleen, as well as the thymus (Kuhn et al., 1995). Thus, homozygously floxed Jag2 mice were crossed with MxCre mice and offspring were injected 5 times with pI-pC in order to inactivate Jag2 in the hematopoietic system.

To confirm efficient excision of the Jag2 deletion arm Cre recombinase expression was induced in a $Jag2^{lox/+}$ MxCre mouse and its littermate control by administering pI-pC every other day for a total of five times. One week after the last injection the $Jag2^{lox/+}$ MxCre and the control mice were sacrificed and genomic DNA was subsequently extracted from their bone marrow cells. Cre-mediated excision of the floxed Jag2 deletion arm was revealed by PCR amplification (Fig.11A). The deletion PCR correctly amplified the excised region of bone marrow DNA derived from the $Jag^{lox/+}$ MxCre mouse (Fig.11B).

Deletion primers: 5’TGTGCAGCAGGCAGTATCTC 3’

5’GTCCCCAAGACCAAGTACCA 3’

To further confirm the correct excision of the floxed Jag2 deletion arm Southern blot analysis was performed. The same DNA as for the deletion PCR was digested with the restriction enzyme BamHI and hybridized as indicated in Fig.11A. The probe was located downstream of the targeting vector, towards the 3’end, and expected fragments were the wt 6.64kb, the floxed 6.07kb and the deleted 8.4kb bands (Fig.11A). The wt 6.64kb band was indeed identified in DNA derived from the heterozygote mouse, and the floxed 6.07kb band was detected in DNA derived from the control $Jag2^{lox/lox}$ mouse. However, instead of the 8.4kb deleted band, an unexpected band above 12kb was detected in the DNA from the $Jag2^{lox/+}$ MxCre mouse (Fig.11C).

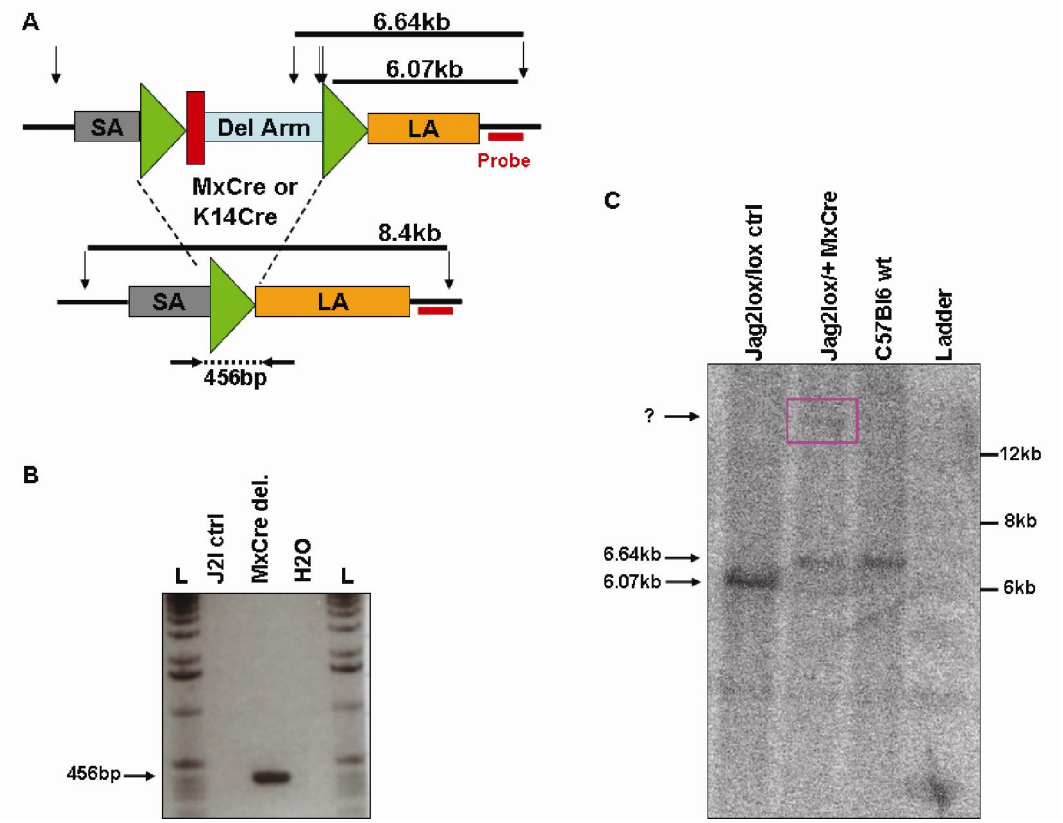

Figure 11. Excision of the floxed Jag2 allele confirmed by PCR and Southern blot analyses. (A) The deletion PCR amplifies a 456bp band (dotted lines) after Cre-mediated excision of Jag2 deletion arm (Del Arm). The Southern blot strategy consists in a BamHI digestion of the genomic DNA (arrows) and subsequent hybridization with a probe located downstream of the targeting vector (red bar). Expected fragments are the wt 6.64kb band, the 6.07kb band for the targeting construct and, after excision of the deletion arm, the 8.4kb band. (B) Deletion PCR on DNA derived from bone marrow of injected Jag2 control and $Jag2^{lox/+}$ MxCre mice amplifies the 456bp product. L: 1kb DNA ladder. (C) Phosphorimager scan of the Southern blot analysis for the excision of the floxed Jag2 allele was performed as depicted in A. 7µg of bone marrow DNA derived from control $Jag2^{lox/lox}$ (first lane), $Jag2^{lox/+}$ MxCre (second lane) and C57Bl/6 wt (third lane) mice were used for digestion and subsequent hybridization. The unexpected band above 12kb is highlighted (pink box). Ladder: 1kb DNA ladder.

Overall, both strategies proved the efficient excision of the floxed Jag2 allele in the bone marrow of the $Jag^{lox/+}$ MxCre mouse. Intriguingly, the Southern blot analysis also revealed a higher band instead of the expected deleted band. These data further suggested an integration of the 5'short arm of the targeting vector. In order to test if transcription of the Jag2 gene occurred despite the partial homologous recombination Jag2 heterozygote mice on the MxCre background were intercrossed. The offspring were genotyped by Southern blot analysis to generate homozygous $Jag2^{lox/lox}$ MxCre mice. It has been previously shown that double negative (DN) thymocytes, as well as CD4 and CD8 single positive T cells, express

Jag2 mRNA (Felli et al., 1999). Therefore, Jag2 mRNA expression was assessed in the deleted $Jag2^{lox/lox}$ MxCre mice by RT-PCR on extracted total RNA from sorted DN thymocytes.

The sorted DN thymocytes were pooled from 11 $Jag2^{lox/lox}$ MxCre and from 6 $Jag2^{lox/lox}$ mice sacrificed 2 weeks after last pI-pC injection. RNA was extracted from the sorted DN cells and, after genomic DNase treatment, cDNA was synthesized. The Jag2 transcript was PCR amplified by using primer sequences which span from exon 22 to exon 25 (Felli et al., 1999). The RT-PCR thus amplified a 592bp band if Jag2 mRNA was present in the samples. Any genomic DNA which might have contaminated the cDNA was not detected as it would have been too long (2.2kb).

Jag2 RT-PCR primers: 5'GTCCTTCCCGCATGGGAGTT 3'

5'GTTTCCACCTTGACCTCGGT 3'

RT-PCR performed on cDNA derived from FACS purified $Jag2^{lox/lox}$ DN cells successfully amplified the 592bp product (Fig.12A). To test the Jag2 deletion efficiency spleens were also isolated from the same mice and their DNA was extracted. Excision of the floxed Jag2 allele was confirmed in each sample by the previously mentioned deletion PCR (data not shown). In addition, DNA was extracted from lin^+ bone marrow (BM) cells isolated from the same mice and used as template for the deletion PCR amplification (Fig.12B). Jag2 genotyping PCR amplification of the same DNA samples identified the wt product in both samples as expected, whereas the floxed allele was only amplified from the $Jag2^{lox/lox}$ control DNA (Fig.12C). These results indicated that the $Jag2^{lox/lox}$ MxCre mice did express the Jag2 mRNA, even though efficient Cre-mediated recombination of the floxed Jag2 allele had occurred.

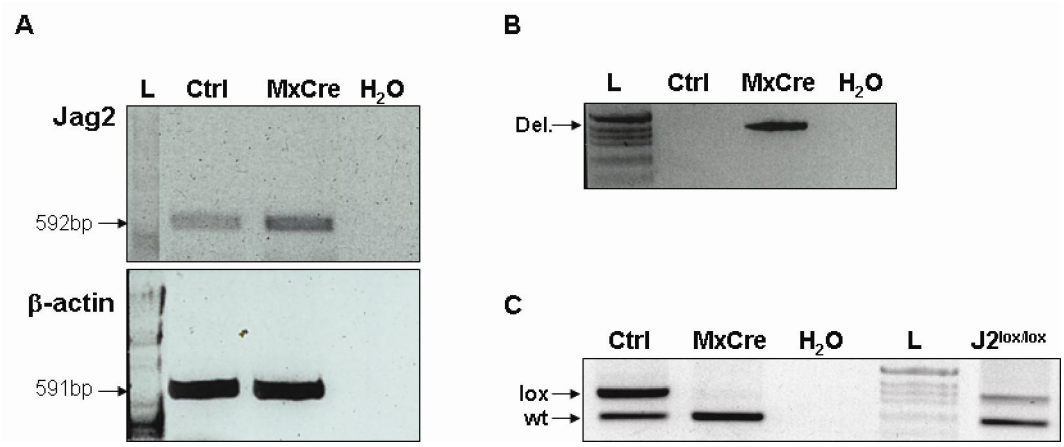

Figure 12. Jag2 expression by RT-PCR and deletion efficiency. (A) Top panel: Jag2 RT-PCR amplification of cDNA derived from sorted DN thymocytes identifies a 592bp product in both control (ctrl) and deleted (MxCre) samples. Bottom panel: β-actin PCR amplification. (B) The deletion PCR of DNA derived from the lin^+ BM cells of the $Jag2^{lox/lox}$ MxCre mice identifies the 456bp deletion band. (C) Jag2 PCR of same DNA as (B) amplifies the lox and the wt products in control samples, but only the wt product in the deleted sample (MxCre). Last lane: $Jag2^{lox/lox}$ tail DNA control. L: 1kb DNA ladder.

In conclusion efficient Cre-mediated recombination of the floxed Jag2 allele did occur when $Jag2^{lox/lox}$ mice were crossed with the inducible MxCre mouse strain. Nevertheless, Jag2 mRNA expression was detectable in the deleted homozygous mice.

3. Discussion and perspectives

The aim of this project was to generate a floxed Jag2 mouse strain in order to study Notch signaling, via the Jagged2 ligand, in an *in vivo* loss-of-function context. Therefore, ES cells carrying a floxed Jag2 allele were used to generate homozygous $Jag2^{lox/lox}$ mice. Successful excision of the Neomycin cassette from the Jag2 recombined targeting vector was also shown. However, a discrepancy between the PCR genotyping and the Southern blot analysis was observed. Several strategies of PCR amplifications and Southern blot analyses have confirmed an incomplete homologous recombination of the targeting vector. These results suggested an integration of the 5'short arm within the 5'UTR of the endogenous Jag2 gene without the replacement of the genomic Jag2 sequence.

Despite the partial recombination event, we further demonstrated efficient Cre-mediated excision of the deletion arm by crossing the Jag2 floxed mice with MxCre transgenic mice. Nevertheless, the Jag2 gene was still expressed in the deleted tissues, as proven by RT-PCR. Since Jag2 mRNA is present in deleted DN thymocytes, its protein should also be expressed. To confirm this hypothesis we performed Western blot analysis on dendritic cells (DC). Jag2 was shown to be expressed in DC, though at higher level when stimulated by mesenchymal stem cells (Zhang et al., 2009). We thus expanded DC isolated from $Jag2^{lox/lox}$ MxCre mice in culture for one week before harvesting and lysing the cells. Jurkat cells were used as a control. Although the Jag2 protein was detected in the Jurkat lysate, no expression could be identified in any of the DC samples. The Western blot conditions were also tested on scraped epidermis from a wt mouse with no result. These experiments need to be repeated and conditions improved.

Alternatively, Jag2 protein expression can also be investigated by crossing Jag2 floxed homozygous mice with K14Cre mice. Immunostaining for Jag2 could then be performed on sections from the skin of $Jag2^{lox/lox}$ K14Cre mice. In parallel, $Jag2^{lox/lox}$ mice could also be crossed with $Jag1^{lox/lox}$ K14Cre mice thereby generating double mutant $Jag1^{lox/lox}Jag2^{lox/lox}$ K14Cre mice. The double knockout mice would be monitored for the severity of their phenotype compared to $Jag1^{lox/lox}$ K14Cre mice. These experiments are ongoing.

In conclusion, the Jag2 mRNA expression in the deleted $Jag2^{lox/lox}$ mice could not be effectively abolished. Consequently, these mice were unsuitable for loss-of-function investigations. Therefore, in order to analyze the role of Jag2 *in vivo* by conditional deletion

in the hematopoietic system or in the skin, floxed Jag2 mice were obtained from the Jackson laboratory in collaboration with Dr. Thomas Gridley. The targeting vector strategy designed by Jingxia Xu is similar to the one described in this chapter. Briefly, the deletion arm flanked by loxP sites also consists of the ATG translation start site and exons 1 and 2 of the Jag2 gene. Efficient excision, which creates a null allele, was confirmed by crossing the floxed homozygous mice with Meox2-Cre mice. The Meox2-Cre mouse strain expresses Cre recombinase in the germline (Tallquist and Soriano, 2000), thus generating embryos bearing a Jag2 null allele. Hence, homozygous Jag2 null mutant mice exhibited an identical phenotype to the null mutant $Jag2^{\Delta DSL/\Delta DSL}$ (Jiang et al., 1998). The mice died at birth and exhibited syndactyly as well as palate-tongue fusion (Xu, 2009).

III. Notch2 reporter

III. Generation of a Notch2 reporter mouse

1. Introduction

Notch signaling is an essential pathway in intercellular communication involved in cell fate determination, stem cell maintenance and differentiation in a variety of tissues during development and homeostasis. The second Notch receptor to be identified in mammals was Notch2 from a rat cDNA library (Weinmaster et al., 1992). *In situ* hybridization analyses of E16 rat embryos have revealed both overlapping and differential expression of Notch1 and Notch2. For example, Notch2 mRNA was highly expressed in the spleen compared to Notch1. Furthermore, Notch1 and Notch2 were expressed in different cell types and at different time points during brain development in rat and in mouse, suggesting that Notch1 and Notch2 may have complimentary roles (Higuchi et al., 1995; Weinmaster et al., 1992). Several other organs were shown to express both receptors, such as the eye, the kidney, the intestine and the skin (Rangarajan et al., 2001; Riccio et al., 2008; Weinmaster et al., 1992).

Moreover, Notch2 expression was shown to be indispensable for post-implantation development in mice by the generation of $Notch2^{-/-}$ mice. A mutation replacing 5 out of 6 ankyrin repeats of the Notch2 receptor by the β-galactosidase gene resulted in embryonic lethality, in homozygous mutants, prior to E11.5. The Notch2-deficient mice died due to the widespread onset of apoptosis throughout the embryo at E9.5 (Hamada et al., 1999).

Since Notch2 knockout mice do not survive into adulthood, a Notch2 conditional mutant mouse was generated to study tissue-specific deletion of the receptor (Saito et al., 2003). Notch2 conditional deletion in the hematopoietic system revealed a role during cell-fate decision in B cells. Loss of Notch2 blocked B cell differentiation during commitment to marginal zone B-cells. The function of Notch2 was restricted as no other B cell lineage was affected by the loss of Notch2 (Saito et al., 2003). Even though Notch2 was shown to be expressed in thymocytes by semi-quantitative RT-PCR (Kaneta et al., 2000), no T cell development defect was observed in the Notch2-deficient mice (Saito et al., 2003). Similarly, although Notch2 is expressed in the murine epidermis its specific deletion in the skin during embryogenesis did not impair skin development and deletion in the adult mouse only resulted in a minor hair phenotype (Rangarajan et al., 2001; Vauclair, 2006).

The function of Notch2 in several organs was also investigated by a hypomorphic Notch2 mutation. The targeted disruption of Notch2 resulted in alternatively spliced

transcripts which had one or two EGF-like repeats deleted. Mice homozygous for the mutation died perinatally from defects in glomerular development in the kidney. The mutant mice also exhibited heart and eye vasculature defects (McCright et al., 2001), thereby suggesting a role for Notch2 in these tissues.

The importance of the Notch2 receptor in many different organs is reflected by its implication in various diseases. As described earlier, Notch2 is crucial during B cell differentiation into marginal zone B cells in mice. Thus, it is not surprising that high Notch2 expression was linked to splenic marginal zone lymphoma (Troen et al., 2004), thereby suggesting that Notch2 might also function as a cell-fate switch in human B cells. Additionally, Notch2 was overexpressed in B-cell chronic lymphocytic leukemia and involved in the overexpression of the glycoprotein CD23, a hallmark of this disease (Hubmann et al., 2002). Notch2 deregulation was also observed in human skin diseases, as its expression was down-regulated in psoriatic plaques and in human basal cell carcinoma (Thelu et al., 2002).

A well-documented illness in which Notch2 plays a role is the Alagille syndrome (AGS). AGS is a dominant highly variable disorder characterized by hepatic bile duct paucity, kidney, cardiac, skeletal and ophthalmologic manifestations. Although mutations in the Jagged1 ligand are associated with 94% of patients suffering from AGS (Li et al., 1997; Oda et al., 1997), the majority of the other 6% of AGS cases have alterations in the Notch2 gene (McDaniell et al., 2006). Accordingly, the described mouse model for AGS is heterozygous for the Jag1 null allele and for a Notch2 hypomorphic allele. The double heterozygous mice exhibited bile duct differentiation defects as well as cardiac, ocular and renal deficiencies (McCright et al., 2002).

Expression and targeted deletion studies of Notch2 suggest diverse roles as well as a complex interplay of receptor-ligand interactions. In spite of its importance in the development and homeostasis of several organs, and of its role in diseases, a precise *in vivo* tool for visualization and identification of Notch2 signaling activity is still lacking. Even though two reporter mice for Notch signaling have recently been described, both transgenic mouse lines respond to canonical Notch signaling mediated by all four receptors.

The first example of a Notch reporter mouse is the Notch activity sensor mouse (NAS). The reporter transgene harbors 12 multimerized head-to-tail RBP-Jκ binding sites upstream of

the lacZ gene. This TP1 promoter is transactivated in a RBP-Jκ dependant manner by all four mammalian Notch receptors. Due to the artificial structure of multiple transcription binding sites, NAS transgenic mice do not display β-galactosidase staining in several tissues known to depend on Notch signaling, such as lymphoid organs (Souilhol et al., 2006).

The second transgenic Notch reporter mouse (TNR), or Tg(Cp-EGFP)25Gaia/J, bares an enhanced green fluorescent protein (EGFP) reporter driven by four tandem copies of the RBP-Jκ binding site consensus sequence. The transgene was used to read out canonical Notch signaling in the hematopoietic and nervous systems. The study reported Notch signaling activity in hematopoietic stem cells *in vivo* and Notch down-regulation upon differentiation (Duncan et al., 2005). Additionally, Notch activity was detected in the epidermis and in regions of the hair follicle (Estrach et al., 2006). These results demonstrate the efficiency of the TNR transgenic mouse line to study Notch signaling *in vivo*. However, similarly to the NAS reporter mouse previously described, the TNR reporter responds to all four Notch receptors through RBP-Jκ binding to an artificial promoter.

In addition to canonical Notch signaling reporter mice, other reports described alternative approaches. The first strategy takes advantage of a Notch target gene promoter, to drive a reporter gene, instead of multimerized RBP-Jκ binding sites. Accordingly, the Hes5 promoter was used to express a GFP reporter gene. The promoter region amplified for the Hes5-reporter was a 3kb fragment, which also included repressor elements and potential binding sites specific for transcription factors other than RBP-Jκ. This method successfully identified multipotent progenitors in the embryonic nervous system but only upon Hes5 expression (Basak and Taylor, 2007). This reporter system is limited due to the need of Notch-induced Hes5 expression and, consequently, is a useful tool in tissues where Hes5 expression correlates with Notch-signaling, such as in the central nervous system (CNS).

Following a similar strategy, two different reporter mice were generated with a GFP-expressing transgene driven by either Hes1 or Hes5 promoters. In this study, a 2.5kb promoter region was used for the Hes1 reporter and less than 1kb for the Hes5 reporter. Both Hes1 and Hes5 are Notch target genes expressed in the developing CNS, although in distinct patterns in different brain regions, suggesting differential regulation. Moreover, their complementary expression pattern was enhanced in the reporter mice (Ohtsuka et al., 2006). Consequently, these results cannot be assimilated to a direct Notch signaling read-out.

The third approach is dependant on Notch1 proteolysis to follow descendants of cells having undergone Notch1 activation. The N1IP (Notch1 intramembrane proteolysis)-Cre reporter (Notch1$^{tm3(cre)Rko}$/J) consists of a Cre recombinase replacing the intracellular domain of Notch1, which is released upon interaction with a ligand (Vooijs et al., 2007). Crossing these reporter mice with the Rosa26R mouse line allows lineage tracing investigations. The Rosa26R mouse line carries a loxP-flanked neo sequence (STOP cassette) which prevents expression of a lacZ reporter gene (Soriano, 1999). Consequently, when crossed with N1IP-Cre mice, the STOP cassette is recombined upon Notch1 signaling-induced Cre. The recombined allele is then inherited in all descendants. A major disadvantage of this system is that β-galactosidase staining does not correspond to the precise timing when the Notch1 signal occurred. Furthermore, because the recombined allele lacking the STOP cassette is inherited by all daughter cells irrespective of an ongoing Notch signaling, Notch1 activation at later time points, such as in the adult, cannot be investigated by this method.

Even though several different Notch signaling reporter mice do exist, none of them specifically responds to Notch2-specific signaling. Therefore, we sought to generate a valuable tool to follow cells which have specifically received a Notch2 signal. The Notch2 reporter strategy consists of two complementary transgenes: a chimeric Notch2 receptor and a secondary reporter. The chimeric Notch2 consists of the extracellular domain of the receptor fused in frame with a DNA binding and a transactivating domain (TAD). Once the chimeric Notch2 receptor is cleaved by interaction with its specific ligand, the intracellular domain, consisting of the DNA binding domain and the TAD, translocates to the nucleus. The Notch2-mediated signal is then conveyed by binding of the intracellular domain to specific response elements of a secondary reporter, which subsequently induces expression of a red fluorescent protein (Fig.1).

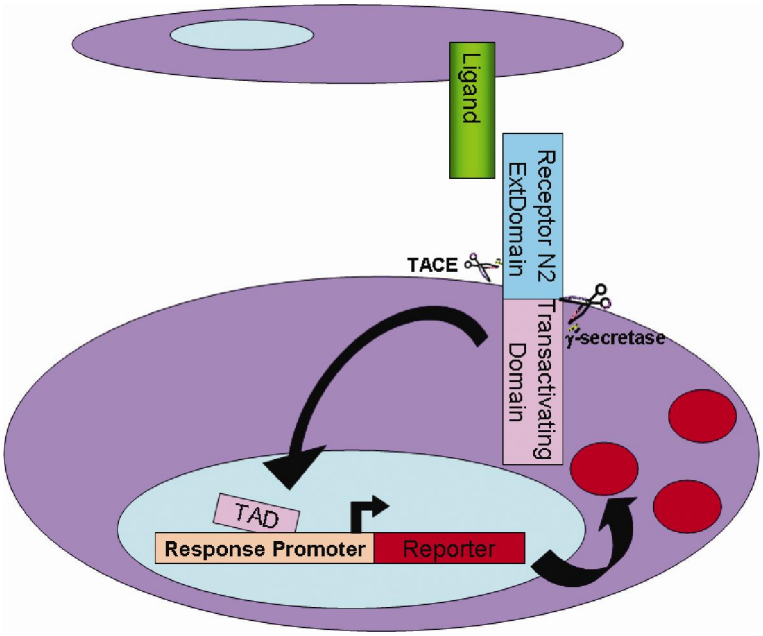

Figure 1. Schematic design of Notch2 reporter signaling activity. A specific ligand, i.e. Jagged or Delta-like, binds to the extracellular domain of the Notch2 receptor, thereby activating the consecutive proteolytic cleavages by TACE and γ-secretase complex which release the DNA binding and transactivating domains (TAD). The TAD of the chimeric construct replaces the intracellular domain of Notch2 and is consequently translocated to the nucleus where it binds to its response elements. The interaction with the response promoter in turn activates transcription of the reporter gene. The latter is a red fluorescent protein which therefore renders the cell receiving a Notch2-mediated signal detectable by becoming red.

This strategy will detect Notch2-mediated signal receiving cells in any tissue at any given point in time. Thus, the genetic design for the Notch2-specific reporter is different in very specific ways than for the previously described reporter mice.

2. Results

2.1 Generation of the chimeric Notch2/tTA2 receptor

As schematicaly shown in Fig.1, the Notch2 reporter strategy consists of two complementary elements: the chimeric Notch2 receptor and its specific reporter. The chimeric Notch2 plasmid was generated by using components of the Tet-Off technology. The rationale behind the system is to replace the cytoplasmic domain of Notch2 with a tetracycline-controlled transactivator (tTA2) which is fused in frame with the extracellular and transmembrane domains of Notch2. The tTA2 transactivator is a fusion protein between the repressor (TetR) of the Tn*10*, the tetracycline resistance operon of *Escherichia coli*, and a C-terminal portion of the minimal transcriptional activation domain derived from Herpes simplex virus protein 16 (VP16). Compared to the first version known as tTA, tTA2 comprises of TetR fused to three activation domains and is tolerated in cells at higher concentrations for the same activity (Baron et al., 1997). This transactivating domain will activate transcription only in the absence of the effector tetracycline, or any of its derivatives such as doxycycline, by binding of TetR to *tet* operator (*tetO*) sequences upstream of a minimal promoter. In contrast, the presence of tetracycline prevents tTA2 from binding to its target, thus abolishing transcription (Fig.2).

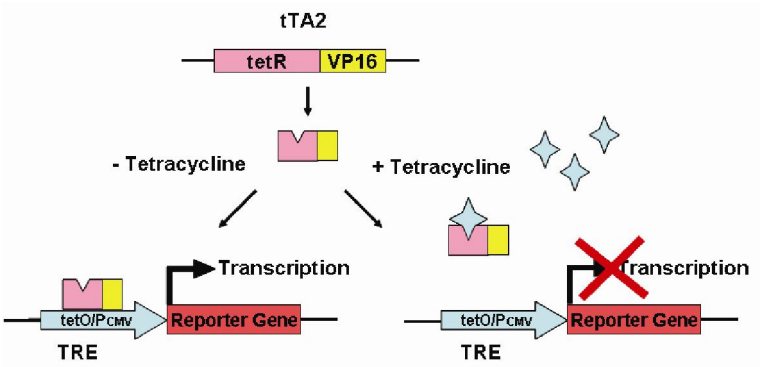

Figure 2. Tet-off system. In absence of tetracycline the transactivating domain tTA2 binds to Tet response elements (TRE) upstream of a minimal promoter (P_{CMV}) and activates transcription of the reporter gene. In presence of tetracycline (blue diamonds) tTA2 can no longer bind to its target thereby abolishing transcription.

Generation of the chimeric Notch2/tTA2 receptor was achieved in several steps. First, the tTA2 transactivator was subcloned from the pUHD20-1 plasmid received from Dr. Bujard (Baron et al., 1997) into the pBluescriptSK backbone. The tTA2 sequence was then amplified

by high-fidelity PCR in order to add the restriction sites PvuI and NotI, up- and downstream of the transgene, respectively.

tTA2 primers with PvuI and NotI restriction sites:

5'AGTTGA**CGATCGAGGCGCCATGTCTAGATTAGATAAAAGTAAAGTGATTAA CAGCG** 3'

5'GCATCA**GCGGCCGCAAGCTTGGTCGAGCTGGATACTTCCC** 3'

Finally, these restriction enzymes were used for digestion of both the tTA2 PCR product and the pTracer-CMV vector containing the full length Notch2 sequence. Subsequent ligation resulted in the fusion in frame of the tTA2 transactivator downstream of the transmembrane domain of the Notch2 receptor. The restriction enzyme PvuI also cut once in the ampicillin resistance cassette of the vector backbone, which is the reason why a three-way ligation was performed (Fig.3B). The unique PvuI restriction site within the Notch2 receptor is located downstream of the RAM domain, precisely 252bp downstream of the TM, which is upstream of the ankyrin repeats (Fig.3A). Ligated clones were tested by two different digestion patterns: EcoRI/NotchI double digest, which resolves two fragments of 5.7kb and 6.6kb in correctly ligated clones, and an HpaI single digest, which is predicted to linearize the vector resulting in a single 12.3kb band if the tTA2 gene is present (Fig.3C). One of the positive vectors was also partially sequenced by custom up- and downstream primers (T7 and BGH rev) as well as by an internal primer designed to sequence the TM region of the chimeric transgene. Obtained sequences aligned as expected.

Internal N2 primer: 5'CAGTGAACTGGAGAGTCC 3'

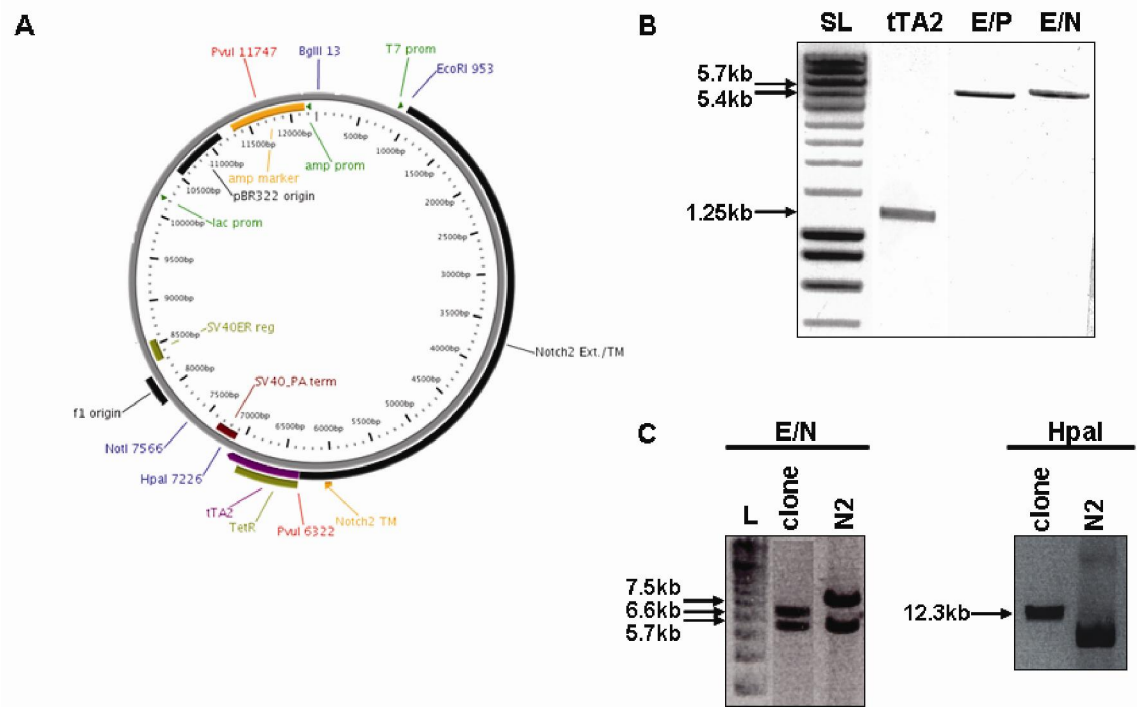

Figure 3. Generation of the chimeric Notch2/tTA2 vector. (A) Plasmid map of the Notch2/tTA2 sequence shows unique restrictions sites in blue and both PvuI restrictions sites in red. The Notch2 extracellular domain, the transmembrane domain (TM), as well as tTA2 gene are indicated. (B) 0.8% TAE agarose gel represents the isolated fragments for the three-way ligation of the chimeric Notch2/tTA2 vector. E/P: EcoRI and PvuI double digest; E/N: EcoRI and NotI double digest of the Notch2 full length plasmid. SL: Smart ladder. (C) Diagnostic digestion patterns for one correctly ligated clone with EcoRI/NotI double digest (E/N) and with HpaI identify the expected band sizes (arrows). L: 1kb DNA ladder.

Once generated, the chimeric Notch2/tTA2 receptor had to be inserted permanently into the mouse genome. One method to integrate and express a transgene is the bacterial artificial chromosome (BAC) technology, which is a plasmid encompassing 100-300kb of genomic DNA. Homologous recombination into a Notch2-containing BAC enables targeted integration of the modified Notch2 gene while conserving regulatory sequences found within its genomic sequence. This strategy enables a similar expression of the chimeric Notch2/tTA2 to the endogenous Notch2 gene.

For recombination into the corresponding BAC, the chimeric Notch2/tTA2 gene was flanked by homologous regions to both the immediate up- and downstream sequences of the Notch2 translation start site (i.e. ATG). For this purpose, three different BAC clones, namely RP23-268C11, -69J13 and -143I22 (Fig.4A), were purchased from the BACPAC Resources Center of the Children's Hospital Oakland Research Institute (CHORI) and a PCR strategy

for both regions was designed. The 5'homologous arm is 566bp long and consists of the genomic region 400bp upstream of exon1 and the portion of exon1 immediately upstream of the initiating ATG. The 3'homologous arm consists of the portion of exon1 immediately downstream of the initiating ATG and 853bp of the first intron (Fig.4B). The 5'arm was directly inserted via restriction enzymes AflII and EcoRI. However, an oligonucleotide sequence containing an AgeI restriction site was added downstream of the Notch2/tTA2 transgene before ligation with the 3'homologous arm. Orientation of the latter and sequences of both homologous arms were confirmed by sequencing with custom primers (CMVfor and BGHrev).

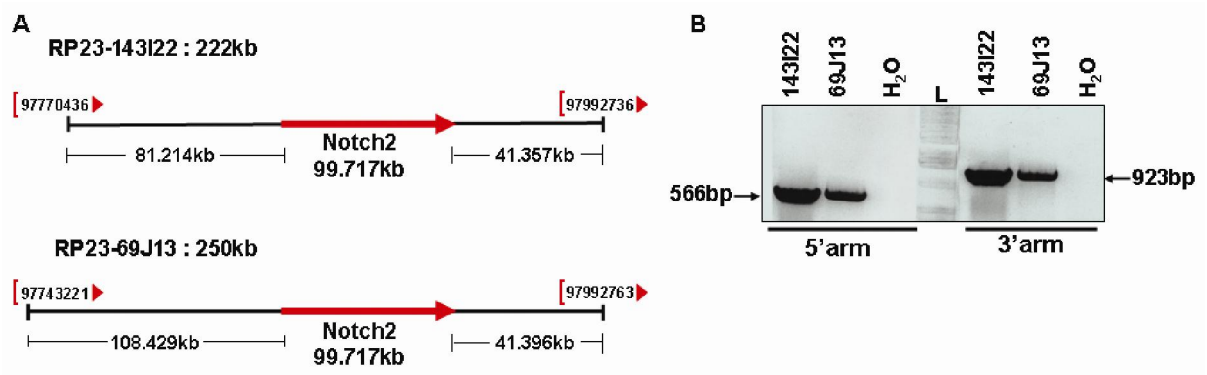

Figure 4. Bacterial artificial chromosomes including the Notch2 genomic sequence. (A) Two BACs, RP23-143I22 and -69J13, are schematically drawn spanning the Notch2 region of the mouse genome (red arrow). Sizes in kb are given up- and downstream of Notch2. (B) Agarose gel electrophoresis of PCR amplifications corresponding to the 5'(566bp) and 3'(923bp) homologous arms of Notch2 from two of the BACs (RP23-143I22 and -69J13). L: 1kb DNA ladder.

In addition to the homologous arms, an ampicillin resistance (Amp) cassette flanked by 34bp FLP1 recombinase target (FRT) sites was cloned between the 5' homologous box and the Notch2/tTA2 gene via the unique EcoRI restriction site (Fig.5A). Ampicillin resistance allows subsequent selection of correctly integrated BAC clones. The Amp cassette can be removed in a second step by FLP-mediated recombination, which induces excision of the intervening sequence and leaves a single FRT site in place. Efficient FLP-mediated recombination of the FRT sites was tested by transforming the final construct into the *E.coli* strain 294-FLP (Buchholz et al., 1996). This bacteria strain was engineered to efficiently express the FLP recombinase gene. Complete excision of the Amp cassette was confirmed by digesting the 294-FLP transformed Notch2/tTA2 vector with the restriction enzyme PvuI. The

Amp sequence bears a PvuI restriction site which is thus lost upon flipase recombination of the resistance cassette (Fig.5).

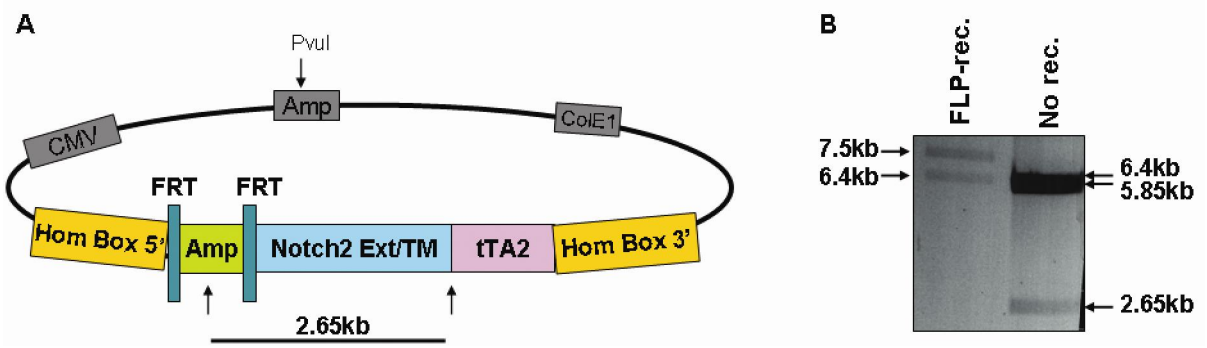

Figure 5. Schematic representation of the chimeric Notch2/tTA2 vector. (A) Homologous boxes to Notch2 genomic sequences, Hom Box 5' and Hom Box 3' (orange), flank Notch2 extracellular (Ext) and transmembrane (TM) domains (dark blue) fused in frame with tTA2 (pink). An ampicillin cassette (Amp; green) flanked by FRT sites (turquoise) is inserted between the Hom Box 5' and the ATG of the Notch2/tTA2 transgene. The three PvuI cutting sites are indicated by arrows. (C) Agarose gel electrophoresis of PvuI digested chimeric Notch2/tTA2 plasmid. FLP-mediated recombination by propagation into 294-FLP bacteria identifies two bands (FLP-rec.) compared to three fragments before transformation (No rec.). Arrows with the band sizes of the fragments are indicated.

2.2 Generation of the secondary reporter

As mentioned earlier, detection of the Notch2-receiving cell is conveyed by binding of the TetR domain of the chimeric Notch2/tTA2 to its specific response transgene. Therefore, the reporter construct harbors a destabilized DsRed coding sequence which is driven by a multimerized Tet Response Element (TRE). The TRE consists of seven *tet* operator sequences upstream of a minimal cytomegalovirus (CMV) promoter. The reporter DsRed is a red-shifted protein derived from the marine organism *Discosoma* (Matz et al., 1999). Several variants of DsRed, such as DsRed.T3 and DsRedExpress, were cloned before settling for the most destabilized form known as DsRedExpressDR. The latter is a fast-maturing version of the red fluorescent protein which is fused to the degradation domain of mouse ornithine decarboxylase at its C-terminal end conferring a short half-life to the reporter protein (Hansson et al., 2006).

The original TRE-Tight-DsRed2 vector from Clontech was used for the backbone of the secondary reporter. The 2.6kb backbone containing the TRE sequence was isolated after a BamHI/NotI digestion. The DsRed2 gene was replaced by the DsRed.T3-c-myc version

kindly provided by Dr. Gérard Eberl. The 700bp transgene was isolated after AscI/NotI digestion. The restriction sites BamHI and AscI were blunted with Klenow DNA polymerase in order to ligate both fragments. Another DsRed version, the DsRedExpress gene, was also cloned into the TRE backbone. The 686bp DsRedExpress gene was isolated from the DsRedExpress-N1 vector (Clontech) by EcoRI/NotI digestion. The same digestion was used to isolate the 2.6kb TRE-containing backbone from the previously cloned TRE-Tight-DsRed.T3-c-myc vector.

The final secondary reporter was cloned in two steps. Firstly, the DsRedExpressDR gene was subcloned into pBluescriptSK, via XhoI/EcoRI digestion, from the 12CSL-DsRedExpressDR vector (kind gift from Dr. Urban Lendahl). The 817bp DsRedExpressDR transgene was then isolated by XhoI/NotI digestion (Fig.6A) and the restriction site XhoI was blunted by Klenow DNA polymerase. This time the 2.6kb TRE-containing backbone from the previously cloned TRE-Tight-DsRed.T3-c-myc vector was isolated by SmaI/NotI digestion. Each cloned vector was checked for correct ligation by diagnostic digestion patterns and subsequently confirmed by sequencing. The table below summarizes the cloning steps performed for the generation of each reporter vector.

Vectors	**Restriction enzymes ([] when blunted)**	**Ligated vectors (backbone with insert)**
TRE-Tight-DsRed2 DsRed.T3-c-myc	[BamHI]/NotI [AscI]/NotI	TRE-Tight-DsRed.T3-c-myc 2.6kb with 700bp
TRE-Tight-DsRed.T3-c-myc DsRedExpress-N1	EcoRI/NotI EcoRI/NotI	TRE-Tight-DsRedExpress 2.6kb with 686bp
12CSL-DsRedExpressDR pBlueScriptSK TRE-Tight-DsRed.T3-c-myc pBS-DsRedExpressDR	XhoI/EcoRI XhoI/EcoRI SmaI/NotI [XhoI]/NotI	pBS-DsRedExpressDR 2.9kb with 817bp TRE-Tight-DsRedExpressDR 2.6kb with 817bp

The TRE-Tight-DsRedExpressDR was digested by StuI and by XhoI and compared to TRE-Tight-DsRed.T3-c-myc digestion patterns. The restriction enzyme StuI excised the DsRedExpressDR gene as expected, which was slightly larger than the DsRed.T3 gene. As the DsRedExpressDR contained an additional XhoI restriction site, three fragments were identified instead of two (Fig.6B).

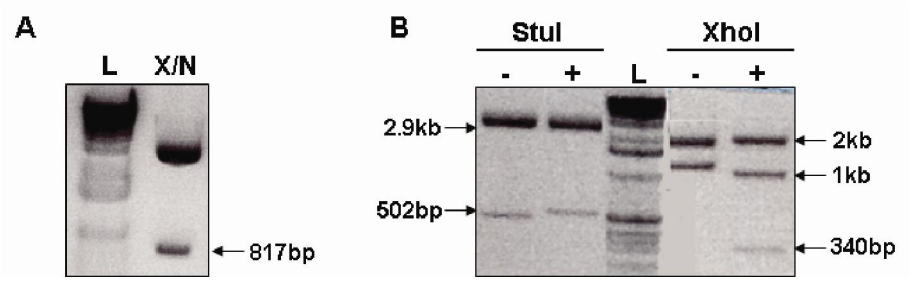

Figure 6. Cloning of the TRE-DsRedExpressDR vector. (A) The 817bp DsRedExpressDR gene is isolated by a double digest XhoI/NotI (X/N) of the pBS-DsRedExpressDR vector. (B) Agarose gel electrophoresis of digestion patterns of a positive clone (+) by restriction enzymes StuI and XhoI identify expected band sizes (arrows). L: 1kb DNA ladder.

The positive clone was then confirmed by sequencing reactions, which were performed by using custom primers (T7 and T3) for the pBS-DsRedExpressDR vector and an internally designed primer for the reporter vector.

Internal DsRedExpress primer: 5'ATGGCCTCCTCCGAGGACGTCATC 3'

2.3 Co-culture assays determine the functionality of the Notch2 reporter system

After generation of both constructs, the complete Notch2 reporter system was tested *in vitro*. Co-cultures of Hela cells expressing a Notch ligand, i.e. Delta-like1 (Dll1), with Hela cells transfected with the TRE-DsRedExpress reporter and with or without the chimeric Notch2/tTA2 construct were set up. Red Hela cells expressing the DsRedExpress reporter were visible when all the elements for the Notch2-mediated signaling were present (Fig.7A). Accordingly, the DsRedExpress protein was only detected when Dll1 cells were co-cultured with Hela cells co-transfected with both the reporter and the chimeric Notch2/tTA2 constructs. Furthermore, the signal was specific to the Notch2 activation since no red cells were detected when the reporter was transfected alone in co-cultures (Fig.7B).

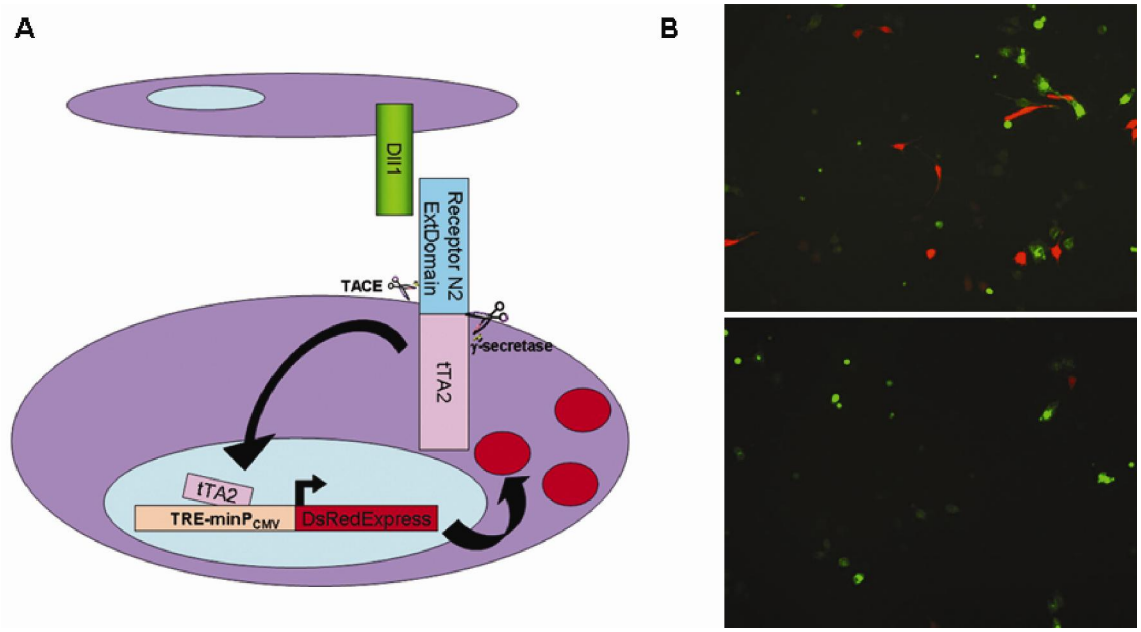

Figure 7. Co-cultures of Dll1-expressing Hela cells with the chimeric Notch2/tTA2 receptor and the DsRedExpress reporter. (A) Schematic representation of the Notch2/tTA2 chimeric receptor (blue) interacting with a specific ligand, e.g. Delta-like 1 (Dll1;green), on the surface of a neighboring cell. This ligand-receptor binding induces proteolytic cleavages which subsequently release the transactivating domain tTA2 (pink). tTA2 binds to the Tet response elements (TRE; light pink) in the nucleus and activates transcription of the reporter gene DsRedExpress (red). (B) Top panel: Co-culture of Hela cells expressing the Dll1-eGFP ligand (green) with co-transfected cells for Notch2/tTA2 and TRE-DsRedExpress proves interaction occurrence by subsequent expression of DsRedExpress protein (red). Bottom panel: Negative control co-culture of Dll1-eGFP Hela cells with Hela cells transfected with the reporter plasmid TRE-DsRedExpress alone.

The functionality of the chimeric Notch2/tTA2 transgene, as well as the robustness of the reporter, was proven *in vitro*. However, for the reporter mouse to be a useful tool the system must not interfere with endogenous Notch2 signaling. As described earlier, the tTA2 gene is fused downstream of the RAM domain. The RAM domain was shown to bind, in conjunction with the ankyrin repeats, to the RBP-Jκ transcription factor in stromal cells isolated from murine bone marrow *in vitro* (Deregowski et al., 2006). Consequently, the presence of the RAM domain in the chimeric Notch2/tTA2 vector could potentially interfere with endogenous Notch2 signaling. This potential interference, although unlikely due to the absence of the ankyrin repeats, was nonetheless analyzed by luciferase co-culture experiments using a Notch signaling reporter. This reporter consisted of 12 multimerized RBP-Jκ binding sites upstream of the firefly luciferase gene. Expression of the luciferase was highly induced when Hela cells are co-transfected with a plasmid containing the Notch1 intracellular domain.

When the chimeric Notch2/tTA2 was co-transfected together with the 12RBP-Jκ luciferase reporter the signal was similar to basal level (Fig.8B). These results verify that the chimeric Notch2/tTA2 receptor does not induce Notch signaling.

Moreover, the Notch2/tTA2 construct had to be specific to ligand-induced Notch proteolytic cleavages. To inhibit Notch signaling, Hela cells co-cultures were treated with the γ-secretase inhibitor DAPT, or *N*-[*N*-(3,5-difluorophenacetyl)-l-alanyl]-*S*-phenylglycine *t*-butyl ester. Compared to control DMSO treated cells, no red fluorescent protein was detectable upon DAPT treatment (Fig.8A). This data demonstrates that specific inhibition of Notch signaling impedes on DsRed expression and hence on Notch2/tTA2 cleavage.

Verification of the reporter system also included testing the Tet-off technology. As schematized in Fig.2, the tTA2 domain can be inactivated by addition of the tetracycline derivative doxycycline. Therefore, Hela co-cultures of Dll1-expressing cells with Notch2/tTA2 transfected cells were treated with 2μg/ml of doxycycline, which indeed hinders the expression of the red fluorescent protein as expected (Fig.8A).

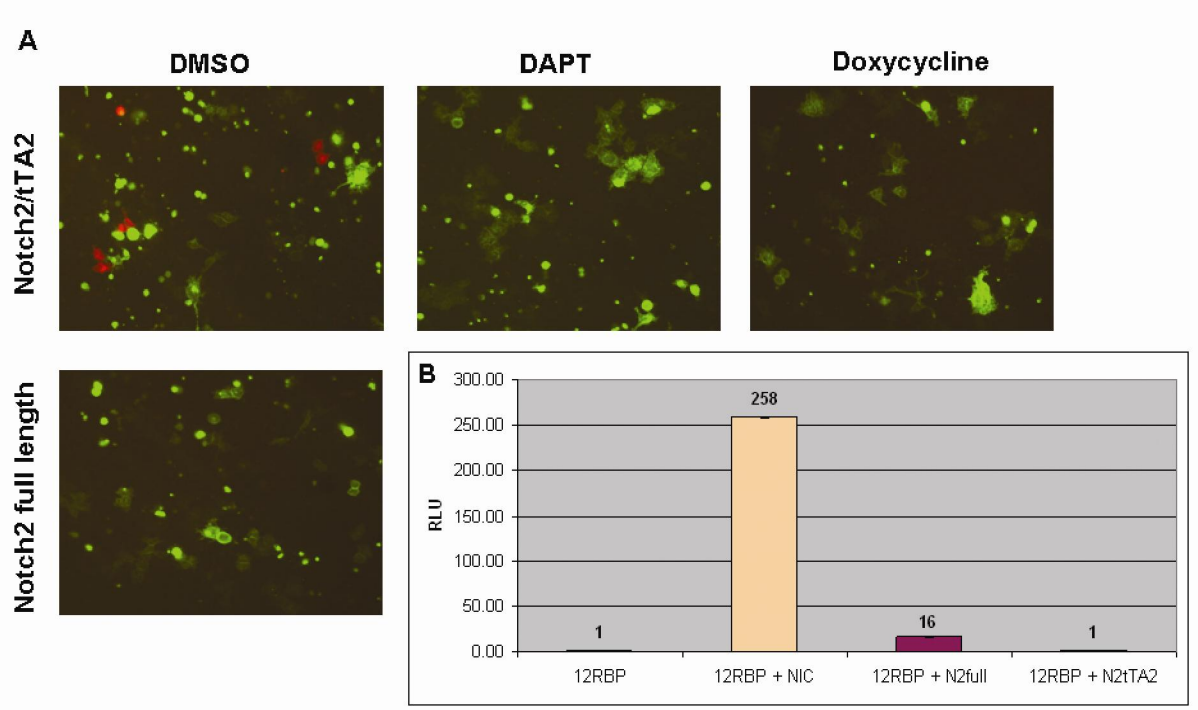

Figure 8. The Notch2/tTA2 reporter system is inhibited by DAPT and by doxycycline. (A) Co-cultures of Notch2/tTA2 and TRE-DsRedExpressDR co-transfected Hela cells (red) with Dll-1 expressing cells (green) were treated with 1mM DAPT or 2µg/ml doxycycline. Equivalent amount of DMSO was added in control. As co-culture negative control the Notch2 full length construct was transfected into Hela cells instead of the chimeric Notch2/tTA2. (B) Luciferase reporter assay was performed on Hela cells co-transfected with 12RBP-Jk-luciferase (12RBP) and Notch2/tTA2 chimeric constructs. NIC: Notch1 intracellular domain; N2full: Notch2 full length; RLU: relative luciferase units normalized to renilla luciferase.

Since the DsRedExpressDR protein is fast-maturing and rapidly degraded, this "real-time" detection does not allow a long-term lineage tracing of cells which have received a Notch2 signal. Therefore, we decided to combine the above strategy with a system to track cells that have once received a Notch2-mediated signal, and which may not signal any longer. For this purpose we focused on an inducible Cre/loxP-based lineage strategy. This method takes advantage of the mutated ligand-binding domain of the human estrogen receptor fused to the Cre recombinase (Cre^{ERT}). The Cre^{ERT} recombinase gene allows conditional site-specific recombination dependant on the estrogen receptor antagonist 4OH-tamoxifen, and not on estradiol (Feil et al., 1996). Lineage tracing is then possible by crossing the reporter mice bearing the Cre^{ERT} with Rosa26R mice (129S-Gt(ROSA)26Sor^{tm1Sor}/J; JAX stock#003310). This Rosa26R mouse line carries a loxP-flanked neo sequence (STOP cassette) which prevents expression of a β-galactosidase (lacZ) reporter gene (Soriano, 1999).

Consequently, when crossed with a Cre-expressing mouse strain the STOP cassette is recombined thereby removing the block for expression of the lacZ reporter (Fig.9B).

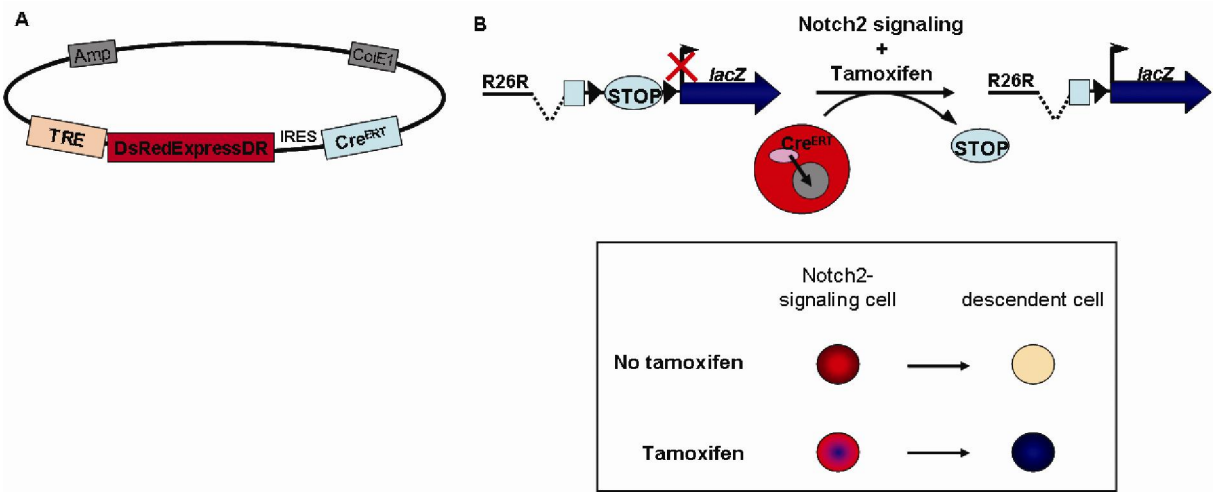

Figure 9. Schematic representation of the secondary reporter and lineage tracing principle. (A) The Tet response element (TRE; light pink) controls the expression of the DsRedExpressDR reporter gene (red) and an internal ribosome entry site (IRES) upstream of the Cre^{ERT} recombinase gene (light blue). (B) Lineage tracing approach involves crossing the Notch2 reporter mouse with a Rosa26R mouse and injecting tamoxifen to the offspring. 4OH-tamoxifen induces expression of the lacZ reporter by removal a STOP cassette. The box below represents the lacZ expression of the Notch2-signaling descendent cells with and without 4OH-tamoxifen injection. DsRedExpressDR expression is in red and lacZ expression is in blue.

Therefore, the tamoxifen-inducible Cre^{ERT} recombinase gene, together with an internal ribosome entry site (IRES), was cloned downstream of the DsRedExpressDR gene (Fig.9A). The TRE-DsRedExpressDR-ires-Cre^{ERT} vector was tested in Hela cell culture experiments *in vitro* to prove the functionality of the system. In order to visualize correct recombination mediated by the Cre^{ERT} recombinase, the reporter construct is co-transfected with a CMV-driven plasmid containing eGFP downstream of a loxP-flanked Stop cassette (Fig.10A). The TRE-DsRedExpressDR-ires-Cre^{ERT} was expressed by co-transfecting with CMV-tTA2, and the inducible Cre ^{ERT} recombinase was subsequently activated by addition of 4OH-tamoxifen directly to the medium for 24 hours. As expected for a successful recombination event, Hela cells expressed the eGFP reporter when induced with tamoxifen as opposed to the ethanol control (Fig.10B).

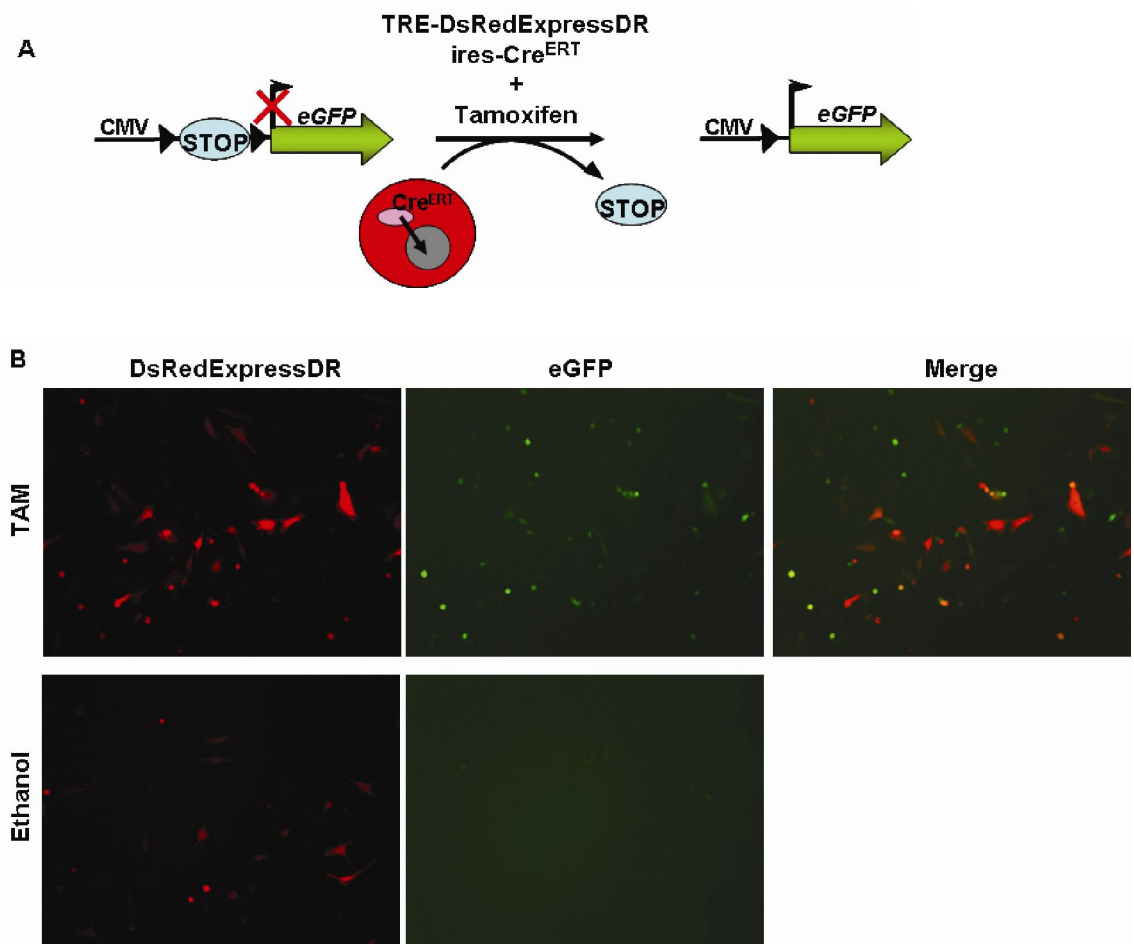

Figure 10. Tamoxifen induced Cre^{ERT}-mediated recombination. (A) The Cre^{ERT} recombinase was tested by using a plasmid containing a CMV promoter and the eGFP reporter separated by a loxP-flanked (full triangles) Stop cassette. 4OH-Tamoxifen addition induces Cre^{ERT}-mediated recombination to remove the Stop sequence, thereby allowing eGFP expression. (B) Hela cells were co-transfected with three plasmids: the response plasmid TRE-DsRedExpressDR-ires-Cre^{ERT}, the CMV-tTA2 plasmid to induce expression of the reporter as well as of the inducible Cre^{ERT} recombinase, and the CMV-Stop-eGFP plasmid. 4OH-tamoxifen (TAM) to a final concentration of 2μM, or an equivalent amount of ethanol as control, was added to the culture medium. Pictures were taken 24h after addition.

2.4 BAC homologous recombination

We have shown that the Notch2 reporter system, i.e. the chimeric Notch2/tTA2 together with the reporter TRE-DsRedExpressDR-ires-Cre^{ERT}, induced expression of the red fluorescent protein upon ligand interaction and was specific to Notch2 signaling *in vitro*. The data indicated that the constructs were suitable to use for the generation of transgenic mouse lines to study Notch2-signaling *in vivo*.

To generate Notch2/tTA2 transgenic mice, we sought to generate BAC clones containing the Notch2/tTA2 transgene within the Notch2 regulatory sequence. Two alternative methods were available. The first consisted of electroporation of the linearized chimeric construct into EL250 bacteria, which were previously electroporated with a Notch2-containing BAC. The EL250 bacteria contain recombination proteins controlled by a temperature-sensitive repressor as well as an arabinose-inducible *flpe* gene (Lee et al. 2001). The 9.25kb Notch2/tTA2 transgene was isolated after linearization by the restriction enzyme PmeI (Fig.11B). Homologous recombination was induced by a temperature shift at 42°C for 15min before chilling the cells on ice for the electroporation step. As the BAC backbone contains a chloramphenicol (chlor) resistance gene, recombined clones containing both BAC and Notch2/tTA2 were selected by double-resistance to ampicillin and chloramphenicol (Fig.11A).

The *flpe* recombinase expression was then induced by incubating the cultures in 0.1% L-arabinose for 1h. This FLP-mediated excision of the Amp cassette generated the final Notch2/tTA2 transgene. A hundred colonies were picked after chloramphenicol selection and digested by the restriction enzyme KpnI. The obtained digestion patterns were compared with that of the original RP23-143I22 BAC and should include an extra fragment at 2.8kb. Intriguingly, several strong bands appeared after agarose gel electrophoresis, but no expected digestion pattern was identified (Fig.11C). Despite several attempts, the chimeric transgene could not be correctly recombined into a Notch2-containing BAC.

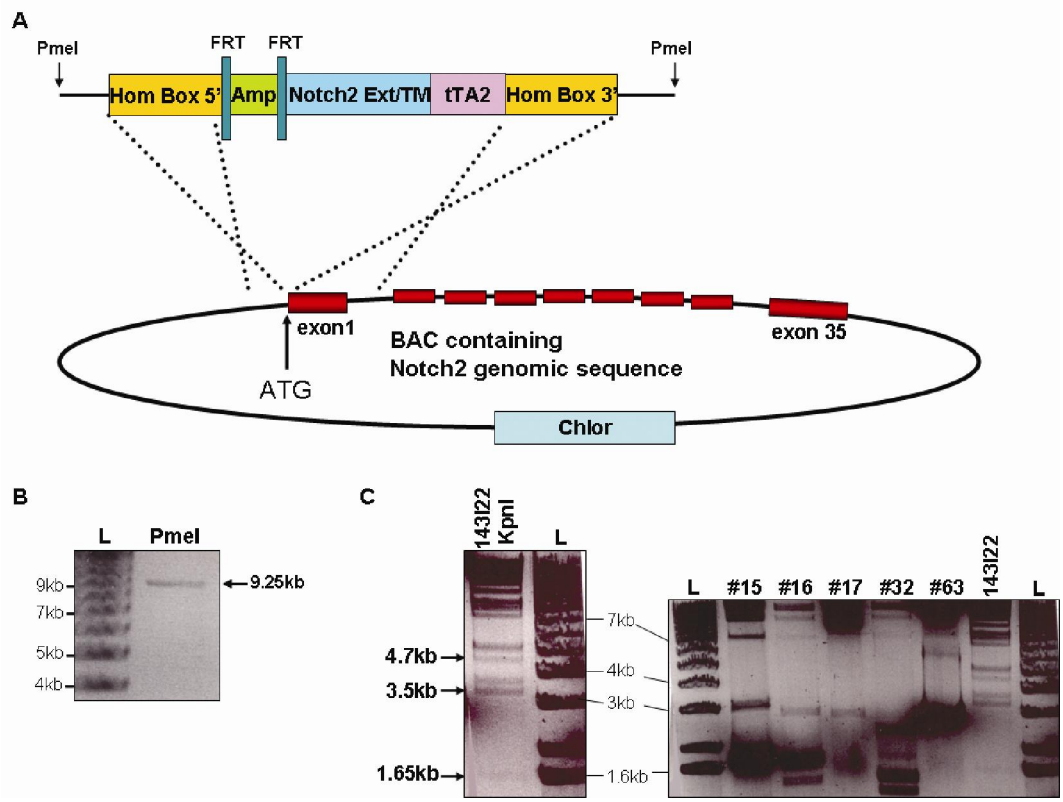

Figure 11. BAC homologous recombination mediated by EL250 bacteria. (A) Linearized chimeric Notch2/tTA2 transgene recombines via the 5' and 3'homologous boxes (orange) into the Notch2-containing BAC. Chlor: chloramphenicol resistance cassette. (B) The 9.25kb chimeric Notch2/tTA2 transgene is linearized by the restriction enzyme PmeI (arrow). (C) Left panel: The restriction enzyme KpnI digests the BAC RP23-143I22 into more than 25 fragments, from which 3 are shown by arrows. Right panel: Several potentially recombined clones (#numbered) are digested by KpnI and compared to the RP23-143I22 original BAC. L: 1kb DNA ladder.

Homologous recombination into the Notch2 genomic sequence was unsuccessful by electroporation into EL250 bacteria. Therefore, we settled for a second method which uses a shuttle vector called pDelsac for targeted recombination into the BAC (Sparwasser et al., 2004). Briefly, the pDelsac, modified to contain the transgene of interest, is first integrated into the BAC via recombination of one of the homologous arms. A second recombination event with the other homologous arm results in excision of the shuttle vector and the resolution of the BAC modification.

Thus, the chimeric Notch2/tTA2 vector, without the Amp cassette, was cloned into the shuttle vector (kindly provided by Dr. Gérard Eberl) by a three-way ligation strategy. Two fragments were isolated from pDelsac: 5.7kb after NotI/NcoI digestion and 1kb after another BamHI/NcoI digestion. The 9.1kb Notch2/tTA2 transgene was isolated from a NotI/BglII

digestion of the chimeric vector. Since the two restriction sites BamHI and BglII formed compatible ends, no blunting was needed (Fig.12A). Correctly ligated clones were identified by the digestion patterns of two restriction enzymes PvuI and XhoI. The Amp sequence, as well as the Notch2/tTA2 transgene, both contain PvuI restriction sites whereas the restriction site XhoI is only present in the Notch2/tTA2 sequence. Consequently, digestion by PvuI resolved two fragments of 12.4kb and 3.2kb while digestion with XhoI resulted in the generation of a 15.8kb band, which corresponded to the linearized product of correctly ligated clones (Fig.12B).

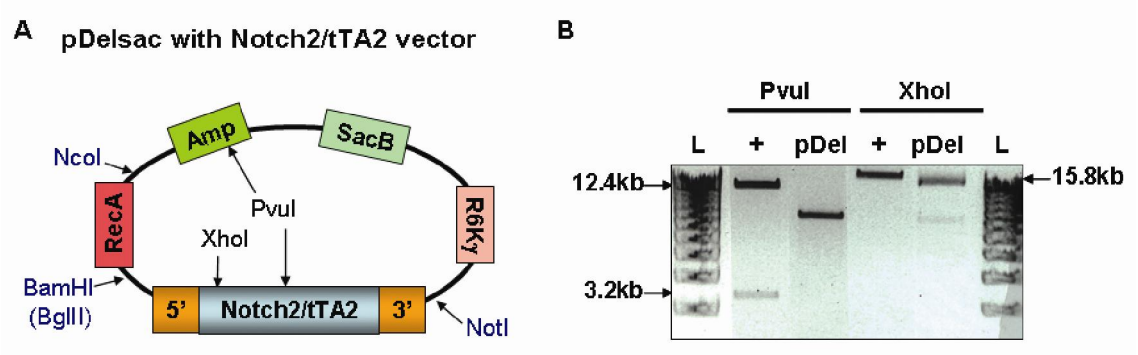

Figure 12. Notch2/tTA2 ligation into shuttle vector pDelsac. (A) pDelsac-Notch2/tTA2, with both 5' and 3'homologous arms (orange boxes), vector is schematically represented with the restriction sites used for ligation marked in blue. The restriction enzymes used for diagnostic digestion patterns shown in B are in black. R6Kγ: origin of replication; Amp: ampicillin resistance gene; SacB: counter-selection gene; RecA: *E.coli* recombinase gene. (B) Digestion of a positive clone by PvuI and by XhoI identifies expected sizes 3.2kb and 12.4kb, and 15.8kb, respectively (arrows). pDel: pDelsac shuttle vector. L: 1kb DNA ladder.

The pDelsac containing Notch2/tTA2 was then successfully recombined by a postdoctoral fellow of our laboratory, Dr. Nicolas Fasnacht, following the previously described protocol (Sparwasser et al., 2004). Clones were first tested for a segment of the Notch2/tTA2 to insure integration of the chimeric transgene. An internal PCR amplification of an 800bp product was designed to span the fusion region between Notch2 and tTA2 (Fig.13).

Internal Notch2/tTA2 primers: 5'CCAACTTGCGCATTAAACAA 3'

5'AGCAAAGCCCGCTTATTTTT 3'

The correctly recombined BAC clones were further verified by two PCR amplifications, one for each recombination region, i.e. at the 5'and the 3'homologous arms.

The expected sizes, 1.3kb and 1.2kb respectively, were indeed amplified in several recombined BAC clones (Fig.13). These results strongly suggested correct homologous recombination of the Notch2/tTA2 transgene within the Notch2 genomic sequence of the BAC.

BACrec5' primers: 5'TCGTAGTTGCCAATTTCGTTC 3'

5'CCAAGAAGCCCTCTGGACAT 3'

BACrec3' primers: 5'CACGCTATCTGTGCAAGGTC 3'

5'AAGACATAGCCCCACTGGAA 3'

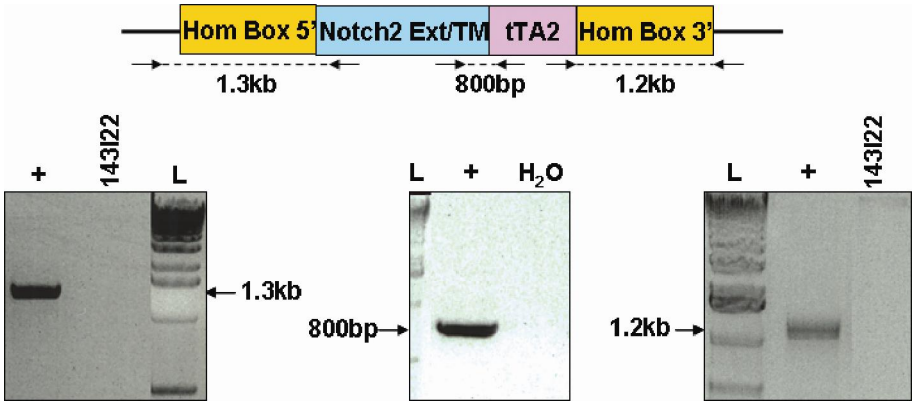

Figure 13. Identification of recombined BAC clones. Top panel: PCR amplifications for three regions of the recombined Notch/tTA2 transgene are schematically drawn by dotted lines with the sizes of the products. Arrows represent the approximate location of the primers. Bottom panels: The three amplification products are shown (arrows) for a potential positive clone by agarose gel electrophoresis. 143I22: RP23-143I22 BAC as negative control. L: 1kb DNA ladder.

Verification of the potentially recombined BAC clones by Southern blot analysis will further confirm the correct BAC homologous recombination event. Once more, both homologous recombination arm regions will be investigated. The 5'homologous arm was used as a probe after an EcoRV digestion of the BAC DNA. The 3.37kb wt band was identified in the original RP23-143I22 BAC. After recombination, clones should have a recombined band at 2.1kb. In addition, the 3'homologous arm was used as a probe after KpnI digestion of the BAC DNA and the 14kb wt band was identified in the RP23-143I22 BAC.

The tTA2 gene could also be used as a probe in this case, and the recombined band would be at 5.5kb (Fig.14).

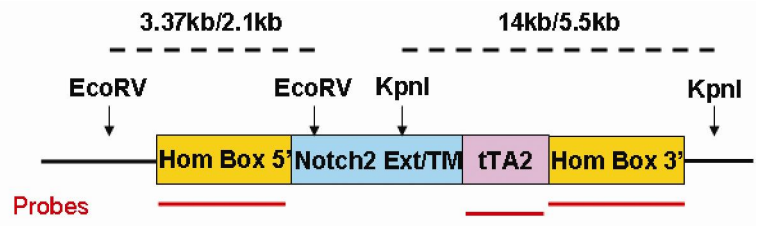

Figure 14. Scheme representing Southern blot analyses of recombined BAC clones. Either an EcoRV or a KpnI digestion (arrows) of the BAC DNA identifies the recombined regions of the 5'or the 3'homologous arm, respectively. Sizes of the expected bands are shown above the dotted lines (wt/recombined) and the probes used are represented by red bars.

If the BAC clones identified by the PCR amplifications are confirmed by the Southern blot analyses described above, then the modified BAC containing the chimeric Notch2/tTA2 will be given to the transgenic animal facility for generation of the Notch2-specific reporter mouse line.

3. Discussion and perspectives

In this section, we have described the successful generation of a Notch2/tTA2 chimeric vector and a TRE-DsRedExpressDR reporter. Both transgenes were designed to generate Notch2-specific reporter mouse lines in order to study Notch2-mediated signaling *in vivo*. The specificity and robustness of the system using both transgenes was demonstrated *in vitro* by co-culture assays indicating that this is a valid strategy for the generation of Notch2 reporter mice.

In order to generate Notch2/tTA2 "pseudo knockin" mice, the chimeric transgene was integrated by homologous recombination into a Notch2-containing BAC. Several clones showed correct recombination by PCR amplifications. However, these potentially modified BAC clones must be confirmed by the Southern blot analyses discussed at the end of chapter 2.4. The Notch2/tTA2 BAC clone will then be given to the transgenic animal facility for pronuclear microinjection and subsequent generation of the Notch2/tTA2 transgenic mice.

Co-injection of the Notch2/tTA2 and the secondary reporter transgenes was also discussed. This method was used for the generation of a Notch1-specific reporter mouse by a postdoctoral fellow of the laboratory, Dr. Emma Smith. The strategy was the same as for the Notch2-specific reporter, but with a Notch1/Gal4VP16 chimeric transgene and a Gal4-Venus-ires-Cre^{ERT} secondary reporter. After pronuclear injection of both constructs, not only was the efficiency extremely low, 6 out 114 mice integrated both transgenes, but more importantly no reporter expression, in this case the green fluorescent protein Venus, was observed in any of the founder lines. These results prompted us to inject the transgenes separately and to increase the efficiency of reporter expression by an alternative method.

The secondary reporter vector TRE-DsRedExpressDR-ires-Cre^{ERT} could be directly injected into murine pronuclei to generate the transgenic mice. However, in order to circumvent variation due to random insertion and copy number, we focused on an alternative strategy by homologous recombination into a known location of the genome. The method integrates a single transgene copy into the X-linked hypoxanthine phosphoribosyltransferase (Hprt) locus, a housekeeping gene, by a directly selectable homologous recombination (Bronson et al., 1996). The subsequent targeted embryonic stem cells are selected by restoration of a functional Hprt gene and injected into blastocysts to generate the transgenic mouse line. A disadvantage of the Hprt targeted integration is the location of the Hprt locus,

which is on the X-chromosome. Thus, the transgene might be silenced in several tissues of female transgenic mice, thereby potentially generating mosaic expressing transgenic females.

Additionally, to increase the efficiency of expression of the reporter DsRedExpressDR, as well as of the Cre^{ERT} gene, both genes can also be cloned into a bidirectional vector. IRES-containing vectors, such as the reporter TRE-DsRedExpressDR-ires-Cre^{ERT}, are known to induce different levels of expression of the genes located up- and downstream of the IRES sequence. Consequently, the DsRedExpressDR protein level is not similar to the level of the Cre^{ERT} recombinase. To circumvent the variation in expression levels, the two reporter genes can be divergently oriented to the central TRE DNA binding sequence. Upon binding of the tTA2 domain, this bidirectional configuration results in initiation of transcription of both transgenes at the same time (Fig.15). Cloning of the bidirectional TRE-DsRedExpressDR-Cre^{ERT} vector is currently pursued by a new PhD student in the laboratory.

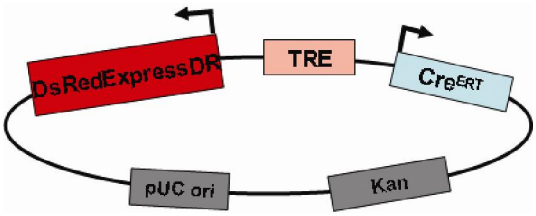

Figure 15. Scheme of the bidirectional TRE-DsRedExpressDR-Cre^{ERT} vector. The backbone depicted is the pENTR1A vector (Invitrogen).

Once both transgenic mouse lines are generated, they will be crossed in order to study *in vivo* Notch2-mediated signaling. Any tissue can be observed at any given time to investigate Notch2 activation during development, self-renewal and tumorigenesis. To control correct reporting of the system red fluorescence can be analyzed at first in organs where Notch2 has been reported to be active, such as in the hematopoietic system. As briefly mentioned earlier, Notch2 is highly expressed in splenic marginal zone B-cells (Kuroda et al., 2003; Saito et al., 2003). Notch2 signaling could also be investigated during hair vibrissae follicle morphogenesis where it has been shown to be expressed in interfollicular dermis and suggested to play a role in dermal papilla formation (Favier et al., 2000). Many other tissues could be analyzed as it has been shown more recently that Notch2 is expressed during intrahepatic bile duct development when hepatoblasts differentiate into biliary epithelial cells (Tchorz et al., 2009).

Moreover, the native microenvironment of Notch2-receiveing cells can be precisely observed by easy detection of red cells in tissue sections. Another application would be to sort the red cells from any given tissue at any time point in order to study their gene expression profile, by microarray analysis for example. Finally, this Notch2-specific reporter mouse will not only allow investigation of Notch2 activation under physiological conditions, but also in challenge situations such as during chemically-induced carcinogenesis. The role of Notch2 signaling can thus be investigated *in vivo* during the process of tumor formation in the skin. This application can also be extended to other disease mouse models by crossing in the Notch2 reporter strains. One example is the Apc^{Min} mutants (C57BL/6J-Apc^{Min}/J; JAX stock#002020) which spontaneously develop intestinal adenomas (Su et al., 1992). Investigating Notch2 in the intestinal tract is of great interest since it is expressed in intestinal crypt cells (Sander and Powell, 2004) and, in addition, we have recently shown that it plays an important role in the gut self-renewal (Riccio et al., 2008).

In conclusion, the Notch2 reporter strategy, comprising of the Notch2/tTA2 chimeric transgene and the TRE-DsRedExpressDR-ires-Cre^{ERT} reporter, was shown to be efficient *in vitro* and will shortly be a useful tool for *in vivo* Notch2-mediated signaling studies.

Materials & Methods

Materials and Methods

Histology, immunohistochemistry and immunofluorescence

Skin samples were fixed with buffered 4% PFA at 4ºC overnight before embedding in paraffin. Skin sections 4µm thick were laid onto slides and dewaxed in three xylene baths before gradually hydrating by an alcohol gradient (3x 100%, 1x 96% and 1x 70%). Deparaffinized sections were then processed for haematoxylin and eosin staining or for immunoreactions. Most immunostainings were set up and performed by the histology core facility. All antibodies and their respective dilutions are listed in Table 1. Pictures of immunostained slides were taken with either one of the Leica microscopes DM5500 or DMI4000.

H&E

Skin sections were stained 5 minutes in haematoxylin, washed in water, dripped into an acidic alcohol bath and incubated for 10 minutes in water. Sections were stained in eosin for 30 seconds and rinsed in water. Sections were gradually dehydrated by increasing the ethanol concentration of the baths (1x 70%, 1x 96%, 3x 100%) and dripped 3 times into xylene. Finally, slides were mounted with Eukitt Solution.

BrdU and RhoV

Proliferation of keratinocytes was analyzed *in vivo* by BrdU (5-Bromo-2'-deoxyuridine) incorporation. Mice were injected intraperitoneally 2 hours prior to sacrifice with 0.1mg/g of body weight. Back skin samples were isolated and processed as previously described.

After dewaxing and rehydrating, skin sections were quenched, to remove endogenous peroxidases, for 10 minutes in 3% H_2O_2 in PBS (phosphate buffered saline). Antigen retrieval was performed on paraffin slides in tri-sodium citrate buffer (10mM tri-sodium and 10mM citric acid in H_2O, pH6) at 95°C for 20 minutes. Sections were blocked in 1% BSA (bovine serum albumin) in PBS for 30 minutes before incubation with a rat anti-BrdU primary antibody overnight at 4°C. Sections were then incubated with a biotinylated donkey anti-rat for 40 minutes at room temperature (RT). Streptavidin-HRP treatment for 30 minutes at RT was followed by incubation with the enzyme substrate DAB in detection buffer (0.05M Tris/HCl pH7.6). The revelation was monitored under a microscope and stopped by washing in the detection buffer alone. Slides were washed in PBS and dipped in 1% BSA between

each step. Finally, the slides were counterstained with nuclear staining Mayer's haematoxylin, dehydrated, and mounted with Eukitt Solution.

This protocol was also applied to the immunostaining for RhoV (or Chp) by using an anti-RhoV (or anti-Chp) primary antibody. However, the results obtained by this method were inconclusive.

Ki67 and myc-tag

Slides for immunostaining of the proliferation marker Ki67 were processed as described for the BrdU staining with the exception of the blocking step and the antibodies used. Blocking of the sections was done in MOM (mouse on mouse) IgG blocking reagent for 60 minutes. The primary antibody, a mouse anti-human Ki67, was incubated overnight at 4°C in MOM diluent. The secondary antibody, an anti-mouse IgG from Envision^{+} system, was incubated for 30 minutes at RT before DAB revelation as previously described.

The myc-tag immunostaining differs from Ki67 by the antibodies tested. Anti-myc 9E10.3 prepared in MOM diluent at 1/50 or 1/10 dilutions, whereas anti-myc 9E10 from the protein expression core facility was diluted 1/200 or 1/100. However, all dilutions resulted in high background.

K14, K1 and loricrin

K14, K1 and loricrin immunostainings were performed by two methods: enzymatic revelation or fluorescent-labeling. For the first method, the processing of the slides was performed as described for the BrdU immunostaining with rabbit anti-K14, rabbit anti-K1, or rabbit anti-loricrin as primary antibodies, followed by incubation with a goat anti-rabbit HRP as secondary antibody. DAB revelation was then used as previously described.

Immunofluorescence: K14, K1, loricrin and Jagged2

In the case of immunofluorescent detection, the secondary antibody was a donkey anti-rabbit Alex568 while the primary antibodies were the same as for the enzymatic revelation described above. Nuclear staining was revealed by incubating the slides in DAPI (1/10.000) for 10 minutes at RT, and subsequently mounted with DABCO anti-bleaching solution.

GFP

For direct visualization of GFP, samples were embedded in OCT compound and immediately frozen at -80°C. Skin sections 8µm thick were cut at -20°C with a cryostat and DAPI stained for nuclear detection. Alternatively, immunostaining was also performed as previously described for BrdU with the exception of the blocking step and the antibodies. Blocking was done in 10% BSA and 0.5% Tween for 30 minutes. Rabbit anti-GFP was diluted 1/50 in 10% BSA for incubation overnight at 4°C. The secondary antibody, anti-rabbit Alexa568 in 10% BSA, was incubated for 2 hours at RT. Another test for the GFP immunostaining was performed with the MOM kit by following the Ki67 protocol.

Antibody	Company	Catalog number	Dilution
Anti-BrdU	Ab Serotec	OBT0030	1/200
Anti-digoxigenin-AP	Roche	11093274910	1/2000
Anti-GFP	Invitrogen	A11122	1/50
Anti-Jagged2	Santa-Cruz	sc-5604	1/100
Anti-K1	Covance	PRB-165P	1/500
Anti-K14	Covance	PRB-155P	1/1000
Anti-Ki67	Novocastra	NCL-L-KI67-MM1	1/100
Anti-Loricrin	Covance	PRB-145P	1/1500
anti-mouse Envision^{+} system labeled polymer-HRP	DakoCytomation	K4001	Ready to use
Anti-myc (clone 9E10.3) Anti-myc	Neomarker (LabVision) EPFL/PECF	MS-139-P0 9E10	1/50 or 1/10 1/200 or 1/100
Anti-rabbit Alexa568	Invitrogen	A21069	1/800
Anti-rabbit HRP	Brunschwig	111-035-003	1/100
Anti-rat biotinylated	Jackson ImmunoResearch	712-065-153	1/200
Anti-RhoV (anti-Chp)	Dr. Ami Aronheim	-	1/50 or 1/10
Streptavidin-HRP	Amersham	RPN-1231	1/100

Table 1. List of antibodies with their manufacturer and catalog number. Dilution ratios used are also described.

Homologous recombination into a BAC

BAC DNA isolation

BAC DNA was purchased from the BACPAC Resources Center of the Children's Hospital Oakland Research Institute (CHORI). The clones were grown in medium containing chloramphenicol (12.5µg/ml) and DNA was isolated following the maxiprep protocol from the Qiagen large-construct kit. In order to extract good quality DNA, resuspension in TE was performed overnight.

For smaller DNA preparations, rapid alkaline lysis minipreps were performed on small cultures (2ml) of BAC clones. The bacteria pellet was resuspended in 300µl of a filter-sterilized solution (15mM Tris pH8, 10mM EDTA, 100µg/ml RNaseA) chilled at 4°C. Bacteria were lysed by addition of 300µl of alkaline lysis buffer (0.2N NaOH, 1% SDS) and incubated for 5 minutes at RT. 300µl of autoclaved, previously chilled 3M KOAc was then added, and the mix was incubated on ice for 5 minutes, which resulted in protein and *E.coli* DNA precipitation. After centrifugation at 10.000rpm at 4°C, the supernatant was transferred into 800µl of ice cold isopropanol and left on ice for 5 minutes. The precipitated DNA pellet was washed with 70% ethanol, air-dried, and finally resuspended in 30 to 45 µl of TE.

Method n°1 using EL250 bacteria

Firstly, the BAC was transformed into EL250 bacteria following a previously described protocol (kindly provided by Dr. Friedrich Beermann). Briefly, EL250 bacteria were grown at 32°C until an OD_{600} of 0.5-0.8 was obtained. They were washed several times with sterile ice cold water before resuspending into 100µl. The BAC DNA (50 to 200ng) was then electroporated (1.75kV, 25µF, 200Ω) using a chilled 1mm gap electroporation cuvette. The electroporated bacteria were immediately grown for 1 hour at 32°C in SOC medium and incubated on a chloramphenicol selective plate overnight at 32°C.

The chimeric Notch2/tTA2 targeting vector was then electroporated into the EL250 bacteria previously transformed with the BAC DNA by the following method. Cultures containing the BAC DNA were grown until an OD_{600} value of 0.5-0.8 had been obtained and the recombination machinery was activated by heating the bacterial culture at 42°C for 15 minutes, before chilling on ice for 20 minutes. The electroporation was then performed as described for the BAC DNA, but this time the linearized targeting vector, without the

backbone, was electroporated. Transformed bacteria were selected by agar plates containing both ampicillin and chloramphenicol.

Method n°2 using the pDelsac shuttle vector

The targeting vector cloned into the pDelsac backbone was transformed into EC100Dpir^{+} bacteria, which express the *pir* gene for replication of R6Kγ origin-containing vectors. The shuttle DNA preparation and the BAC homologous recombination were performed as previously described (Sparwasser et al., 2004).

***In situ* hybridization (ISH)**

RhoV probes were transcribed using the pCMV-SPORT6 plasmid (Table 3) which contains mouse RhoV cDNA flanked by two promoters, namely SP6 and T7. The sense probe was obtained by linearization with NotI and transcription by SP6 RNA polymerase. For the antisense probe the restriction enzyme used was EcoRI and transcription was performed by the T7 RNA polymerase (Fig.1).

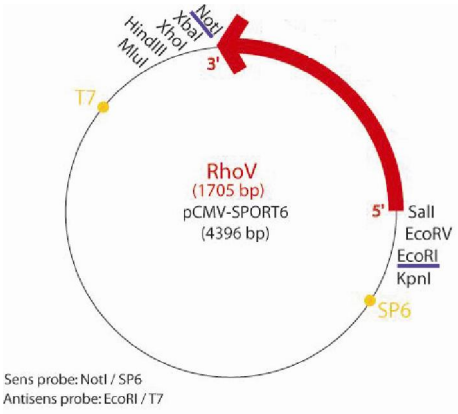

Figure 1. Plasmid map of pCMV-SPORT6 containing the RhoV cDNA sequence. Restriction enzymes used for linearization are underlined in blue. T7 and SP6 promoters for their respective RNA polymerases are depicted in yellow.

The linearized plasmid was purified by phenol-chloroform extraction. Briefly, 1/10 volume of 3M NaAc pH5.2 was added to the DNA before addition of 200µl of phenol and 200µl of chloroform. The mix was vortexed and centrifuged for 5min at maximum speed. The upper aqueous layer could then be cleaned from phenol traces by adding only chloroform and repeating the centrifugation. The DNA was then precipitated with 1ml ice cold 100% ethanol and left for at least 20min at -20°C. After 20min centrifugation, the pellet was washed with 70% ethanol, air-dried, and resuspended in DEPC-treated water.

Subsequently, 1µg of the purified linearized plasmid was used for the labeling reaction. The probes were labeled with digoxigenin-UTP following the DIG RNA labeling mix

protocol. Once labeled, the probe can be stored at -80°C for up to a year. *In situ* hybridization was then performed on skin sections fixed overnight in buffered 4% PFA at 4°C and embedded in paraffin. Alternatively, skin isolated from newborn pups was fixed in Bouin's fixative solution (30ml picric acid, 10ml 37% formamide, 4ml glacial acetic acid). Briefly, samples were fixed overnight at 4°C, washed several times with 1x PBS, washed several times in 70% ethanol, and then incubated in 70% ethanol overnight. Skin samples were then embedded in paraffin. 8µm sections, either from 4% PFA or Bouin fixed paraffin blocks, were prepared no longer than 1 week before ISH to avoid RNA degradation of the sample. The hybridization was either performed by following a previously described protocol (kindly provided by Dr. Hans Clevers), or by an automated ISH instrument.

For both methods, a pre-treatment of the slides by dewaxing three times in xylene, gradual re-hydration (ethanol 100%, 95%, 70% and 1x PBS) and soaking in 0.2N HCl for 15 minutes was necessary. Pre-treated slides were then incubated with PBS buffered proteinase K (30µg/ml) at 37°C for 10 minutes. The slides were post-fixed for 10min in 4% PFA then incubated for 5min in acetic anhydride solution (1.34% v/v tri-ethanolamine pH8, 0.6% v/v acetic anhydride). After two washes in 1x PBS and in 5x SSC (0.75M NaCl, 75mM Na-citrate pH7) sections were completely covered by pre-hybridization solution (50% formamide, 5x SSC pH4.5, 2% block solution, 5mM EDTA, 0.05% Chaps, 50µg/ml heparin, 1µg/ml yeast total RNA). The slides were kept in a humidified environment (5x SSC, 50% formamide) at 70°C for at least 1 hour. The DIG-labeled probe was then added at a final concentration of 1µg/ml before incubation at 68-70°C for 12 to 72 hours.

Post-hybridization were performed in 2x SSC, 50% formamide/2x SSC and TBST (1x TBS, 0.1% Tween), prior to immunological detection. The sections were then blocked for 30 minutes with 0.5% blocking powder using 100µl/slide. After subsequent addition of sheep anti-digoxigenin-AP (diluted 1/2000 – Table 1), the slides were incubated at 4°C overnight. Slides were then washed several times in TBST. Fresh NTMT solution (0.1M Tris pH 9.5, 0.05M $MgCl_2$, 0.1M NaCl, Tween 1%) was used to wash slides before revelation. NBT/BCIP solution was prepared by adding NBT and BCIP to NTMT at 4.5 and 7µl/ml, respectively. Slides were then wrapped in aluminum foil, incubated at 37°C, and monitored for revelation. The reaction was stopped by rinsing in PBS when the signal was strong enough. Finally, slides were mounted with PBS buffered 50% glycerol.

Alternatively, ISH was also performed with the automated system Discovery® XT from Ventana Medical Systems Inc. This instrument processes several slides rapidly by following a protocol set by the user. The amount of the probe added varied from 50ng to 100ng per slide.

Mice

Notch1$^{lox/lox}$ (Radtke et al., 1999), Jagged1$^{lox/lox}$ (Mancini et al., 2005), and RosaNIC (Murtaugh et al., 2003) mice were crossed with K14Cre transgenic mice (Indra et al., 2000). Controls were littermates which lacked Cre recombinase but carried the floxed alleles, or were homo- and heterozygous for the RosaNIC transgene. The Jagged2 floxed mice we generated were first crossed with Flpe^{+} deleter mice (Rodriguez et al., 2000), then with MxCre (Kuhn et al., 1995), or K14Cre and Jagged1$^{lox/lox}$ mice.

Genotyping of the mice was done by PCR on genomic DNA extracted from about 5mm of tail. Digestion was carried out at 56°C with maximum shaking in a buffer containing non-ionic detergents (50mM KCl, 10mM Tris-HCl pH8.3, 2.5mM $MgCl_2$, 0.1mg/ml gelatin, 0.45% v/v Nonidet P40, 0.45% v/v Tween 20) and proteinase K. After 2 hours the digestion was heat-inactivated for 10 min at 99°C. Standard PCR conditions were used: 30 seconds at 95°C before annealing for 30 seconds at a temperature specific for the primer pair, then an elongation step of 30 seconds (1min per kb) at 72°C, and this cycle was repeated 30 times. Primer sequences for each gene can be found in Table 2.

Gene	Primers' sequences [5' to 3']	Annealing temperature [°C]	Band sizes [bp]
β-actin	TGG GTC AGA AGG ACT CCT ATG CAG GCA GCT CAT AGC TCT TCT	60	591 wt
Cre	CTA GAG CCT GTT TTG CAC GTT C GTT CGC AAG AAC CTG ATG GAC A	60	339 Tg
eGFP	AAG TTC ATC TGC ACC ACC G TCC TTG AAG AAG ATG GTG CG	60	173 Tg
FLPe	CTT TAG CGC AAG GGG TAG GAT CAA CTC CGT TAG GCC CTT CA	60	200 Tg
Jagged1	GCA AGT CTG TCT GCT TTC ATC AGG TTG GCC ACC TCT AAA TC	56	317 lox 267 wt
Jagged2	GCT CCA AAT CGC TAC CTG AG GTC CCC AAG ACC AAG TAC CA	60	392 lox 200 wt
Notch1	CTG ACT TAG TAG GGG GAA AAC AGT GGT CCA GGG TGT GAG TGT	64	350 lox 300 wt
RhoV	CGC CTG GAG AAG AAA CTG AA ACA CCG GCC TTA TTC CAA G	60	612 Tg
RosaNeo	AAA GTC GCT CTG AGT TGT TAT GCG AAG AGT TTG TCC TCA ACC GGA GCG GGA GAA ATG GAT ATG	60	600 wt 200 neo

Table 2. Primer sequences for the PCR reactions. The annealing temperature and the product sizes are noted.

Plasmids

Plasmids used for the generation of the various transgenic mice were kindly provided by several sources: the human keratin14 promoter by Dr. Joerg Huelsken, the involucrin promoter by Dr. Fiona Watt, and the MHKA1 promoter by Dr. Raphael Kopan. The Jagged2 targeting vector was generated by the company Nucléis (Lyon, France; bankruptcy in 2006).

Various plasmids were used for transfection assays, which are described in the corresponding paragraphs, and are listed in Table 3.

Plasmid	Source/Company	Catalog number
12RBPJκ-luciferase	Dr. Freddy Radtke laboratory	-
pAdEasy-1 from AdEasy™ adenoviral vector system	Stratagene	240009
PCMV-Dll1	Dr. Freddy Radtke laboratory	-
pCMV-Notch2 full length	Dr. Freddy Radtke laboratory	-
pCMV-Notch1IC	Doorbar *et al.*, 2000	-
pCMV-SPORT6 from SuperScript® plasmid system with Gateway® technology	Invitrogen	19625-011
pCMV-Stop-eGFP	Dr. Friedrich Beermann	-
pGL4.26[luc2/minP/Hygro]	Promega	E8441
pGL4.74 [hRluc/TK]	Promega	E6921
pRL-CMV-Renilla-luciferase	Promega	E2261
pUHD20-1	Dr. Hermann Bujard	-

Table 3. List of plasmids and their respective source.

Primary keratinocytes

Primary keratinocytes were prepared from 2-3 day-old Notch1$^{lox/lox}$ mice as previously described (Rangarajan et al., 2001). Briefly, newborn mice were decapitated, limb and tails were amputated and a longitudinal incision was performed from tail to snout. The skin was peeled off the body using forceps and rinsed in 70% ethanol, then in PBS. Each skin was carefully deposited with the epidermis facing upwards on the surface of a 0.25% trypsin solution and left at 4°C for at least 15 hours. The epidermis was then separated from the dermis with forceps, minced and filtered through a sterile 70µm nylon cell strainer.

The culture dishes were coated with 2ml of a solution containing 1ml BSA, 1mg fibronectin and 1ml purified collagen (3mg/ml) added to 95ml of DMEM without FCS, and left at 37°C for at least 30 minutes before plating the cells. Primary keratinocytes were cultured in a minimum essential medium (MEM Eagle with Earle's BSS calcium-free) containing 8% fetal bovine serum (FBS) pretreated with Chelex resin (20g for 500ml) for calcium removal. The MEM/8%FBS medium contained a Ca^{2+} concentration of 0.05mM,

which was required to maintain primary keratinocytes in an undifferentiated state. To induce differentiation, Ca^{2+} concentration in the medium was increased to 2mM. The growth medium was also supplemented with antibiotics (100 units/ml penicillin, 0.1 mg/ml streptomycin). The culture medium was replaced every 2 days or earlier if necessary.

RT-PCR

Keratinocytes were scraped from the frozen skin of transgenic and littermate control mice and total RNA was isolated using TRIZOL reagent. The working area was previously cleaned with RNase AWAY in order to work in an RNase-free environment before handling RNA samples. RNA was quantified using a ND-100 NanoDrop spectrophotometer from NanoDrop Technologies. 1µg of total RNA was reverse-transcribed using the QuantiTect reverse transcription kit. For each sample, a reaction with and without reverse transcriptase was performed. The resulting cDNA was used for PCRs for RhoV, eGFP and β-actin as control (primers in Table 2).

Real-time quantitative RT-PCR

Primary keratinocytes in culture were washed once with PBS before total RNA was isolated following the TRIZOL reagent protocol. The quality of the RNA was tested on a 1% TAE (Tris-acetate-EDTA) agarose gel where two sharp bands should appear. The higher 28S band should be more intense than the lower 18S band. Moreover, the small 5S band was also visible in a few samples.

For one reverse transcription reaction a mix of 1µl of the reverse transcriptase M-MLV, 4µl of the enzyme's buffer, 2µl DTT (0.1M), 1µl RNase inhibitor (10U), 1µl oligodT (10µM) and 1µl dNTPs (10µM) was prepared. Meanwhile, RNA was heated at 65°C for 10 minutes and later left on ice for another 5 minutes. The mix was added to the RNA before incubation for 50 minutes at 37°C. Once reverse transcription had occurred the reaction was deactivated by heating at 95°C for 2 minutes. The resulting cDNA was stored at -20°C until usage.

The real-time RT-PCR was carried out in optical 96-well fast thermal cycler plates with barcodes. For each gene of interest 1µl of its specific TaqMan® probe was mixed with 10µl of TaqMan® Universal PCR master mix and dispensed into the corresponding wells. The cDNA was diluted with RNase-free water to a final concentration of 10ng/µl, and 9µl was added to each well. The plate was processed by the Applied Biosystems' 7500 System. The data were

normalized to the housekeeping gene GAPDH and the final fold changes included three independent experiments for each gene tested (Table 4).

Gene name	Gene ID	Applied Biosystems Number
BMP receptor 1A	12166	Mm00477650_m1
Casein kinase 1α (CKIα)	93687	Mm00521599_m1
Casein kinase 1ε (CKIε)	27373	Mm00443344_m1
CyclinD1	12443	Mm00432358_g1
DEPP	213393	Mm00524329_g1
Frizzled6	14368	Mm00433383_m1
Glyceraldehyde-3-phosphate dehydrogenase (GAPDH)	14433	Mm99999915_g1
Inhibitor of DNA binding 1 (Id1)	15901	Mm00775963_g1
Mitogen activated protein kinase kinase 1 (MEK1)	26395	Mm00435940_m1
Prickle2	243548	Mm01182432_m1
Prostaglandin-endoperoxide synthase 1 (Ptgs1)	19224	Mm00477214_m1
Ras-related C3 botulinum substrate 1 (Rac1)	19353	Mm01201654_g1
RhoV	228543	Mm00523731_g1
SMAD specific E3 ubiquitin protein ligase 2 (Smurf2)	66313	Mm01242752_g1

Table 4. List of genes and their respective probe numbers from Applied Biosystems.

Southern blot analysis

DNA digestion and gel electrophoresis

A small piece of mouse tail or scraped epidermis from frozen skin was digested overnight at 56°C in 400µl of proteinase K solution (0.5% SDS, 0.1M NaCl, 50mM Tris pH8, 7.5mM EDTA and 0.5mg/ml proteinase K). DNA was extracted with 100µl of 8M KOAc and 600µl chloroform. After centrifugation, the DNA-containing upper phase was transferred to a new tube and mixed with 500µl of 100% ethanol. After centrifugation, the DNA pellet was

washed with 70% ethanol and resuspended overnight at 37°C in 50µl of TE (10mM Tris, 1mM EDTA, pH8).

8-10µg of DNA was digested overnight with restriction enzymes EcoRI and HindIII for Jagged2, and with NcoI for the RhoV transgenic mice. Digested DNA was loaded onto a 0.8% TAE agarose gel and run overnight at 50 Volts. The gel was then depurinated for 20 minutes in 0.2N HCl, denatured for 2x 20 minutes in 1.5M NaCl/0.5N NaOH, neutralized 2x 20 minutes in 1M ammonium acetate/ 20mM NaOH, each time with gentle rocking at RT, and was finally soaked 5 minutes in 20x SSC (3M NaCl, 0.3M Na-citrate). The nylon membrane was first soaked in water and then in 20x SSC before assembling with the gel on a vacuum blotter at 50mbar for 4 hours. The DNA transferred onto the membrane was UV cross-linked at 1.200J.

Probe labeling

While blotting, the probe was prepared with the High prime DNA labeling kit. Between 50 and 75ng of template DNA in 8µl final volume was denatured for 5 minutes in a heat block at 99°C and chilled on ice. After addition of 4µl of High prime reaction mixture, 5µl of dNTP mix (dATP, dGTP, dTTP) and 7µl of radioactively labeled (^{32}P) dCTP (3.000Ci/mmol), the reaction solution was incubated for 2 hours at 37°C. The probe was then isolated and quantified before boiling for 5 minutes. The membrane was incubated in pre-hybridization solution (1.5x SSPE (225mM NaCl, 15mM NaH2PO4, 1mM EDTA), 10% PEG, 7% SDS and 10µg/ml salmon sperm DNA) for at least 15 minutes before addition of the probe (about 0.5 x10^6cpm per ml of hybridization solution).

Membrane hybridization

The membrane was incubated overnight at 65°C, then rinsed in 2x SSC, washed for 20 minutes in 2x SSC/0.1% SDS (pre-heated at 65°C) and washed another 20 minutes in 0.2x SSC/0.1% SDS (also pre-heated at 65°C). The membrane was exposed either on a phosphorimager for 5 hours to overnight, or on an X-ray film at –80°C for a few days, depending on the intensity of the signal. Copy number was quantified using the phosphorimager and the image analyzer software Aida.

Thymocytes and dendritic cells

Adult Jagged2$^{lox/lox}$ MxCre and littermate control (Jagged2$^{lox/lox}$) mice received 5 intraperitoneal injections of 2µg/g body weight pI-pC at 2-day intervals. Mice were sacrificed 2 weeks after the last injection, and RNA was prepared from single cell suspension of sorted DN thymocytes. Genomic DNA was isolated from total bone marrow (BM) cells and from spleens. mRNA levels of Jagged2 in sorted double-negative (DN) thymocytes cells was assessed by RT-PCR and the deletion efficiency of whole BM from control and Jagged2$^{lox/lox}$ MxCre was assessed by deletion PCR. BM-derived dendritic cells (DC) were cultured and subsequently lysed for protein analysis by Western blot.

Preparation of sorted DN (DN3 and DN4) thymocytes

DN thymocytes were prepared from Jagged2$^{lox/lox}$ MxCre and littermate control mice as previously described (Wolfer et al., 2001). Briefly, total thymocytes were resuspended in Hanks Balanced salt solution (HBSS) supplemented with newborn calf serum (2% NCS) and 25mM Hepes (staining medium) at 10x10^6 cells/ml and incubated on ice with antibodies directed against CD8 (clone 31M) and CD4 (clone RL172.4). To kill the targeted cells, rabbit complement and DNaseI 0.1 % were added and incubated at 37 °C for 1 hour. A Lympholyte®-M gradient was performed to eliminate dead cells and debris. DN-enriched thymocytes were stained with the indicated antibody cocktail (see table below) and sorted for Lin$^-$CD44$^-$CD25$^+$ (DN3) and CD44$^-$CD25$^-$ (DN4) fraction by gating out the Lin$^-$ CD44$^+$CD117$^-$ cells using a BD FACSAria™ II cell sorter.

Antibody	Conjugation
Lin$^+$ cocktail: CD4, CD8, B220, CD19, CD11b, Gr1	PE-Cy7
CD44	PE
CD25	APC-Cy7
CD117 (c-kit receptor)	APC

Purity of the cell fractions was greater than 98%. The DN3 and DN4 fraction was pooled from an individual sample and per sample 1-2x10^6 cells were sorted. RNA was extracted using TRIZOL reagent following standard protocol and RT-PCR for Jagged2 was performed.

Culture of dendritic cells

Single cell suspensions of BM cells were isolated and lineage depleted by magnetic cell sorting. Bone marrow cells (B6.CD45.1) expressing markers of the myeloid (GR-1, Mac-1), lymphoid (B220, CD4, CD8, and CD3), and erythroid (TER-119) lineages were removed using sheep anti-rat IgG magnetic beads from Dynabeads® and purified rat antibodies directed against the lineage markers.

The lineage negative fraction was collected, counted and seeded onto 10cm culture dishes at a density of $5x10^6$ cells per dish in complete Iscoves medium. Iscoves medium was supplemented with gentamicin (100ng/ml), 25mM HEPES, non-essential amino acids, and the growth factors SCF (100ng/ml; SCF was removed from the culture medium after 48 hrs), GM-CSF (20ng/ml) and IL-4 (10ng/ml). To generate BM-derived DCs, the cultures were maintained for 10 days and the supplemented culture medium was exchanged every 3 days by gently aspirating 75% of the culture medium and adding back the same amount. On day 10 of the culture, DCs were easily observed morphologically and harvested. Cells were further processed for whole protein extraction.

Jurkat cells

As a control for the Western blot analysis on protein extracts from the cultured DCs, Jurkat cells (an immortalized T cell line) were cultured in RPMI/2-mercaptoethanol before stimulation of the cells for 1 hour with GM-CSF (25ng/ml). Stimulated and non-stimulated cells were harvested 48 hours later for protein lysis and Jag2 Western blot analysis.

Transient transfection and luciferase assays

All transient transfections were performed with JetPEI transfection reagent following the specific protocol, and in duplicates for each experiment. Transfected cells were lysed 24 to 48 hours after transfection, and firefly and renilla luciferase values were measured using the Dual-Luciferase reporter assay system. Normalized firefly luciferase values were reported on the graphs as RLU (relative luciferase units). All studies are representative of at least three independent experiments.

Cell lines

The cell line used for transfection assays was a cervical carcinoma (Hela) cultured at 37°C with 5% CO_2 in 10% FCS/DMEM medium. Another cell line cultured under the same conditions was abandoned because of the high background results during the investigations: the 293T cells, or human embryonic kidney (HEK) 293 cells containing the SV40 large T-antigen.

Notch2/tTA2 assays

For the chimeric Notch2/tTA2 tests, Hela cells were co-transfected with 1µg of Notch2/tTA2 plasmid and 1µg of 12RBPJκ-Luc, together with 200ng of pRL-CMV-Renilla luciferase plasmid as an internal control. Transfection controls were cells co-transfected with 1µg 12RBPJκ-Luc and 1µg pCMV-Notch1IC, or pCMV-Notch2 full length. Inhibition of Notch signaling was induced by treating the cells with 1mM γ-secretase inhibitor DAPT, directly added to the medium, or the equivalent amount of DMSO in control. To investigate the Tet-off system, 2µg/ml of doxycycline, or the equivalent amount of H_2O in control was added to the culture medium.

For the assays on the proof of principle of the Notch2/tTA2 transgene, Hela cells were co-transfected with 1µg of the chimeric plasmid and 1µg of the secondary reporter plasmid, such as TRE-DsRedExpressDR. The transfected cells were subsequently co-cultured with Hela cells transfected with 1µg of pCMV-Dll1.

In order to test the Cre recombinase efficiency, Hela cells were co-transfected with 1µg TRE-DsRedExpressDR-ires-Cre^{ERT} together with 1µg pUHD20-1, which expressed tTA2, and 1.3µg pCMV-Stop-eGFP. 4OH-tamoxifen was added to the culture medium at a final concentration of 2µM, and the equivalent amount in µl of ethanol was added to control cells. Fluorescence was monitored 24 to 48 hours later by using the Leica microscope DMI4000.

RhoV promoter analysis

For the RhoV promoter studies, Hela cells were co-transfected with 1µg of one of the generated pGL4.26 plasmids containing sequences of potential RBPJκ binding sites (RhoVprom or RhoVint2), 1µg pCMV-Notch1IC, and 200ng of internal control pGL4.74

renilla luciferase plasmid. In order to evaluate the transfection efficiency, cells were co-transfected with 1μg 12RBPJκ-Luc and 1μg pCMV-Notch1IC.

Viruses

Generation of recombinant adenoviruses was performed by following the pAdEasy1 adenoviral vector system (He et al., 1998). Adeno-NIC (gift from Dr. Paolo Dotto) was generated by inserting the corresponding cDNA for the constitutively active form of Notch1, i.e. amino acids 1852-2125 of human Notch1 (Capobianco et al., 1997) into BamHI-XhoI sites of plasmid pAdTrack-CMV and then recombined into the adenoviral vector pAdEasy1 in bacteria. The recombinant adenovirus expressing the Cre-recombinase was previously generated by the same method after inserting the corresponding cDNA into pAdTrack-PJK vector. Both adenoviruses also express GFP to track infection efficiency.

Each pAd-Track-CMV plasmid was then transfected into 293 cells that were 80% confluent. Once the cells started detaching, and before viral-induced lysis, the infected 293 cells were washed with PBS before recovering them by centrifugation. Viruses were extracted by 4 rounds of freeze/thaw using dry ice in methanol and a 37°C water bath. After centrifugation, the supernatant containing the virus was titrated and stored at –20°C. Infection efficiency was monitored by an estimation of the amount of GFP-expressing 293 cells after infection with various quantities of the viral supernatant.

Once the optimal conditions were determined, Notch1$^{lox/lox}$ primary keratinocytes were infected after 24 hours in culture with either adeno-NIC or adeno-Cre in parallel with control adeno-GFP viruses. In the gain of function experiment, medium was removed and infected cells were scraped and washed with PBS after 12 hours of infection. In the loss of function conditions, keratinocytes were scraped after 24 hours of infection or induced to differentiate during an additional 24 hours by increasing the medium's calcium concentration to 2mM. Subsequently in all settings, RNA was isolated by TRIZOL extraction for real-time RT-PCR analysis.

Western blot analysis

Protein extraction

Whole cell lysate of scraped epidermis or of scraped cells was obtained by washing with PBS and incubating on ice for 10 minutes in about 40μl of RIPA lysis buffer (1%

Nonidet P40, 150mM NaCl, 80mM Tris/HCl pH 7.5, 2mM EDTA, 0.1% SDS, 1% Na deoxycholate) containing protease inhibitors (1 tablet of Complete EDTA-free inhibitor cocktail in 500µl). Supernatant was extracted after 15 minutes centrifugation at maximum speed at 4°C and protein concentration was determined by Bradford protein assay.

Proteins from hair samples were extracted as previously described (Nakamura et al., 2002). At first, hairs plucked from the back pelage of Tg and control mice were washed with ethanol. Then, lipids were removed by adding chloroform/methanol in a 2:1 (v:v) volume enough to cover the hairs, and left shaking for 24 hours. Delipidized hair samples were weighed and the Shindai mix was added in a ratio of 5ml for 20mg of hair. The Shindai mix consists of 25mM Tris/HCl pH8.5, 2.6M thiourea, 5M urea, and 5% 2-mercaptoethanol. The samples were incubated on a shaking heating block at 50°C for 2 days. The samples were then centrifuged at maximum speed for 20 minutes at RT and the supernatant extracted. Finally, protein concentration was determined by Bradford protein assay.

Gel electrophoresis and protein transfer

A solution of 2x loading dye (150mM Tris/HCl pH 6.8, 1.2% SDS, 30% glycerol, 15% β-mercaptoethanol, and 1.8mg per 100ml bromophenol blue) was added to 50µg of protein, which were subsequently boiled for 5 minutes. The linearized proteins were loaded onto a SDS-polyacrylamide gel of 8 to 10%, depending on expected protein size. Electrophoresis was performed at 60-70mA without exceeding 180V (SDS-Page running buffer 24.8mM Tris, 192mM glycine, 0.1% SDS). Subsequently, proteins were transferred onto a nitrocellulose membrane for 1 hour at 400mA and 100V maximum voltage (the same solution as the running buffer, but with 20% methanol).

Protein hybridization

The membrane containing the proteins was blocked with 5% milk in TBST (5mM Tris/HCl pH 7.5, 15mM NaCl, 0.1% Tween 20) for 1 hour at RT before adding the primary antibody for hybridization overnight at 4°C. After several washes with TBST, the secondary antibody was added in 5% milk TBST and incubated for 1 hour at RT. Proteins detected by the antibody were revealed by enhanced chemiluminescence using an ECL detection kit. Primary and secondary antibodies, as well as their respective dilution ratios, are listed in Table 5.

Antibody	Company	Catalog number	Dilution
Anti-GFP (rabbit)	Invitrogen	A11122	1/3.000
Anti-Jagged2 (rabbit)	Santa-Cruz	sc-5604	1/100
Anti-myc (mouse)	EPFL/PECF	9E10	1/5.000
Anti-myc (mouse)	Neomarker (LabVision)	MS-139-P0	1/100
Anti-RhoV (anti-Chp; rabbit)	Dr. Ami Aronheim	-	1/1.000
Anti-αtubulin (mouse)	Sigma	T5168	1/3.000
ECL Anti-mouse HRP	Amersham	NA931	1/5.000
ECL Anti-rabbit HRP	Amersham	NA934	1/5.000

Table 5. List of antibodies for Western immunoblot analysis and their respective dilution ratios.

Wound healing assay

Mice were anaesthetized by intraperitoneal injection of 100µl ketamine (10g/l)/xyline (8g/l) solution or by isoflurane (induction 5% and maintenance 1-2%). Their back skin was shaved and washed with ethanol. Full-thickness excisional wounds of 5mm in diameter were made on the back of both the transgenic and the littermate control mice. Wounds were left uncovered and were regularly monitored. Mice were injected with buprenorphine twice a day for 2 or 3 days if pain was observed. The complete wounds, including approximately 2mm of the epithelial margins, were excised and fixed in 4% PFA before embedding in paraffin wax.

All surgical procedures were according to Swiss guidelines and authorized by the veterinarian authorities of the canton de Vaud.

Products & Kits (non-exhaustive list)

Product	Company	Catalog number
[α^{32}P]dCTP 3000Ci/mmol	Hartmann	SRP-205
2-mercaptoethanol	Invitrogen	31350010
70µm nylon cell strainer	BD Falcon	352350
Accuprime *Pfx* DNA polymerase	Invitrogen	12344-024
BCIP (25mg/ml in 50% dimethylformamide)	Chemie Brunschwig Biotium	10001
Bradford protein assay	Bio-Rad	500-0006
BrdU (5-Bromo-2'-deoxyuridine)	Sigma	858811
Chelex resin	BioRad	142-2842
Collagen	Vitrogen	FXP-019
Complete EDTA-free inhibitor cocktail	Roche	11836170001
DAB (3,3'-diaminobenzidine)	Sigma	D-5905
DABCO (1,4-diazabicyclo[2.2.2]octane).	Sigma	D-2522
DAPI (4,6-diamino-2-phenylindole)	Sigma	D-9542
DAPT (N-[N-(3,5-Difluorophenacetyl-L-alanyl)]-S-phenylglycine *t*-Butyl Ester)	Calbiochem	565770
DEPC (diethyl pyrocarbonate)	Axon Applichem	A0881.0100
DIG RNA labeling mix	Roche	11 277 073 910
DMEM	Invitrogen	31906-021
DMSO (dimethyl sulfoxide)	Sigma	D-2650
DNaseI	Roche	104159
Doxycycline hyclate	Sigma-Aldrich/Fluka	D9891
Dual-Luciferase reporter assay	Promega	E1910
Dynabeads® M-450 sheep anti-rat IgG	Dynal Biotech	110.07
EC100D™ *pir*$^{+}$ electrocompetent *E.coli*	Epicentre (Connectorate)	ECP09500
ECL Western blotting detection reagents	Amersham/GE Healthcare	RPN2106
Eukitt solution	Fluka/O. Kindler GmbH & Co	03989
Fetal bovine serum	Gibco (lot #41G6550K)	10270-106
Fibronectin	Calbiochem	341635
Gentamicin	Invitrogen	15710049
GM-CSF (granulocyte-macrophage colony stimulating factor)	Peprotech	315-03
HBSS (Hank's balanced salt solution)	Invitrogen	14175129
Hepes	Bioconcept	5-31F00-H

Product	Company	Catalog number
High prime DNA labeling kit	Roche	1158559200
Hybond N+ membrane	Amersham/GE Healthcare	RPN303S
Hybond-ECL nitrocellulose membrane	Amersham	RPN303D
IL-4 (interleukin 4)	Peprotech	214-14
Iscoves modified Dulbeccos medium (IMDM)	Invitrogen	12440046
JetPEI	Polyplus transfection	101-10
Large-construct kit	Qiagen	12462
Lympholyte®-M	Bioconcept	CL5035
MEM Eagle with Earle's BSS calcium free	Invitrogen	041-94775M
M-MLV reverse transcriptase	Invitrogen	28025-013
MOM kit	Vector Lab	BMK-2202
NBT (75mg/ml in 70% dimethylformamide)	Chemie Brunschwig Eurobio	GAUNTBT00
Optical 96-well Fast Thermal Cycler Plate with Barcode	Applied Biosystems	4346906
Penicillin/Streptomycin solution	Invitrogen	15070-063
PFA (paraformaldehyde)	VWR (Merck)	1.04005.1000
pI-pC	InvivoGen	tlrl-pic-5
Proteinase K	Roche	03115879001
QIAquick nucleotide removal kit	Qiagen	23306
QuantiTect reverse transcription kit	Qiagen	205311
Rabbit complement	Saxon Europe Ltd, HD supplies	RC1
RNase AWAY	Catalys	7002
RNase inhibitor (10U) RNAguard	Amersham	27-0815-01
RPMI 1640 medium	Invitrogen	61870044
SCF (stem cell factor)	Peprotech	250-03
SOC medium	Invitrogen	15544034
Tamoxifen	Sigma	T5648-1G
TaqMan® Universal PCR Master Mix, No AmpErase® UNG	Applied Biosystems	4324018
TRIZOL reagent	Invitrogen	15596-026
Trypsin 0.25%	Invitrogen	25050-014

Abbreviations

Abbreviations

AD	Atopic dermatitis
AGS	Alagille syndrome
Amp	Ampicillin
BAC	Bacterial artificial chromosome
BCC	Basal cell carcinoma
BM	Bone marrow
BMP	Bone morphogenic protein
bp	Base pair
Cdnk1a	Cyclin-dependent kinase inhibitor 1a
Chlor	Chloramphenicol
Chp	Cdc42 homolog protein
CMV	Cytomegalovirus
c-Myc	c-Myelocytomatosis oncogene
CNS	Central nervous system
cpm	Counts per minute
Cre	Cyclic recombinase
CSL	CBF1/Su(H)/LAG1
DC	Dendritic cell
DEPP	Decidual protein induced by progesterone
Dll1, 3, 4	Delta-like 1, 3, 4
DN	Double negative
DP	Dermal papilla
DSL	Delta Serrate Lag
DsRed	*Discosoma*-derived red fluorescent protein
DTA	Diphtheria toxin A-chain
E	Embryonic day
ECM	Extracellular matrix
EGF	Epidermal growth factor
EGFP or eGFP	Enhanced green fluorescent protein
EPU	Epidermal proliferative unit
ERT	Mutated ligand-binding domain of human estrogen receptor
ES	Embryonic stem cell
F0	Founder line
FACS	Fluorescence activated cell sort
FGF	Fibroblast growth factor
FIG	Fasting-induced gene
FRT	FLP1 recombinase target
FSEG	Fat-specific expressed gene
GAP	GTPase-activating protein
GEF	Guanine nucleotide exchange factor
GFP	Green fluorescent protein
H&E	Haematoxylin/eosin
HairKRNB	MHKA1-driven RhoV dominant negative
Hes	Hairy/Enhancer of Split
HF	Hair follicle
Hh	Hedgehog

HKRAB	Human keratin14-driven RhoV dominant active
Hprt	Hypoxanthine phosphoribosyltransferase
HRP	Horse radish peroxidase
HS	Hair shaft
IFE	Interfollicular epidermis
IFNα or β	Interferon-α or -β
Ig	Immunoglobulin
IL1	Interleukin-1
IRES	Internal ribosome entry site
IRNB	Involucrin-driven RhoV dominant negative
IRS	Inner root sheath
ISH	*In situ* hybridization
Jag1, 2	Jagged1, 2
JNK	c-Jun-N-terminal kinase
K	Keratin
kb	Kilo base
KGF	Keratinocyte growth factor
Klf4	Krüppel-like factor 4
LEF1	Lymphoid enhancer factor 1
Lgr5	Leucine-rich G protein-coupled receptor 5
LoxP	Locus of crossing-over from phage P1
LRC	Label-retaining cell
Lrig1	Immunoglobulin-like domain protein 1
MAML	Mastermind-like
MHKA1	Mouse hair keratin A1
MNNL	Conserved N terminus of Notch ligands
MOM	Mouse on mouse
mTORC2	Mammalian target of rapamycin complex 2
Mx1	Myxovirus influenza resistance 1
MZB	Marginal zone B cell
N1IP	Notch1 intramembrane proteolysis
NAS	Notch activity sensor mouse
NCS	Newborn calf serum
NFAT	Nuclear factors of activated T cells
NIC or NICD	Notch intracellular domain
OCT	Optimal cutting temperature
OD	Optical density
ORS	Outer root sheath
P	Postnatal day
Pak1, 2, 3	p21-activated kinase 1, 2, 3
PCP	Planar cell polarity
PCR	Polymerase chain reaction
pI-pC	Polyinosinic-polycytidylic acid (Toll-like receptor 3 ligand)
Psen1	Presenilin-1
qRT-PCR	Quantitative reverse transcription PCR
Rac1	Ras-related C3 botulinum substrate 1
RAM domain	Regulation of amino-acid metabolism domain
Ras	Retrovirus-associated DNA sequences

Rho	Ras homologue
RLU	Relative luciferase unit
rpm	Revolutions per minute
RT	Room temperature
SC	Stem cell
SCC	Squamous cell carcinoma
Shh	Sonic hedgehog
TA	Transient-amplifying cell
TACE	TNFα converting enzyme
TAD	Transactivating domain
T-ALL	T cell acute lymphoblastic leukemia
TAM	4OH-tamoxifen
TAN1	Translocation-associated Notch homologue 1
TCF1	T cell-specific transcription factor 1
TCR	T cell receptor
tetO	Tet operator
TetR	Tetracycline repressor
Tg	Transgenic
TGFα or β	Transforming growth factor-α or -β
TM	Transmembrane domain
TNFα	Tumor necrosis factor-α
TNR	Transgenic Notch reporter mouse
TRE	Tet response element
tTA2	Tetracycline-controlled transactivator 2
UI	Upper isthmus
UV	Ultraviolet
VP16	Virus protein 16
Wrch	Wnt-regulated Cdc42 homolog
wt	Wild-type

References

References

Allen, T.D. and Potten, C.S. (1974) Fine-structural identification and organization of the epidermal proliferative unit. *J Cell Sci*, **15**, 291-319.

Ambler, C.A. and Maatta, A. (2009) Epidermal stem cells: location, potential and contribution to cancer. *J Pathol*, **217**, 206-216.

Arnold, I. and Watt, F.M. (2001) c-Myc activation in transgenic mouse epidermis results in mobilization of stem cells and differentiation of their progeny. *Curr Biol*, **11**, 558-568.

Aronheim, A., Broder, Y.C., Cohen, A., Fritsch, A., Belisle, B. and Abo, A. (1998) Chp, a homologue of the GTPase Cdc42Hs, activates the JNK pathway and is implicated in reorganizing the actin cytoskeleton. *Curr Biol*, **8**, 1125-1128.

Artavanis-Tsakonas, S., Rand, M.D. and Lake, R.J. (1999) Notch signaling: cell fate control and signal integration in development. *Science*, **284**, 770-776.

Aspenstrom, P., Ruusala, A. and Pacholsky, D. (2007) Taking Rho GTPases to the next level: the cellular functions of atypical Rho GTPases. *Exp Cell Res*, **313**, 3673-3679.

Baron, U., Gossen, M. and Bujard, H. (1997) Tetracycline-controlled transcription in eukaryotes: novel transactivators with graded transactivation potential. *Nucleic Acids Res*, **25**, 2723-2729.

Basak, O. and Taylor, V. (2007) Identification of self-replicating multipotent progenitors in the embryonic nervous system by high Notch activity and Hes5 expression. *Eur J Neurosci*, **25**, 1006-1022.

Benitah, S.A., Frye, M., Glogauer, M. and Watt, F.M. (2005) Stem cell depletion through epidermal deletion of Rac1. *Science*, **309**, 933-935.

Bettenhausen, B., Hrabe de Angelis, M., Simon, D., Guenet, J.L. and Gossler, A. (1995) Transient and restricted expression during mouse embryogenesis of Dll1, a murine gene closely related to Drosophila Delta. *Development*, **121**, 2407-2418.

Blanpain, C., Lowry, W.E., Pasolli, H.A. and Fuchs, E. (2006) Canonical notch signaling functions as a commitment switch in the epidermal lineage. *Genes Dev*, **20**, 3022-3035.

Blaumueller, C.M., Qi, H., Zagouras, P. and Artavanis-Tsakonas, S. (1997) Intracellular cleavage of Notch leads to a heterodimeric receptor on the plasma membrane. *Cell*, **90**, 281-291.

Blessing, M., Nanney, L.B., King, L.E., Jones, C.M. and Hogan, B.L. (1993) Transgenic mice as a model to study the role of TGF-beta-related molecules in hair follicles. *Genes Dev*, **7**, 204-215.

Botchkarev, V.A., Botchkareva, N.V., Sharov, A.A., Funa, K., Huber, O. and Gilchrest, B.A. (2002) Modulation of BMP signaling by noggin is required for induction of the secondary (nontylotrich) hair follicles. *J Invest Dermatol*, **118**, 3-10.

Bronson, S.K., Plaehn, E.G., Kluckman, K.D., Hagaman, J.R., Maeda, N. and Smithies, O. (1996) Single-copy transgenic mice with chosen-site integration. *Proc Natl Acad Sci U S A*, **93**, 9067-9072.

Bruckner, K., Perez, L., Clausen, H. and Cohen, S. (2000) Glycosyltransferase activity of Fringe modulates Notch-Delta interactions. *Nature*, **406**, 411-415.

Buchholz, F., Angrand, P.O. and Stewart, A.F. (1996) A simple assay to determine the functionality of Cre or FLP recombination targets in genomic manipulation constructs. *Nucleic Acids Res*, **24**, 3118-3119.

Capobianco, A.J., Zagouras, P., Blaumueller, C.M., Artavanis-Tsakonas, S. and Bishop, J.M. (1997) Neoplastic transformation by truncated alleles of human NOTCH1/TAN1 and NOTCH2. *Mol Cell Biol*, **17**, 6265-6273.

Cavani, A., Zambruno, G., Marconi, A., Manca, V., Marchetti, M. and Giannetti, A. (1993) Distinctive integrin expression in the newly forming epidermis during wound healing in humans. *J Invest Dermatol*, **101**, 600-604.

Chenette, E.J., Abo, A. and Der, C.J. (2005) Critical and distinct roles of amino- and carboxyl-terminal sequences in regulation of the biological activity of the Chp atypical Rho GTPase. *J Biol Chem*, **280**, 13784-13792.

Chenette, E.J., Mitin, N.Y. and Der, C.J. (2006) Multiple sequence elements facilitate Chp Rho GTPase subcellular location, membrane association, and transforming activity. *Mol Biol Cell*, **17**, 3108-3121.

Chiang, C., Swan, R.Z., Grachtchouk, M., Bolinger, M., Litingtung, Y., Robertson, E.K., Cooper, M.K., Gaffield, W., Westphal, H., Beachy, P.A. and Dlugosz, A.A. (1999) Essential role for Sonic hedgehog during hair follicle morphogenesis. *Dev Biol*, **205**, 1-9.

Chuang, Y.Y., Valster, A., Coniglio, S.J., Backer, J.M. and Symons, M. (2007) The atypical Rho family GTPase Wrch-1 regulates focal adhesion formation and cell migration. *J Cell Sci*, **120**, 1927-1934.

Cotsarelis, G., Sun, T.T. and Lavker, R.M. (1990) Label-retaining cells reside in the bulge area of pilosebaceous unit: implications for follicular stem cells, hair cycle, and skin carcinogenesis. *Cell*, **61**, 1329-1337.

Dassule, H.R., Lewis, P., Bei, M., Maas, R. and McMahon, A.P. (2000) Sonic hedgehog regulates growth and morphogenesis of the tooth. *Development*, **127**, 4775-4785.

Deans, M.R., Antic, D., Suyama, K., Scott, M.P., Axelrod, J.D. and Goodrich, L.V. (2007) Asymmetric distribution of prickle-like 2 reveals an early underlying polarization of vestibular sensory epithelia in the inner ear. *J Neurosci*, **27**, 3139-3147.

del Amo, F.F., Gendron-Maguire, M., Swiatek, P.J., Jenkins, N.A., Copeland, N.G. and Gridley, T. (1993) Cloning, analysis, and chromosomal localization of Notch-1, a mouse homolog of Drosophila Notch. *Genomics*, **15**, 259-264.

Deregowski, V., Gazzerro, E., Priest, L., Rydziel, S. and Canalis, E. (2006) Role of the RAM domain and ankyrin repeats on notch signaling and activity in cells of osteoblastic lineage. *J Bone Miner Res*, **21**, 1317-1326.

Dumortier, A., Durham, AD., Di Piazza, M., Vauclair, S., Koch, U., Ferrand, G., Ferrero, I., Demehri, S., Li Song, L., Farr, AG., Leonard, WJ., Kopan, R., Miele, L., Hohl, D., Finke, D., Radtke, F. (2010) Atopic Dermatitis-Like Disease and Associated Lethal Myeloproliferative Disorder Arise from Loss of Notch Signaling in the Murine Skin. *PLoS One*, **5**.

Duncan, A.W., Rattis, F.M., DiMascio, L.N., Congdon, K.L., Pazianos, G., Zhao, C., Yoon, K., Cook, J.M., Willert, K., Gaiano, N. and Reya, T. (2005) Integration of Notch and Wnt signaling in hematopoietic stem cell maintenance. *Nat Immunol*, **6**, 314-322.

Dunwoodie, S.L., Henrique, D., Harrison, S.M. and Beddington, R.S. (1997) Mouse Dll3: a novel divergent Delta gene which may complement the function of other Delta homologues during early pattern formation in the mouse embryo. *Development*, **124**, 3065-3076.

Ellisen, L.W., Bird, J., West, D.C., Soreng, A.L., Reynolds, T.C., Smith, S.D. and Sklar, J. (1991) TAN-1, the human homolog of the Drosophila notch gene, is broken by chromosomal translocations in T lymphoblastic neoplasms. *Cell*, **66**, 649-661.

Estrach, S., Ambler, C.A., Lo Celso, C., Hozumi, K. and Watt, F.M. (2006) Jagged 1 is a beta-catenin target gene required for ectopic hair follicle formation in adult epidermis. *Development*, **133**, 4427-4438.

Estrach, S., Cordes, R., Hozumi, K., Gossler, A. and Watt, F.M. (2008) Role of the Notch ligand Delta1 in embryonic and adult mouse epidermis. *J Invest Dermatol*, **128**, 825-832.

Fanto, M. and Mlodzik, M. (1999) Asymmetric Notch activation specifies photoreceptors R3 and R4 and planar polarity in the Drosophila eye. *Nature*, **397**, 523-526.

Favier, B., Fliniaux, I., Thelu, J., Viallet, J.P., Demarchez, M., Jahoda, C.A. and Dhouailly, D. (2000) Localisation of members of the notch system and the differentiation of vibrissa hair follicles: receptors, ligands, and fringe modulators. *Dev Dyn*, **218**, 426-437.

Feil, R., Brocard, J., Mascrez, B., LeMeur, M., Metzger, D. and Chambon, P. (1996) Ligand-activated site-specific recombination in mice. *Proc Natl Acad Sci U S A*, **93**, 10887-10890.

Felli, M.P., Maroder, M., Mitsiadis, T.A., Campese, A.F., Bellavia, D., Vacca, A., Mann, R.S., Frati, L., Lendahl, U., Gulino, A. and Screpanti, I. (1999) Expression pattern of notch1, 2 and 3 and Jagged1 and 2 in lymphoid and stromal thymus components: distinct ligand-receptor interactions in intrathymic T cell development. *Int Immunol*, **11**, 1017-1025.

Fre, S., Huyghe, M., Mourikis, P., Robine, S., Louvard, D. and Artavanis-Tsakonas, S. (2005) Notch signals control the fate of immature progenitor cells in the intestine. *Nature*, **435**, 964-968.

Fuchs, E. (2007) Scratching the surface of skin development. *Nature*, **445**, 834-842.

Fuchs, E. and Green, H. (1980) Changes in keratin gene expression during terminal differentiation of the keratinocyte. *Cell*, **19**, 1033-1042.

Fuchs, E. and Raghavan, S. (2002) Getting under the skin of epidermal morphogenesis. *Nat Rev Genet*, **3**, 199-209.

Fukata, M., Nakagawa, M., Kuroda, S. and Kaibuchi, K. (1999) Cell adhesion and Rho small GTPases. *J Cell Sci*, **112 (Pt 24)**, 4491-4500.

Ghaleb, A.M., Aggarwal, G., Bialkowska, A.B., Nandan, M.O. and Yang, V.W. (2008) Notch inhibits expression of the Kruppel-like factor 4 tumor suppressor in the intestinal epithelium. *Mol Cancer Res*, **6**, 1920-1927.

Ghazizadeh, S. and Taichman, L.B. (2001) Multiple classes of stem cells in cutaneous epithelium: a lineage analysis of adult mouse skin. *Embo J*, **20**, 1215-1222.

Go, M.J., Eastman, D.S. and Artavanis-Tsakonas, S. (1998) Cell proliferation control by Notch signaling in Drosophila development. *Development*, **125**, 2031-2040.

Greenwald, I. (1998) LIN-12/Notch signaling: lessons from worms and flies. *Genes Dev*, **12**, 1751-1762.

Gruneberg, H. (1956) Genetical studies on the skeleton of the mouse. XVIII. Three genes for syndactylism. *J Genet*, **54**, 113-145.

Guo, L., Yu, Q.C. and Fuchs, E. (1993) Targeting expression of keratinocyte growth factor to keratinocytes elicits striking changes in epithelial differentiation in transgenic mice. *Embo J*, **12**, 973-986.

Gupta-Rossi, N., Le Bail, O., Gonen, H., Brou, C., Logeat, F., Six, E., Ciechanover, A. and Israel, A. (2001) Functional interaction between SEL-10, an F-box protein, and the nuclear form of activated Notch1 receptor. *J Biol Chem*, **276**, 34371-34378.

Gurtner, G.C., Werner, S., Barrandon, Y. and Longaker, M.T. (2008) Wound repair and regeneration. *Nature*, **453**, 314-321.

Hamada, Y., Kadokawa, Y., Okabe, M., Ikawa, M., Coleman, J.R. and Tsujimoto, Y. (1999) Mutation in ankyrin repeats of the mouse Notch2 gene induces early embryonic lethality. *Development*, **126**, 3415-3424.

Hansson, E.M., Teixeira, A.I., Gustafsson, M.V., Dohda, T., Chapman, G., Meletis, K., Muhr, J. and Lendahl, U. (2006) Recording Notch signaling in real time. *Dev Neurosci*, **28**, 118-127.

Hardy, M.H. (1992) The secret life of the hair follicle. *Trends Genet*, **8**, 55-61.

He, T.C., Zhou, S., da Costa, L.T., Yu, J., Kinzler, K.W. and Vogelstein, B. (1998) A simplified system for generating recombinant adenoviruses. *Proc Natl Acad Sci U S A*, **95**, 2509-2514.

Hebert, J.M., Rosenquist, T., Gotz, J. and Martin, G.R. (1994) FGF5 as a regulator of the hair growth cycle: evidence from targeted and spontaneous mutations. *Cell*, **78**, 1017-1025.

Hicks, C., Johnston, S.H., diSibio, G., Collazo, A., Vogt, T.F. and Weinmaster, G. (2000) Fringe differentially modulates Jagged1 and Delta1 signalling through Notch1 and Notch2. *Nat Cell Biol*, **2**, 515-520.

Higuchi, M., Kiyama, H., Hayakawa, T., Hamada, Y. and Tsujimoto, Y. (1995) Differential expression of Notch1 and Notch2 in developing and adult mouse brain. *Brain Res Mol Brain Res*, **29**, 263-272.

Hori, K., Fuwa, T.J., Seki, T. and Matsuno, K. (2005) Genetic regions that interact with loss- and gain-of-function phenotypes of deltex implicate novel genes in Drosophila Notch signaling. *Mol Genet Genomics*, **272**, 627-638.

Hubmann, R., Schwarzmeier, J.D., Shehata, M., Hilgarth, M., Duechler, M., Dettke, M. and Berger, R. (2002) Notch2 is involved in the overexpression of CD23 in B-cell chronic lymphocytic leukemia. *Blood*, **99**, 3742-3747.

Huelsken, J., Vogel, R., Erdmann, B., Cotsarelis, G. and Birchmeier, W. (2001) beta-Catenin controls hair follicle morphogenesis and stem cell differentiation in the skin. *Cell*, **105**, 533-545.

Indra, A.K., Li, M., Brocard, J., Warot, X., Bornert, J.M., Gerard, C., Messaddeq, N., Chambon, P. and Metzger, D. (2000) Targeted somatic mutagenesis in mouse epidermis. *Horm Res*, **54**, 296-300.

Indra, A.K., Warot, X., Brocard, J., Bornert, J.M., Xiao, J.H., Chambon, P. and Metzger, D. (1999) Temporally-controlled site-specific mutagenesis in the basal layer of the epidermis: comparison of the recombinase activity of the tamoxifen-inducible Cre-ER(T) and Cre-ER(T2) recombinases. *Nucleic Acids Res*, **27**, 4324-4327.

Iseki, S., Araga, A., Ohuchi, H., Nohno, T., Yoshioka, H., Hayashi, F. and Noji, S. (1996) Sonic hedgehog is expressed in epithelial cells during development of whisker, hair, and tooth. *Biochem Biophys Res Commun*, **218**, 688-693.

Ishibashi, M., Ang, S.L., Shiota, K., Nakanishi, S., Kageyama, R. and Guillemot, F. (1995) Targeted disruption of mammalian hairy and Enhancer of split homolog-1 (HES-1) leads to up-regulation of neural helix-loop-helix factors, premature neurogenesis, and severe neural tube defects. *Genes Dev*, **9**, 3136-3148.

Ishida-Yamamoto, A., Tanaka, H., Nakane, H., Takahashi, H. and Iizuka, H. (1999) Antigen retrieval of loricrin epitopes at desmosomal areas of cornified cell envelopes: an immunoelectron microscopic analysis. *Exp Dermatol*, **8**, 402-406.

Jaffe, A.B. and Hall, A. (2005) Rho GTPases: biochemistry and biology. *Annu Rev Cell Dev Biol*, **21**, 247-269.

Jaks, V., Barker, N., Kasper, M., van Es, J.H., Snippert, H.J., Clevers, H. and Toftgard, R. (2008) Lgr5 marks cycling, yet long-lived, hair follicle stem cells. *Nat Genet*, **40**, 1291-1299.

Jarriault, S., Le Bail, O., Hirsinger, E., Pourquie, O., Logeat, F., Strong, C.F., Brou, C., Seidah, N.G. and Isra l, A. (1998) Delta-1 activation of notch-1 signaling results in HES-1 transactivation. *Mol Cell Biol*, **18**, 7423-7431.

Jehn, B.M., Bielke, W., Pear, W.S. and Osborne, B.A. (1999) Cutting edge: protective effects of notch-1 on TCR-induced apoptosis. *J Immunol*, **162**, 635-638.

Jenny, A. and Mlodzik, M. (2006) Planar cell polarity signaling: a common mechanism for cellular polarization. *Mt Sinai J Med*, **73**, 738-750.

Jenny, A., Reynolds-Kenneally, J., Das, G., Burnett, M. and Mlodzik, M. (2005) Diego and Prickle regulate Frizzled planar cell polarity signalling by competing for Dishevelled binding. *Nat Cell Biol*, **7**, 691-697.

Jensen, K.B., Collins, C.A., Nascimento, E., Tan, D.W., Frye, M., Itami, S. and Watt, F.M. (2009) Lrig1 expression defines a distinct multipotent stem cell population in mammalian epidermis. *Cell Stem Cell*, **4**, 427-439.

Jensen, U.B., Yan, X., Triel, C., Woo, S.H., Christensen, R. and Owens, D.M. (2008) A distinct population of clonogenic and multipotent murine follicular keratinocytes residing in the upper isthmus. *J Cell Sci*, **121**, 609-617.

Jiang, C.K., Magnaldo, T., Ohtsuki, M., Freedberg, I.M., Bernerd, F. and Blumenberg, M. (1993) Epidermal growth factor and transforming growth factor alpha specifically induce the activation- and hyperproliferation-associated keratins 6 and 16. *Proc Natl Acad Sci U S A*, **90**, 6786-6790.

Jiang, R., Lan, Y., Chapman, H.D., Shawber, C., Norton, C.R., Serreze, D.V., Weinmaster, G. and Gridley, T. (1998) Defects in limb, craniofacial, and thymic development in Jagged2 mutant mice. *Genes Dev*, **12**, 1046-1057.

Kaneta, M., Osawa, M., Sudo, K., Nakauchi, H., Farr, A.G. and Takahama, Y. (2000) A role for pref-1 and HES-1 in thymocyte development. *J Immunol*, **164**, 256-264.

Karlsson, R., Pedersen, E.D., Wang, Z. and Brakebusch, C. (2009) Rho GTPase function in tumorigenesis. *Biochim Biophys Acta*, **1796**, 91-98.

Kidd, S., Kelley, M.R. and Young, M.W. (1986) Sequence of the notch locus of Drosophila melanogaster: relationship of the encoded protein to mammalian clotting and growth factors. *Mol Cell Biol*, **6**, 3094-3108.

Komine, M., Rao, L.S., Freedberg, I.M., Simon, M., Milisavljevic, V. and Blumenberg, M. (2001) Interleukin-1 induces transcription of keratin K6 in human epidermal keratinocytes. *J Invest Dermatol*, **116**, 330-338.

Komine, M., Rao, L.S., Kaneko, T., Tomic-Canic, M., Tamaki, K., Freedberg, I.M. and Blumenberg, M. (2000) Inflammatory versus proliferative processes in epidermis. Tumor necrosis factor alpha induces K6b keratin synthesis through a transcriptional complex containing NFkappa B and C/EBPbeta. *J Biol Chem*, **275**, 32077-32088.

Kuhn, R., Schwenk, F., Aguet, M. and Rajewsky, K. (1995) Inducible gene targeting in mice. *Science*, **269**, 1427-1429.

Kulessa, H., Turk, G. and Hogan, B.L. (2000) Inhibition of Bmp signaling affects growth and differentiation in the anagen hair follicle. *Embo J*, **19**, 6664-6674.

Kuroda, K., Han, H., Tani, S., Tanigaki, K., Tun, T., Furukawa, T., Taniguchi, Y., Kurooka, H., Hamada, Y., Toyokuni, S. and Honjo, T. (2003) Regulation of marginal zone B cell development by MINT, a suppressor of Notch/RBP-J signaling pathway. *Immunity*, **18**, 301-312.

Lardelli, M., Dahlstrand, J. and Lendahl, U. (1994) The novel Notch homologue mouse Notch 3 lacks specific epidermal growth factor-repeats and is expressed in proliferating neuroepithelium. *Mech Dev*, **46**, 123-136.

Lefort, K., Mandinova, A., Ostano, P., Kolev, V., Calpini, V., Kolfschoten, I., Devgan, V., Lieb, J., Raffoul, W., Hohl, D., Neel, V., Garlick, J., Chiorino, G. and Dotto, G.P. (2007) Notch1 is a p53 target gene involved in human keratinocyte tumor suppression through negative regulation of ROCK1/2 and MRCKalpha kinases. *Genes Dev*, **21**, 562-577.

Lehar, S.M. and Bevan, M.J. (2006) T cells develop normally in the absence of both Deltex1 and Deltex2. *Mol Cell Biol*, **26**, 7358-7371.

Levy, V., Lindon, C., Harfe, B.D. and Morgan, B.A. (2005) Distinct stem cell populations regenerate the follicle and interfollicular epidermis. *Dev Cell*, **9**, 855-861.

Li, A., Pouliot, N., Redvers, R. and Kaur, P. (2004) Extensive tissue-regenerative capacity of neonatal human keratinocyte stem cells and their progeny. *J Clin Invest*, **113**, 390-400.

Li, L., Krantz, I.D., Deng, Y., Genin, A., Banta, A.B., Collins, C.C., Qi, M., Trask, B.J., Kuo, W.L., Cochran, J., Costa, T., Pierpont, M.E., Rand, E.B., Piccoli, D.A., Hood, L. and Spinner, N.B. (1997) Alagille syndrome is caused by mutations in human Jagged1, which encodes a ligand for Notch1. *Nat Genet*, **16**, 243-251.

Li, T., Ma, G., Cai, H., Price, D.L. and Wong, P.C. (2003) Nicastrin is required for assembly of presenilin/gamma-secretase complexes to mediate Notch signaling and for processing and trafficking of beta-amyloid precursor protein in mammals. *J Neurosci*, **23**, 3272-3277.

Lin, M.H., Leimeister, C., Gessler, M. and Kopan, R. (2000) Activation of the Notch pathway in the hair cortex leads to aberrant differentiation of the adjacent hair-shaft layers. *Development*, **127**, 2421-2432.

Lindsell, C.E., Shawber, C.J., Boulter, J. and Weinmaster, G. (1995) Jagged: a mammalian ligand that activates Notch1. *Cell*, **80**, 909-917.

Liu, A.X., Rane, N., Liu, J.P. and Prendergast, G.C. (2001) RhoB is dispensable for mouse development, but it modifies susceptibility to tumor formation as well as cell adhesion and growth factor signaling in transformed cells. *Mol Cell Biol*, **21**, 6906-6912.

Lock, F.E. and Hotchin, N.A. (2009) Distinct roles for ROCK1 and ROCK2 in the regulation of keratinocyte differentiation. *PLoS One*, **4**, e8190.

Logeat, F., Bessia, C., Brou, C., LeBail, O., Jarriault, S., Seidah, N.G. and Israel, A. (1998) The Notch1 receptor is cleaved constitutively by a furin-like convertase. *Proc Natl Acad Sci U S A*, **95**, 8108-8112.

Lowell, S., Jones, P., Le Roux, I., Dunne, J. and Watt, F.M. (2000) Stimulation of human epidermal differentiation by delta-notch signalling at the boundaries of stem-cell clusters. *Curr Biol*, **10**, 491-500.

Luo, B., Aster, J.C., Hasserjian, R.P., Kuo, F. and Sklar, J. (1997) Isolation and functional analysis of a cDNA for human Jagged2, a gene encoding a ligand for the Notch1 receptor. *Mol Cell Biol*, **17**, 6057-6067.

Mammucari, C., Tommasi di Vignano, A., Sharov, A.A., Neilson, J., Havrda, M.C., Roop, D.R., Botchkarev, V.A., Crabtree, G.R. and Dotto, G.P. (2005) Integration of Notch 1 and calcineurin/NFAT signaling pathways in keratinocyte growth and differentiation control. *Dev Cell*, **8**, 665-676.

Mancini, S.J., Mantei, N., Dumortier, A., Suter, U., MacDonald, H.R. and Radtke, F. (2005) Jagged1-dependent Notch signaling is dispensable for hematopoietic stem cell self-renewal and differentiation. *Blood*, **105**, 2340-2342.

Manser, E., Leung, T., Salihuddin, H., Zhao, Z.S. and Lim, L. (1994) A brain serine/threonine protein kinase activated by Cdc42 and Rac1. *Nature*, **367**, 40-46.

Marionnet, C., Lalou, C., Mollier, K., Chazal, M., Delestaing, G., Compan, D., Verola, O., Vilmer, C., Cuminet, J., Dubertret, L. and Basset-Seguin, N. (2003) Differential molecular profiling between skin carcinomas reveals four newly reported genes potentially implicated in squamous cell carcinoma development. *Oncogene*, **22**, 3500-3505.

Matz, M.V., Fradkov, A.F., Labas, Y.A., Savitsky, A.P., Zaraisky, A.G., Markelov, M.L. and Lukyanov, S.A. (1999) Fluorescent proteins from nonbioluminescent Anthozoa species. *Nat Biotechnol*, **17**, 969-973.

McCright, B., Gao, X., Shen, L., Lozier, J., Lan, Y., Maguire, M., Herzlinger, D., Weinmaster, G., Jiang, R. and Gridley, T. (2001) Defects in development of the kidney, heart and eye vasculature in mice homozygous for a hypomorphic Notch2 mutation. *Development*, **128**, 491-502.

McCright, B., Lozier, J. and Gridley, T. (2002) A mouse model of Alagille syndrome: Notch2 as a genetic modifier of Jag1 haploinsufficiency. *Development*, **129**, 1075-1082.

McDaniell, R., Warthen, D.M., Sanchez-Lara, P.A., Pai, A., Krantz, I.D., Piccoli, D.A. and Spinner, N.B. (2006) NOTCH2 mutations cause Alagille syndrome, a heterogeneous disorder of the notch signaling pathway. *Am J Hum Genet*, **79**, 169-173.

Mehrel, T., Hohl, D., Rothnagel, J.A., Longley, M.A., Bundman, D., Cheng, C., Lichti, U., Bisher, M.E., Steven, A.C., Steinert, P.M. and et al. (1990) Identification of a major keratinocyte cell envelope protein, loricrin. *Cell*, **61**, 1103-1112.

Moloney, D.J., Panin, V.M., Johnston, S.H., Chen, J., Shao, L., Wilson, R., Wang, Y., Stanley, P., Irvine, K.D., Haltiwanger, R.S. and Vogt, T.F. (2000) Fringe is a glycosyltransferase that modifies Notch. *Nature*, **406**, 369-375.

Morgan, T.H. (1917) The Theory of the Gene. *The American Naturalist*, **51**, 513.

Moriyama, M., Durham, A.D., Moriyama, H., Hasegawa, K., Nishikawa, S., Radtke, F. and Osawa, M. (2008) Multiple roles of Notch signaling in the regulation of epidermal development. *Dev Cell*, **14**, 594-604.

Morris, R.J., Liu, Y., Marles, L., Yang, Z., Trempus, C., Li, S., Lin, J.S., Sawicki, J.A. and Cotsarelis, G. (2004) Capturing and profiling adult hair follicle stem cells. *Nat Biotechnol*, **22**, 411-417.

Mumm, J.S., Schroeter, E.H., Saxena, M.T., Griesemer, A., Tian, X., Pan, D.J., Ray, W.J. and Kopan, R. (2000) A ligand-induced extracellular cleavage regulates gamma-secretase-like proteolytic activation of Notch1. *Mol Cell*, **5**, 197-206.

Murtaugh, L.C., Stanger, B.Z., Kwan, K.M. and Melton, D.A. (2003) Notch signaling controls multiple steps of pancreatic differentiation. *Proc Natl Acad Sci U S A*, **100**, 14920-14925.

Nakamura, A., Arimoto, M., Takeuchi, K. and Fujii, T. (2002) A rapid extraction procedure of human hair proteins and identification of phosphorylated species. *Biol Pharm Bull*, **25**, 569-572.

Nguyen, B.C., Lefort, K., Mandinova, A., Antonini, D., Devgan, V., Della Gatta, G., Koster, M.I., Zhang, Z., Wang, J., Tommasi di Vignano, A., Kitajewski, J., Chiorino, G., Roop, D.R., Missero, C. and Dotto, G.P. (2006) Cross-regulation between Notch and p63 in keratinocyte commitment to differentiation. *Genes Dev*, **20**, 1028-1042.

Nicolas, M. (2003) The role of murine Notch1 in skin homeostasis and tumorigenesis. *Faculté des Sciences*. Université de Lausanne, Lausanne, Vol. PhD, p. 119.

Nicolas, M., Wolfer, A., Raj, K., Kummer, J.A., Mill, P., van Noort, M., Hui, C.C., Clevers, H., Dotto, G.P. and Radtke, F. (2003) Notch1 functions as a tumor suppressor in mouse skin. *Nat Genet*, **33**, 416-421.

Nijhof, J.G., Braun, K.M., Giangreco, A., van Pelt, C., Kawamoto, H., Boyd, R.L., Willemze, R., Mullenders, L.H., Watt, F.M., de Gruijl, F.R. and van Ewijk, W. (2006) The cell-surface marker MTS24 identifies a novel population of follicular keratinocytes with characteristics of progenitor cells. *Development*, **133**, 3027-3037.

Nye, J.S. and Kopan, R. (1995) Developmental signaling. Vertebrate ligands for Notch. *Curr Biol*, **5**, 966-969.

Oberg, C., Li, J., Pauley, A., Wolf, E., Gurney, M. and Lendahl, U. (2001) The Notch intracellular domain is ubiquitinated and negatively regulated by the mammalian Sel-10 homolog. *J Biol Chem*, **276**, 35847-35853.

Oda, T., Elkahloun, A.G., Pike, B.L., Okajima, K., Krantz, I.D., Genin, A., Piccoli, D.A., Meltzer, P.S., Spinner, N.B., Collins, F.S. and Chandrasekharappa, S.C. (1997) Mutations in the human Jagged1 gene are responsible for Alagille syndrome. *Nat Genet*, **16**, 235-242.

Ohtsuka, T., Imayoshi, I., Shimojo, H., Nishi, E., Kageyama, R. and McConnell, S.K. (2006) Visualization of embryonic neural stem cells using Hes promoters in transgenic mice. *Mol Cell Neurosci*, **31**, 109-122.

Oka, C., Nakano, T., Wakeham, A., de la Pompa, J.L., Mori, C., Sakai, T., Okazaki, S., Kawaichi, M., Shiota, K., Mak, T.W. and Honjo, T. (1995) Disruption of the mouse RBP-J kappa gene results in early embryonic death. *Development*, **121**, 3291-3301.

Okuda, H., Miyata, S., Mori, Y. and Tohyama, M. (2007) Mouse Prickle1 and Prickle2 are expressed in postmitotic neurons and promote neurite outgrowth. *FEBS Lett*, **581**, 4754-4760.

Okuyama, R., Ogawa, E., Nagoshi, H., Yabuki, M., Kurihara, A., Terui, T., Aiba, S., Obinata, M., Tagami, H. and Ikawa, S. (2007) p53 homologue, p51/p63, maintains the immaturity of keratinocyte stem cells by inhibiting Notch1 activity. *Oncogene*, **26**, 4478-4488.

Oswald, F., Winkler, M., Cao, Y., Astrahantseff, K., Bourteele, S., Knochel, W. and Borggrefe, T. (2005) RBP-Jkappa/SHARP recruits CtIP/CtBP corepressors to silence Notch target genes. *Mol Cell Biol*, **25**, 10379-10390.

Pellegrini, G., Dellambra, E., Golisano, O., Martinelli, E., Fantozzi, I., Bondanza, S., Ponzin, D., McKeon, F. and De Luca, M. (2001) p63 identifies keratinocyte stem cells. *Proc Natl Acad Sci U S A*, **98**, 3156-3161.

Perumalsamy, L.R., Nagala, M., Banerjee, P. and Sarin, A. (2009) A hierarchical cascade activated by non-canonical Notch signaling and the mTOR-Rictor complex regulates neglect-induced death in mammalian cells. *Cell Death Differ*, **16**, 879-889.

Powell, B.C., Passmore, E.A., Nesci, A. and Dunn, S.M. (1998) The Notch signalling pathway in hair growth. *Mech Dev*, **78**, 189-192.

Pui, J.C., Allman, D., Xu, L., DeRocco, S., Karnell, F.G., Bakkour, S., Lee, J.Y., Kadesch, T., Hardy, R.R., Aster, J.C. and Pear, W.S. (1999) Notch1 expression in early lymphopoiesis influences B versus T lineage determination. *Immunity*, **11**, 299-308.

Radtke, F., Schweisguth, F. and Pear, W. (2005) The Notch 'gospel'. *EMBO Rep*, **6**, 1120-1125.

Radtke, F., Wilson, A., Stark, G., Bauer, M., van Meerwijk, J., MacDonald, H.R. and Aguet, M. (1999) Deficient T cell fate specification in mice with an induced inactivation of Notch1. *Immunity*, **10**, 547-558.

Rangarajan, A., Talora, C., Okuyama, R., Nicolas, M., Mammucari, C., Oh, H., Aster, J.C., Krishna, S., Metzger, D., Chambon, P., Miele, L., Aguet, M., Radtke, F. and Dotto, G.P. (2001) Notch signaling is a direct determinant of keratinocyte growth arrest and entry into differentiation. *Embo J*, **20**, 3427-3436.

Riccio, O., van Gijn, M.E., Bezdek, A.C., Pellegrinet, L., van Es, J.H., Zimber-Strobl, U., Strobl, L.J., Honjo, T., Clevers, H. and Radtke, F. (2008) Loss of intestinal crypt progenitor cells owing to inactivation of both Notch1 and Notch2 is accompanied by derepression of CDK inhibitors p27Kip1 and p57Kip2. *EMBO Rep*, **9**, 377-383.

Rice, R.H. and Green, H. (1979) Presence in human epidermal cells of a soluble protein precursor of the cross-linked envelope: activation of the cross-linking by calcium ions. *Cell*, **18**, 681-694.

Rodriguez, C.I., Buchholz, F., Galloway, J., Sequerra, R., Kasper, J., Ayala, R., Stewart, A.F. and Dymecki, S.M. (2000) High-efficiency deleter mice show that FLPe is an alternative to Cre-loxP. *Nat Genet*, **25**, 139-140.

Saito, T., Chiba, S., Ichikawa, M., Kunisato, A., Asai, T., Shimizu, K., Yamaguchi, T., Yamamoto, G., Seo, S., Kumano, K., Nakagami-Yamaguchi, E., Hamada, Y., Aizawa, S. and Hirai, H. (2003) Notch2 is preferentially expressed in mature B cells and indispensable for marginal zone B lineage development. *Immunity*, **18**, 675-685.

Samarin, S. and Nusrat, A. (2009) Regulation of epithelial apical junctional complex by Rho family GTPases. *Front Biosci*, **14**, 1129-1142.

Sander, G.R. and Powell, B.C. (2004) Expression of notch receptors and ligands in the adult gut. *J Histochem Cytochem*, **52**, 509-516.

Scott, I.R. and Harding, C.R. (1986) Filaggrin breakdown to water binding compounds during development of the rat stratum corneum is controlled by the water activity of the environment. *Dev Biol*, **115**, 84-92.

Shawber, C., Boulter, J., Lindsell, C.E. and Weinmaster, G. (1996) Jagged2: a serrate-like gene expressed during rat embryogenesis. *Dev Biol*, **180**, 370-376.

Shin, D. and Anderson, D.J. (2005) Isolation of arterial-specific genes by subtractive hybridization reveals molecular heterogeneity among arterial endothelial cells. *Dev Dyn*, **233**, 1589-1604.

Shutes, A., Berzat, A.C., Chenette, E.J., Cox, A.D. and Der, C.J. (2006) Biochemical analyses of the Wrch atypical Rho family GTPases. *Methods Enzymol*, **406**, 11-26.

Shutter, J.R., Scully, S., Fan, W., Richards, W.G., Kitajewski, J., Deblandre, G.A., Kintner, C.R. and Stark, K.L. (2000) Dll4, a novel Notch ligand expressed in arterial endothelium. *Genes Dev*, **14**, 1313-1318.

Sidow, A., Bulotsky, M.S., Kerrebrock, A.W., Bronson, R.T., Daly, M.J., Reeve, M.P., Hawkins, T.L., Birren, B.W., Jaenisch, R. and Lander, E.S. (1997) Serrate2 is disrupted in the mouse limb-development mutant syndactylism. *Nature*, **389**, 722-725.

Simon, M. and Green, H. (1988) The glutamine residues reactive in transglutaminase-catalyzed cross-linking of involucrin. *J Biol Chem*, **263**, 18093-18098.

Soriano, P. (1999) Generalized lacZ expression with the ROSA26 Cre reporter strain. *Nat Genet*, **21**, 70-71.

Souilhol, C., Cormier, S., Monet, M., Vandormael-Pournin, S., Joutel, A., Babinet, C. and Cohen-Tannoudji, M. (2006) Nas transgenic mouse line allows visualization of Notch pathway activity in vivo. *Genesis*, **44**, 277-286.

Sparwasser, T., Gong, S., Li, J.Y. and Eberl, G. (2004) General method for the modification of different BAC types and the rapid generation of BAC transgenic mice. *Genesis*, **38**, 39-50.

Strutt, D., Johnson, R., Cooper, K. and Bray, S. (2002) Asymmetric localization of frizzled and the determination of notch-dependent cell fate in the Drosophila eye. *Curr Biol*, **12**, 813-824.

Swiatek, P.J., Lindsell, C.E., del Amo, F.F., Weinmaster, G. and Gridley, T. (1994) Notch1 is essential for postimplantation development in mice. *Genes Dev*, **8**, 707-719.

Tallquist, M.D. and Soriano, P. (2000) Epiblast-restricted Cre expression in MORE mice: a tool to distinguish embryonic vs. extra-embryonic gene function. *Genesis*, **26**, 113-115.

Tao, W., Pennica, D., Xu, L., Kalejta, R.F. and Levine, A.J. (2001) Wrch-1, a novel member of the Rho gene family that is regulated by Wnt-1. *Genes Dev*, **15**, 1796-1807.

Tchorz, J.S., Kinter, J., Muller, M., Tornillo, L., Heim, M.H. and Bettler, B. (2009) Notch2 signaling promotes biliary epithelial cell fate specification and tubulogenesis during bile duct development in mice. *Hepatology*, **50**, 871-879.

Thelu, J., Rossio, P. and Favier, B. (2002) Notch signalling is linked to epidermal cell differentiation level in basal cell carcinoma, psoriasis and wound healing. *BMC Dermatol*, **2**, 7.

Trempus, C.S., Morris, R.J., Bortner, C.D., Cotsarelis, G., Faircloth, R.S., Reece, J.M. and Tennant, R.W. (2003) Enrichment for living murine keratinocytes from the hair follicle bulge with the cell surface marker CD34. *J Invest Dermatol*, **120**, 501-511.

Troen, G., Nygaard, V., Jenssen, T.K., Ikonomou, I.M., Tierens, A., Matutes, E., Gruszka-Westwood, A., Catovsky, D., Myklebost, O., Lauritzsen, G., Hovig, E. and Delabie, J. (2004) Constitutive expression of the AP-1 transcription factors c-jun, junD, junB, and c-fos and the marginal zone B-cell transcription factor Notch2 in splenic marginal zone lymphoma. *J Mol Diagn*, **6**, 297-307.

Tsai, S., Fero, J. and Bartelmez, S. (2000) Mouse Jagged2 is differentially expressed in hematopoietic progenitors and endothelial cells and promotes the survival and proliferation of hematopoietic progenitors by direct cell-to-cell contact. *Blood*, **96**, 950-957.

Tumbar, T., Guasch, G., Greco, V., Blanpain, C., Lowry, W.E., Rendl, M. and Fuchs, E. (2004) Defining the epithelial stem cell niche in skin. *Science*, **303**, 359-363.

Uyttendaele, H., Marazzi, G., Wu, G., Yan, Q., Sassoon, D. and Kitajewski, J. (1996) Notch4/int-3, a mammary proto-oncogene, is an endothelial cell-specific mammalian Notch gene. *Development*, **122**, 2251-2259.

Uyttendaele, H., Panteleyev, A.A., de Berker, D., Tobin, D.T. and Christiano, A.M. (2004) Activation of Notch1 in the hair follicle leads to cell-fate switch and Mohawk alopecia. *Differentiation*, **72**, 396-409.

van Es, J.H., van Gijn, M.E., Riccio, O., van den Born, M., Vooijs, M., Begthel, H., Cozijnsen, M., Robine, S., Winton, D.J., Radtke, F. and Clevers, H. (2005) Notch/gamma-secretase inhibition turns proliferative cells in intestinal crypts and adenomas into goblet cells. *Nature*, **435**, 959-963.

van Genderen, C., Okamura, R.M., Farinas, I., Quo, R.G., Parslow, T.G., Bruhn, L. and Grosschedl, R. (1994) Development of several organs that require inductive epithelial-mesenchymal interactions is impaired in LEF-1-deficient mice. *Genes Dev*, **8**, 2691-2703.

Vassar, R., Rosenberg, M., Ross, S., Tyner, A. and Fuchs, E. (1989) Tissue-specific and differentiation-specific expression of a human K14 keratin gene in transgenic mice. *Proc Natl Acad Sci U S A*, **86**, 1563-1567.

Vauclair, S. (2006) Role of Notch signaling in epidermis and appendages. *Faculté de biologie et de médecine*. Université de Lausanne, Lausanne, Vol. Thèse de doctorat ès sciences de la vie (PhD), p. 184.

Vauclair, S., Nicolas, M., Barrandon, Y. and Radtke, F. (2005) Notch1 is essential for postnatal hair follicle development and homeostasis. *Dev Biol*, **284**, 184-193.

Vooijs, M., Ong, C.T., Hadland, B., Huppert, S., Liu, Z., Korving, J., van den Born, M., Stappenbeck, T., Wu, Y., Clevers, H. and Kopan, R. (2007) Mapping the consequence of Notch1 proteolysis in vivo with NIP-CRE. *Development*, **134**, 535-544.

Waikel, R.L., Kawachi, Y., Waikel, P.A., Wang, X.J. and Roop, D.R. (2001) Deregulated expression of c-Myc depletes epidermal stem cells. *Nat Genet*, **28**, 165-168.

Watanabe, H., Nonoguchi, K., Sakurai, T., Masuda, T., Itoh, K. and Fujita, J. (2005) A novel protein Depp, which is induced by progesterone in human endometrial stromal cells activates Elk-1 transcription factor. *Mol Hum Reprod*, **11**, 471-476.

Watt, F.M., Estrach, S. and Ambler, C.A. (2008) Epidermal Notch signalling: differentiation, cancer and adhesion. *Curr Opin Cell Biol*, **20**, 171-179.

Watt, F.M., Kubler, M.D., Hotchin, N.A., Nicholson, L.J. and Adams, J.C. (1993) Regulation of keratinocyte terminal differentiation by integrin-extracellular matrix interactions. *J Cell Sci*, **106 (Pt 1)**, 175-182.

Weinmaster, G., Roberts, V.J. and Lemke, G. (1992) Notch2: a second mammalian Notch gene. *Development*, **116**, 931-941.

Weisz Hubsman, M., Volinsky, N., Manser, E., Yablonski, D. and Aronheim, A. (2007) Autophosphorylation-dependent degradation of Pak1, triggered by the Rho-family GTPase, Chp. *Biochem J*, **404**, 487-497.

Weng, A.P., Ferrando, A.A., Lee, W., Morris, J.P.t., Silverman, L.B., Sanchez-Irizarry, C., Blacklow, S.C., Look, A.T. and Aster, J.C. (2004) Activating mutations of NOTCH1 in human T cell acute lymphoblastic leukemia. *Science*, **306**, 269-271.

Wharton, K.A., Johansen, K.M., Xu, T. and Artavanis-Tsakonas, S. (1985) Nucleotide sequence from the neurogenic locus notch implies a gene product that shares homology with proteins containing EGF-like repeats. *Cell*, **43**, 567-581.

Wherlock, M. and Mellor, H. (2002) The Rho GTPase family: a Racs to Wrchs story. *J Cell Sci*, **115**, 239-240.

Wilson, A., MacDonald, H.R. and Radtke, F. (2001) Notch 1-deficient common lymphoid precursors adopt a B cell fate in the thymus. *J Exp Med*, **194**, 1003-1012.

Wilson, A. and Radtke, F. (2006) Multiple functions of Notch signaling in self-renewing organs and cancer. *FEBS Lett*, **580**, 2860-2868.

Wilson, N., Hynd, P.I. and Powell, B.C. (1999) The role of BMP-2 and BMP-4 in follicle initiation and the murine hair cycle. *Exp Dermatol*, **8**, 367-368.

Wolfer, A., Bakker, T., Wilson, A., Nicolas, M., Ioannidis, V., Littman, D.R., Lee, P.P., Wilson, C.B., Held, W., MacDonald, H.R. and Radtke, F. (2001) Inactivation of Notch 1 in immature thymocytes does not perturb CD4 or CD8T cell development. *Nat Immunol*, **2**, 235-241.

Wong, P. and Coulombe, P.A. (2003) Loss of keratin 6 (K6) proteins reveals a function for intermediate filaments during wound repair. *J Cell Biol*, **163**, 327-337.

Wong, P.C., Zheng, H., Chen, H., Becher, M.W., Sirinathsinghji, D.J., Trumbauer, M.E., Chen, H.Y., Price, D.L., Van der Ploeg, L.H. and Sisodia, S.S. (1997) Presenilin 1 is required for Notch1 and DII1 expression in the paraxial mesoderm. *Nature*, **387**, 288-292.

Wu, G., Lyapina, S., Das, I., Li, J., Gurney, M., Pauley, A., Chui, I., Deshaies, R.J. and Kitajewski, J. (2001) SEL-10 is an inhibitor of notch signaling that targets notch for ubiquitin-mediated protein degradation. *Mol Cell Biol*, **21**, 7403-7415.

Wu, L., Aster, J.C., Blacklow, S.C., Lake, R., Artavanis-Tsakonas, S. and Griffin, J.D. (2000) MAML1, a human homologue of Drosophila mastermind, is a transcriptional co-activator for NOTCH receptors. *Nat Genet*, **26**, 484-489.

Wu, X., Quondamatteo, F., Lefever, T., Czuchra, A., Meyer, H., Chrostek, A., Paus, R., Langbein, L. and Brakebusch, C. (2006) Cdc42 controls progenitor cell differentiation and beta-catenin turnover in skin. *Genes Dev*, **20**, 571-585.

Xia, X., Qian, S., Soriano, S., Wu, Y., Fletcher, A.M., Wang, X.J., Koo, E.H., Wu, X. and Zheng, H. (2001) Loss of presenilin 1 is associated with enhanced beta-catenin signaling and skin tumorigenesis. *Proc Natl Acad Sci U S A*, **98**, 10863-10868.

Xu, J. (2009) Generation of mice with a conditional null allele of the Jagged2 gene. *Thomas Gridley*. The Jackson Laboratory, Bar Harbor, Maine 04609 USA.

Xue, Y., Gao, X., Lindsell, C.E., Norton, C.R., Chang, B., Hicks, C., Gendron-Maguire, M., Rand, E.B., Weinmaster, G. and Gridley, T. (1999) Embryonic lethality and vascular defects in mice lacking the Notch ligand Jagged1. *Hum Mol Genet*, **8**, 723-730.

Yang, A., Schweitzer, R., Sun, D., Kaghad, M., Walker, N., Bronson, R.T., Tabin, C., Sharpe, A., Caput, D., Crum, C. and McKeon, F. (1999) p63 is essential for regenerative proliferation in limb, craniofacial and epithelial development. *Nature*, **398**, 714-718.

Yuspa, S.H., Kilkenny, A.E., Steinert, P.M. and Roop, D.R. (1989) Expression of murine epidermal differentiation markers is tightly regulated by restricted extracellular calcium concentrations in vitro. *J Cell Biol*, **109**, 1207-1217.

Zhang, B., Liu, R., Shi, D., Liu, X., Chen, Y., Dou, X., Zhu, X., Lu, C., Liang, W., Liao, L., Zenke, M. and Zhao, R.C. (2009) Mesenchymal stem cells induce mature dendritic cells into a novel Jagged-2-dependent regulatory dendritic cell population. *Blood*, **113**, 46-57.

Zhao, Z.S. and Manser, E. (2005) PAK and other Rho-associated kinases--effectors with surprisingly diverse mechanisms of regulation. *Biochem J*, **386**, 201-214.

Zhou, P., Byrne, C., Jacobs, J. and Fuchs, E. (1995) Lymphoid enhancer factor 1 directs hair follicle patterning and epithelial cell fate. *Genes Dev*, **9**, 700-713.

Acknowledgements

I would like to thank Freddy for giving me the opportunity to pursue my PhD thesis in his laboratory, as well as all the members of the lab, past and present, for their friendship and good times. I really enjoyed working and sharing jokes, meals and coffees with all of you!

I would also like to thank all the people around the institute, friends and colleagues, for their help and advice, particularly the animal and the histology core facilities. I warmly thank Prof. Nouria Hernandez for her precious support and motivation, which were badly needed by times.

A special thank you goes to my dears Caro and Emma, who have been present during the ups and downs. These years would not have been the same without you!

My dear Sonja, you know how much our talks about work and life are precious to me! I can only thank you for your support and friendship.

Big kisses, hugs and thank yous go to my Mom Jacqueline, my Dad Jerry and my dear sister Maddy for their priceless support, motivation, advice, and love. I have done it because you were all there for me all the way!! Love you tons. Warm hugs go to my grandparents, wherever they are.

Merci à mon amour, mon gros chat (v. et r.), mon mari Raphaël pour tout ce que tu m'apportes. Tu as vécu ces quatre années de thèse à mes côtés, sans trop broncher, et surtout en me motivant durant les moments difficiles. Tu m'as toujours épaulée et soutenue avec les meilleures intentions du monde. Merci pour tout mon beau.

Curriculum Vitae

April Bezdek Pomey
Av. des Oiseaux 9
1018 Lausanne, VD, Switzerland
Tel: +41 78 825 6303 [mobile]
+41 21 646 1126 [private]
Email: april.bezdek_pomey@a3.epfl.ch
Nationalities: CH and USA
Age: 27 years old

Current Position	**PhD student** in **Life Sciences** at the Swiss Federal Institute of Technology Lausanne (EPFL) Working in the field of **Molecular Biology of Cancer and Infection**

My PhD thesis investigated the role of a specific pathway, also involved in cancer, called Notch, during differentiation of the epidermis. More specifically, one of my projects focused on deciphering the role of a potential downstream target gene by the generation of several transgenic mice. Analyses of the transgenic skin during homeostasis as well as during wound healing did not reveal any overt dysregulation. These results suggest a more complex interplay of signals involved in skin development.

Formal Education

2001-2005	Biochemistry Diploma (Master's degree equivalent),University of Fribourg, Switzerland Undergraduate independent research thesis on Circadian Rhythms and Apoptosis During my diploma year I contributed to finding a link between programmed cell death and the murine circadian clock. I also investigated the potential role of the neurotransmitter acetylcholine in the effect of ethanol consumption on the central pacemaker. In addition, I preformed behavioral wheel-running tests on mice.
1996-2001	Baccalaureate diploma in sciences, Sion, Switzerland

Professional Experiences

2004-2005	Translation (French/English), University of Fribourg, Switzerland
2004	Swiss institute for experimental cancer research (ISREC) Summer Research Program in the laboratory of Prof. Dr. Pierre Gönczy, Switzerland Private English teaching

Fellowships/Awards

2009	Selected for the Youth Forum of the Global Humanitarian Forum, Switzerland
2008-2009	Selected in the "women mentoring program" supported by the Swiss Confederation
2007	EMBO workshop "Practical course on RNAi"- Travel fellowship, Germany
2005	Onassis Foundation Lecture Series - Travel fellowship, Greece "Programmed Cell Death and Cell Signaling in Development and Disease"

Meetings attended with poster presentation

2009	Hydra Summer School Stem Cells & Regenerative Medicine, EuroSystem, Greece
2008	Cancer and the Cell Cycle, EPFL Life Science Symposium, Lausanne
2007	Practical course on RNAi, EMBO, Heidelberg
2006	Advances in Stem Cell Research, EuroStemCell, Lausanne

Publications

Riccio O, van Gijn ME; Bezdek AC, Pellegrinet L, van Es JH, Zimber-Strobl U, Strobl Lj, Honjo T, Clevers H, Radtke F. Loss of intestinal crypt progenitor cells due to inactivation of both Notch1 and Notch2 is accompanied by derepression of cyclin-dependent (CDK) inhibitors p27Kip1 and p57Kip2, EMBO Rep. 2008, 9(4):377-83.

Schaub M, Bezdek A, Henzinger T, Radtke F, and Fisher J. Qualitative Crosstalk Analysis of Wnt and Notch Signaling in Mammalian Skin, RECOMB Satellite Conference on Systems Biology, 2007.

Language skills

French	Mother tongue
English	Mother tongue
German	Good conversational knowledge

IT skills

Microsoft Office, Adobe Photoshop, Bioinformatics tools (e.g. BLAST, NCBI, Primer3Plus, Ensembl, Lalign), FileMakerPro, EndNote

Personal Information

2008	Member of the PhD committee for ISREC PhD students
2006-2009	Member of the Swiss Society for Biochemistry
Interests	Hiking, fitness, travel